Renewable and Sustainable Energy Reviews 226 (2026) 116324

Contents lists available at ScienceDirect

Renewable and Sustainable Energy Reviews

journal homepage: www.elsevier.com/locate/rser

A comprehensive review of frequency response and control strategies for grid-connected solar photovoltaic systems

Ateeb Hassan, Jubaer Ahmed *, Savvas Papadopoulos, Fadi Kahwash, Keng Goh

School of Computing, Engineering and Built-Environment, Edinburgh Napier University, 10 Colinton Road, EH10 5DT, United Kingdom

ARTICLE INFO

Keywords:
Renewable energy integration
Frequency control
Solar PVs
MPPT
FPPT
De-loading
Power reserve control (PRC)

ABSTRACT

Renewable energy is the future of energy generation to meet the growing electricity demand worldwide. The extensive integration of Renewable Energy Sources (RESs) is causing a paradigm shift in the power network. Integrating RESs reduces the overall inertia of the system, which could result in occasional unstable frequency and may lead to cascading blackouts. This paper performs an overarching analysis of different frequency control techniques that support seamless integration of solar photovoltaic systems to the grid. These techniques are extensively compared based on various parameters and are categorised based on control actions and implementation to highlight their effectiveness and limitations. Before exploring frequency regulation methods, a primer on PV system modelling and configuration is given to comprehend PV integration to the grid. Furthermore, a brief synopsis of strategies utilising Energy Storage Devices (ESSs) is provided, emphasising methods that do not require ESSs. Beyond this, an overview of optimisation algorithms used in the literature for frequency regulation is given, providing a holistic understanding. Recent research highlights the growing interest in hybrid power reserve approaches, as combining diverse optimisation algorithms offers robust, reliable, fast, and adaptive solutions. This paper endeavours to provide a holistic review for researchers interested in developing frequency regulation methods for PV systems and to support industry practitioners in finding the appropriate solutions for frequency regulation-related applications.

1. Introduction

Renewable Energy Sources (RESs) have gained more traction in recent years due to growing concerns about global warming and rising electricity usage. The primary source of greenhouse gases is the electricity generated from traditional sources (coal, oil, and gas). The initiative to lower carbon emissions from these sources using a surplus energy mix from different renewable energy sources is being led by utilities [1]. According to the latest report by Ref. [2], the capacity of Renewable Energy (RE) increased by 36 % on a worldwide scale in 2023, adding 473 GW to reach a total of 3870 GW at the end of the year, demonstrating notable expansion and advancement in the global integration of RESs. Over time, this upward tendency has persisted, with RE playing an important role in the global energy mix. Due to rapid developments in technology and favourable local Government rules, these RESs are economical and readily accessible [3]. This benefit facilitates the simplicity of maintaining the electrical infrastructure in remote and rural areas, besides reducing fossil fuel imports [4].

The large-scale integration of RESs in the electricity network replaces the conventional Synchronous Generator (SG). The government-funded and large-scale corporate RE projects with a 100 kW or higher capacity are called “large-scale renewable energy”. In conventional grids, SGs are grid-connected and in the event of power failure, their stored Kinetic Energy (KE) (referred to as ‘inertia’) is promptly utilised [5]. For instance, when there is an abrupt rise in the power demand or when a significant generator connected to the grid fails, it can cause the equipment within the grid to decelerate. Consequently, this can lead to a decrease in the grid’s frequency. Maintaining this frequency’s stability is paramount in contemporary power systems to function safely and reliably [6]. While RESs provide clean energy, among these various RESs, the high penetration of wind and Photovoltaic (PV) brings operational intricacies to the grid, such as instability in frequency and voltage. These two sources are coupled via a power electronics inverter, which eliminates their inertia, and therefore, their high integration reduces the overall inertia of the grid that could result in an increased rate of change of frequency (RoCoF) and triggering of load-shedding controllers [7].

Ireland was the first country globally to recognise elevated RoCoF rates as a potential problem in 2010, together with the power systems of

* Corresponding author.
E-mail address: J.ahmed@napier.ac.uk (J. Ahmed).

https://doi.org/10.1016/j.rser.2025.116324
Received 3 July 2025; Received in revised form 22 August 2025; Accepted 18 September 2025
Available online 30 September 2025

EirGrid and the System Operator of Northern Ireland (SONI). In July 2010, Hawaii witnessed a high RoCoF of 0.373 Hz/s and frequency nadir (f_{nadir}) of 57.7 Hz/s, necessitating modification to the power plant control parameters. The frequency nadir is a key indicator of power stability and resilience, which refers to the lowest point where the system frequency reaches after a disturbance before recovery begins. New Zealand's power system faced disturbance the following year when the Northern Island's frequency nadir was 47.5 Hz, and the RoCoF values reached 0.73 Hz/s. A similar event occurred on the island of Cyprus, where RoCoF values beyond relay thresholds (1.3 Hz/s vs 1.25 Hz/s) resulted in the shutdown of 68 MW of wind power [8]. In August 2019, the UK grid's frequency dropped to 49.1 Hz, which led to the disconnection of 350 MW of Distributed Generators (DGs), impacting around 1 million customers [1]. The primary duty of power system operators is to ensure the dependability and safety of the power supply.

On the other hand, these low-inertia systems can bring forth new provocations such as complicated frequency control mechanisms, fault-prone systems, and unstable voltages. These challenges are overcome by employing ancillary services called grid support services. A crucial element of this security is the equilibrium between load and generation; any discrepancy between the power produced by the generator and the electrical load can lead to a shift in frequency, which can impair the performance of the power system. Therefore, the frequency serves as a valuable measure of the level of harmony between generator and load [9].

1.1. ESS for frequency stability

Incorporating ESSs into integrated PV systems is a frequent or traditional way to minimise frequency variations. More inertia can be mimicked with the proper control for robustness and frequency stability. Several ESSs have been researched, including Battery Energy Storage System (BESS), Flywheel Energy Storage (FES), super capacitors, fuel cells, and Superconducting Magnetic Energy Storage (SMES). Fig. 1 displays the overall schematic diagram of the PV-BESS grid-connected system based on a virtual synchronous generator [10].

In [11], a summary of several methods for frequency regulation in PV plants and wind turbines with ESS support is provided. To mitigate the intermittent nature of PV power that affects the electrical grid's stability [12], presented a new algorithm in conjunction with a storage system for the Energy Management System (EMS) of a grid-connected PV system. An investigation into ESS's ability to enhance the frequency response in situations with high PV penetration was conducted by Ref. [13]. In Refs. [14,15], ESSs have been used to lessen voltage fluctuations in integrated PV systems. To reduce output power fluctuations, optimise power flow on the energy transmission side, adjust the frequency of the electrical grid, and analyse distributed and mobile energy storage systems on the distribution side [16], conducted an analysis of the significant state of BESS development and its application scenarios. A control strategy was put forth in Ref. [17] to control the voltages at the Point of Common Coupling (PCC) by ESS. The algorithm mostly used reactive power to regulate the voltage. A bi-directional converter was proposed in Ref. [18] to compensate for the sporadic nature of battery-powered PV arrays. To contribute to PFR/PFC, enhance the frequency dynamics, and support BESS long-term performance, a control strategy that combines adaptive control of statism and State of Charge (SOC) recovery was developed by Ref. [19]. The Multipurpose Control and Planning (MCP) method was developed by Ref. [11] to address the growing number of large-scale PV installations in distribution networks for BESS. For hybrid PV-ESS systems, the energy and power management controls have been covered in Refs. [20,21], and [22], respectively. Fig. 2 shows the configuration of a hybrid power system [1,20]. Despite variations in PV power, these controllers guarantee the nominal power supply to loads. An admittance-based control was proposed in Refs. [23,24] to enhance the power quality of a PV-diesel-battery hybrid system. This setting effectively eliminates harmonics in addition to load balancing.

Besides BESS, an FES spins a heavy rotor at high speeds to store energy and release the stored kinetic energy by slowing down the rotor. Using a small signal analysis and time domain simulations, a sample 50 MW FES plant model providing transient support for PFC was evaluated in the Argentinian Interconnected System (AIS) and Northern Chile Interconnected System (NCIS) [7]. A highly penetrated PV power islanded grid in Ref. [25] was investigated for frequency control utilising dual and Single Magnet SMES Systems (SMESS). Furthermore, it examines the transient states of a microgrid from grid-connected to islanded to demonstrate the usefulness of a dual magnet SMES system for frequency regulation in islanded mode. A novel multi-stage frequency control method was proposed in Ref. [26] to increase the SMESS's efficiency and lengthen its discharge period. Depending on the number of stages, the system's ability to support power-connected loads during a power outage can vary, offering the choice of an isolated or grid-connected Uninterruptible Power Supply (UPS). To boost the SMESS's capacity to mitigate Low Frequency Oscillations (LFOs) in power systems with high PV penetration, a Fractional-Order PID (FOPID) controller was developed in Ref. [27], with the PSO approach optimising the controller's parameters.

This overview reveals that various ESSs have been developed and tested, showcasing numerous benefits (rapid response, reliable, more stable solution) and their role towards frequency stability; however, they also present some disadvantages, such as high cost, frequent maintenance, and shorter lifespan. Nevertheless, BESS's cycle efficiency and life span are still developing and immature [1]. According to a study

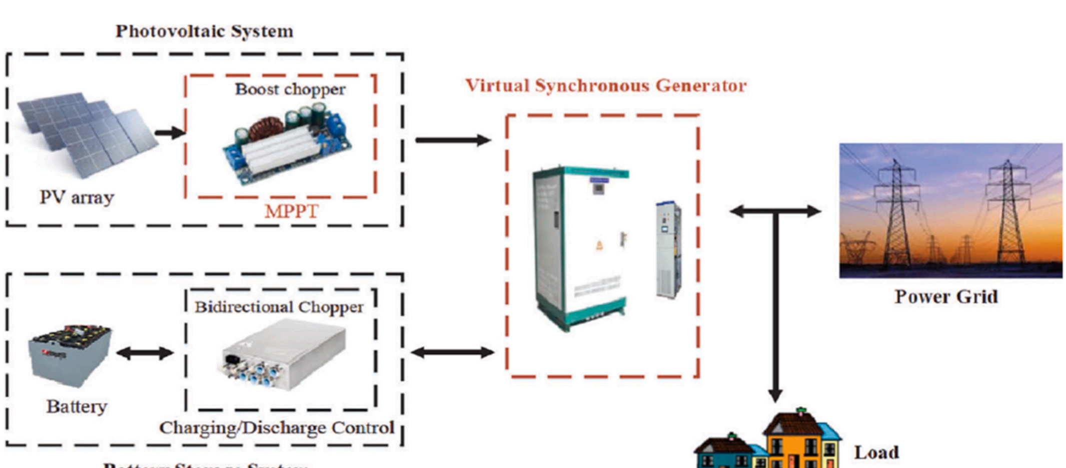

Fig. 1. Schematic of a PV-BESS System based on VSG.

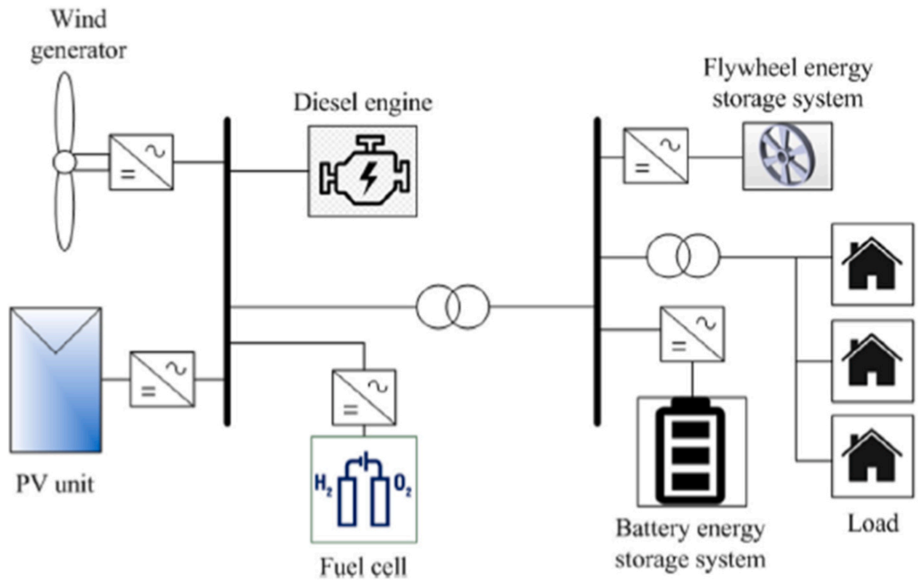

Fig. 2. Configuration of a hybrid power system.

in Ref. [28], BESS is not cost-effective, especially for large-scale power plants. Similarly, the authors of [29] address the detrimental effects (resource depletion, toxic waste, recycling, etc.) of BESS on the environment during construction and operation. The United Nations' SDGs 7 and 13 also focus on achieving net-zero greenhouse gas emissions by 2050, including supplying clean energy by 2030 [30]. However, achieving this target could be challenging if no proper measures are taken to reduce carbon emissions.

1.2. Effect of PV on power grids

Distribution grids used to function as passive components, allowing unidirectional power flow from the source substation to the end users. The integration of decentralised production influences power flows and voltages due to the influence of sources and loads. The connection of PV systems to the grid can substantially impact their functioning due to the technological peculiarities of photovoltaic installations [10].

The primary influence of PV systems on the power grids is as follows.

- *Regarding Voltage Quality:* PV generators affect the voltage plane and the grid's control devices. These effects can be summed up as an increase in power losses, reverse power flow, voltage rise, voltage imbalance, voltage fluctuations, and fluctuations in reactive power flow.
- *Regarding Power Quality:* The deviations in frequency, rising harmonics, shifting power factor, and occurrence of voltage sag all impact power quality.
- *Regarding Stability:* Systems with high PV penetration rates integrated into power systems significantly impact small signal, static, and dynamic voltage stability, which leads to disturbances in system stability.
- *Regarding the Protective System:* PV integration increases complicated fault detection and substantially impacts protection issues with increased fault current.

An extensive analysis of rooftop PV on distribution networks was done by Ref. [31], where the aforementioned impacts of PV systems are discussed in detail. PV systems are becoming increasingly prevalent in countries with high solar irradiance at the residential and utility scales due to their numerous advantages over other RESs. According to Ref. [32], the world's total cumulative installed PV capacity in 2023 was about 1.5 TW. PV systems are anticipated to grow steadily and become increasingly important in the global energy transition. A potential solution to the frequency instability issue is to emulate the inertial response of SGs through RESs, especially using PV systems and Energy Storage System (ESS).

1.3. Contributions and literary gaps

Therefore, to the best of the author's knowledge and based on the projections for PV systems and BESS, this review paper provides an in-depth exploration of PV systems' capability to provide frequency ancillary services. While briefly acknowledging the ESS-based techniques, its primary emphasis remains on storage-less solutions, providing a complete picture for the readers without diluting the core focus, serving as a comprehensive guide for researchers and engineers interested in the PV's intrinsic capabilities for grid stability.

Existing literature includes similar kinds of studies, with the majority of them focusing on the provision of frequency response services through battery energy storage systems [33–35]; likewise, a few of them have considered both PV and wind systems. A review on PV was done by Ref. [1], where BESS, hybrid, and without BESS methods have been reviewed, but no detailed overview of power reserve methods was provided. A good review focused on PV and methods with ESSs for frequency regulation was published by Ref. [3], but there is a lack of a detailed summary on power reserve techniques. Contrarily [36], focused on methods with power reserve (without BESS), but there was no overview of the optimisation algorithm used in PV power systems. Likewise [37], provided a good survey of grid support services, but it was devoid of comprehensive summary tables that might have highlighted the software and hardware tools utilised in the reviewed studies. A summary of the various optimisation techniques employed in the literature was also missing. A good overview of methods with and without ESS was presented by Ref. [7], but no detailed analysis of the literature was provided. Finally, another good review on frequency regulation methods with and without auxiliary devices was published by Ref. [5], but it is not particularly focused on PV systems. Besides, the comparison tables provided do not include other important parameters.

A comprehensive technical analysis of various battery-less PV frequency response techniques is provided in this paper, along with a meticulous review of each method. Therefore, the following methodology is employed to accomplish this goal.

- An extensive corpus of 51 recent research papers has been analysed, providing a clear understanding of operational principles, advantages/contributions/summary, and limitations of all techniques, with a summary table provided at the end of each technique section. These tables offer a highly organised and accessible overview, addressing the limitations of less comprehensive comparisons/summary tables in previous reviews and facilitating quick reference for researchers.
- A dedicated section of 26 diverse optimisation algorithms employed in this research domain with targeted objective functions, which also addresses a significant gap identified in prior reviews like [36,37], offering researchers insights into the computational tools and strategies used to enhance the performance of PV-based frequency response.

The remainder of the paper is structured as follows. SECTION II contains the foundations of power system dynamics and modelling; SECTION III represents the frequency control schemes in PV systems, SECTION IV contains recommendations and outlook, and SECTION IV comprises the conclusion.

2. Foundations of power system dynamics and modelling

2.1. Dynamic characteristics and frequency response

2.1.1. Power system inertia

In Physics, inertia is often defined as the ability of an object to stay unaltered in the absence of an external force, whether moving or stationary. SGs and turbines account for most of the inertia in the power system. The resistance to a change in the rotational speed is defined as inertia in a power system. The relationship between system inertia and power exchange is given in equation (1) [36].

$$H_{sys}.\frac{d\omega_e}{dt} = P_g - P_l \quad (1)$$

Here, H_{sys} is the inertial time constant, ω_e is the angular frequency, P_g is the generated power, and P_l is the load power.

When the load power increases, $P_g - P_l < 0$ becomes valid, and consequently, the power system encounters a shortage in power. In this case, the energy stored in the rotational masses of synchronous generators is injected into the system to counter the frequency deviation, reducing the generators' speed. On the other hand, if $P_g - P_l > 0$ becomes valid, meaning the load power decreases, then the direction of energy exchange is reversed. This exchange will increase the speed of the generators. The system's damping ability and sensitivity to abrupt changes in load are directly correlated with its level of inertia.

Moreover, to investigate the impact of system inertia on f_{nadir}, RoCoF and power system dynamics [1], created a small-signal model. Each machine ran at a step load change of 0.02 p.u., while maintaining a steady 50 Hz synchronous speed at t = 2 s. The results are shown in Fig. 3, which shows the increase in RoCoF and the decrease in f_{nadir} as inertia reduces. Conversely, since governor droop is the only mechanism causing the steady-state frequency variation, inertia does not affect it.

2.1.2. Frequency response in conventional systems

When a frequency disturbance occurs in the power grid, it is restored in different stages, and therefore, it is crucial to comprehend these stages. Primary, secondary, or Automatic Generation Control (AGC), Load Frequency Control (LFC), and tertiary controls are responsible for frequency regulation in a power system. Primary Frequency Control (PFC)/Primary Frequency Regulation (PFR) consists of two subparts: inertial response and governor response. Fig. 4 represents the frequency response of a typical power system, where f_o is the nominal frequency, and Δf is the permitted frequency limit, which varies depending on the system operator and region to region.

The contingency begins to occur when the system is perturbed at point A, reducing frequency until point B, also known as the frequency nadir (f_{nadir}). An inverse relationship between the inertia constant and the curve's slope connecting points A and B represents the RoCoF. In contingency, the PFC triggers an inertial and governor response for 20–30 s. At point C, the secondary control comes into action, which is the state attained after governor control action and lasts for 5–10 min. The tertiary control is the last stage, lasting more than 30 min and bringing the frequency to its nominal value. Equation (2) makes it abundantly evident that inertia significantly affects the initial RoCoF and f_{nadir}. These two are the most significant parameters during frequency contingency [1].

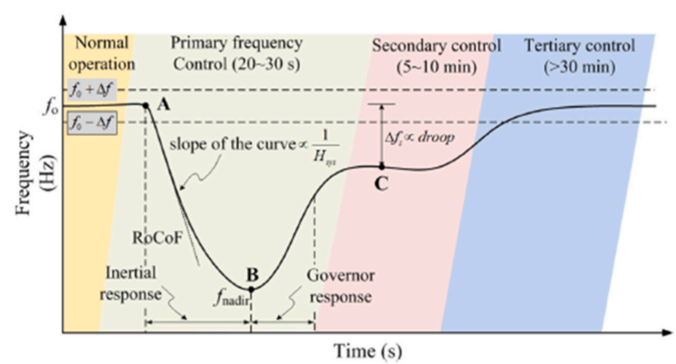

Fig. 4. Graphical Representation of the system's frequency response and the period involved [1].

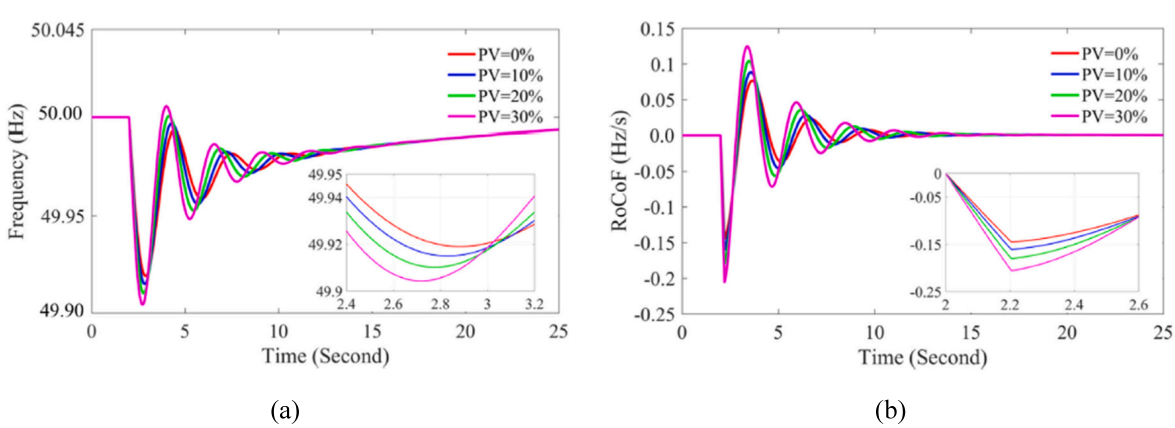

Fig. 3. Influence of inertia on f_{nadir} and RoCoF for step load change at different PV penetration levels: (a) Frequency response of power system, (b) RoCoF response of power system.

$$\frac{d\Delta f}{dt} = \frac{\Delta P_m - \Delta P_e}{2H} \tag{2}$$

Where Δf is the change in system frequency, ΔP_m and ΔP_e are a change in mechanical and electrical power per unit, respectively, and H is the inertia constant of the system, which is proportional to the stored rotational kinetic energy.

This multi-stage sequential nature of traditional frequency control, especially since it can take 30 min to hours for tertiary control to restore the frequency completely. This protracted response constitutes a significant limitation in modern grids demanding enhanced agility and resilience. Developing grid-connected power electronics inverters offers a revolutionary solution, particularly in PV and wind systems. By leveraging the rapid controllability of these inverters, Virtual Inertia (VI) is emulated, thereby addressing a significant drawback of conventional frequency controllers.

2.2. Power system modelling and configuration

Before delving into the frequency control methods, this section will give a general overview of the power system modelling and how solar PV systems are connected or integrated with the grid.

The three stages of the power system are generation, transmission, and distribution. A detailed analysis of the power system modelling was conducted by Refs. [38,39], where the former provided an extensive analysis of supply-side and power system modelling for frequency stability, and the latter presented a comprehensive review on AGC of interconnected power systems integrated with conventional, renewable, and sustainable energy sources. The different areas of power systems including single-area, two-area, three area and nth area. A geographical location with several power plants operating concurrently is referred to as an "area, " indicating that every generator in that area is linked together and operates at the same frequency, comprehending the behaviour of large-scale power systems, creating advanced control schemes, and analysing power system dynamics depend on understanding multi-area power systems. A detailed analysis of AGC of these multiple area systems, microgrids, smart grids, restructured power systems, and renewable energy sources was provided in Ref. [39].

2.2.1. Conventional system models for frequency analysis

Generally, an equivalent power system model can be represented by considering the swing equation, which summarises all SGs into an equivalent rotating mass with an equivalent inertia constant, denoted as H_{eq}, which can be calculated by (3).

$$H_{eq} = \frac{\sum_{i=1}^{SG} H_i \,.P_{r,i}}{P_r} \tag{3}$$

Where the inertia constant and rated power of the SG (i) are denoted by H_i and $P_{r,i}$, respectively. The total number of SGs linked to the grid is represented by SG, and the rated power of the power system is represented by P_r. Accordingly, the power system's swing equation can be expressed as (4) [38].

$$\Delta f = \frac{1}{(2.H_{eq})\ .\ s + D} . (\Delta P_g - \Delta P_L) \tag{4}$$

where, H_{eq} [s] is the equivalent inertia of the grid, and D [W/Hz] is the damping factor, which depicts how a load power changes with frequency, even though a power system has more damping elements such as excitation system, speed governing, etc [40]. According to Ref. [38], several authors substitute M[s] for $2.H_{eq}$, whereas some studies suggest and employ the following expression (5).

$$\Delta f = \frac{K_P}{T_P\ .\ s + 1} . (\Delta P_g - \Delta P_L) \tag{5}$$

Being $K_P = \frac{1}{D}\left[\frac{Hz}{W}\right]$ and $T_P = 2.\frac{H_{eq}}{D}\ [W^{-1}]$. Because both H_{eq} and D lessen the effect of power changes in frequency, regardless of the equation applied, they are essential variables for the stability of the power system [41]. The chronologically arranged, summarised values for H_{eq} and D from literature, as well as the H_{eq} values of the studies where $H_{eq} = M/2$, and values of K_P and T_P have been reported in Ref. [38]. Which states that the parameters considered to simulate the equivalent power system model varied significantly, and this has a significant impact on the related frequency fluctuations in terms of both f_{nadir} and RoCoF. In each research study, many synchronous power plants linked to the grid contribute to a pertinent variability in the equivalent power system inertia values that could be attributed to the significant variations in power plant inertia constants, primarily based on type and rated power. Moreover, literature presents a wide range of damping factor values, and a precise estimation of the damping factor is essential for power system stability analysis under disturbances, given its substantial influence on the results. Significantly, frequency control is sensitive to damping factor variations. The development of virtual damping and inertia strategies based on small-signal stability is currently a research focus.

2.2.2. PV system modelling

PV power stations typically consist of several arrays of PV cells linked to the grid via an inverter and an optional DC-DC converter. Models of PV cells have long been used to describe the behaviour of PV cells. The single-diode five-parameter model is the most widely used PV cell model [42,43]. Fig. 5 shows a circuit diagram of a single-diode model.

The figure includes a current source, which depends on solar irradiance and cell temperature, a diode in which the inverse saturation current depends on the operating temperature, a series resistor, and a shunt resistor, considering the resistive load. It can be mathematically expressed as (6) [42];

$$I_{pv} = I_L - I_o\left[exp\left(\frac{V + IR_S}{V_t}\right) - 1\right] - \frac{V + IR_S}{R_{sh}} \tag{6}$$

Where, I_L is the photocurrent, I_o is the diode saturation current, R_S is the series resistance, R_{sh} is the shunt resistance and V_t is the thermal voltage.

As reported by Ref. [38], few studies have restructured equation (6) for a PV module and represented it as equation (7).

$$I_{pv} = N_p\ .\ I_{ph} - N_p\ .\ I_{rs}\left(e^{\frac{q.V_{mpp}}{k.T.A.N_s}} - 1\right) \tag{7}$$

Where, N_p and N_s are no. of cells in parallel and series, respectively, A is the ideality factor, V_{mpp} is the voltage at the maximum power point, I_{ph} is the short-circuit current for a single PV panel string. Many research studies analyse the frequency stability of the power system by modelling the PV system just using a first-order transfer function, which ignores any dynamic behaviour (non-linearities of P-V and I-V curves) of the PV power conversion systems, as shown in Fig. 6 [38].

The cell temperature, incident solar irradiance, and their reference values are the three factors that affect the five parameters of the PV model. PV module manufacturers typically supply these reference values

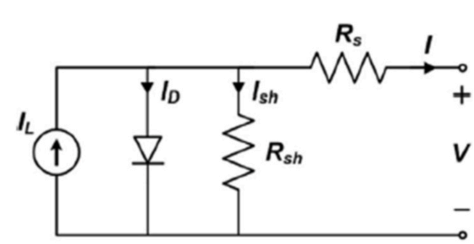

Fig. 5. A single-diode model of PV cell [42].

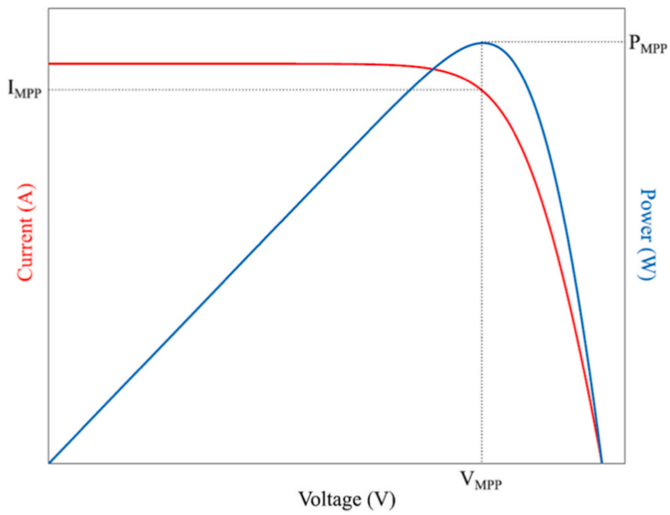

Fig. 6. P-V and I-V curves of a PV module.

under specific working conditions, such as Standard Test Conditions (STC), where the cell temperature is 25 °C and irradiance is 1000 W/m^2. The STC and operating conditions are never the same, and mismatch factors may also impact the fundamental values of these mean parameters. The manufacturer's reference parameters are not accurate at STC. Therefore, a methodology to ascertain reference values for the five model parameters utilising outdoor data collection and mathematical analysis has been proposed by Ref. [43]. These benchmarks are then employed to evaluate the parameters in the context of actual irradiance and temperature experienced by the PV module.

2.2.3. Grid-integrated PV configuration

Using a power electronics converter to integrate a solar PV system with a utility grid, Fig. 7 shows the general layout of the grid-connected PV system, highlighting the controller functions. This structure consists of a PV array, an optional DC/DC Boost converter, a DC/AC inverter (VSI), an LC or any other type of filter, an isolation transformer, and a power grid. Power conversion from the PV array to the grid occurs in two steps. Two controllers, one on the PV side (DC side controller) and the other on the grid side (AC side controller), perform various ancillary functions while supplying real power to the grid [44]. The photoelectric effect of the PV array converts sunlight into low-voltage DC power. This power is transferred to the DC/DC converter via boost circuit control to generate stable high-voltage DC power. The MPPT control strategy is then implemented to guarantee the maximum output from PV. Different MPPT algorithms are available, like hill climbing [45], P&O [46], incremental conductance [47], and parabolic prediction-based MPPT [48], etc. The grid-connected inverter transforms the DC power into AC power, which satisfies grid-connected requirements and feeds the AC power into the electrical grid at the same frequency and phase [49].

The parameters of the grid-connected PV system can be found in Ref. [50]. The system's configuration and size depend on its intended application. Residential PV systems typically have a capacity of less than 20 kW, while commercial systems range from 20 kW to 1 MW, and utility-scale systems are greater than 1 MW. The power handling capacity of the PV systems varies based on their architecture. Importantly, real-world arrays are typically formed by connecting multiple solar panels in series and parallel connections. Inverters play a crucial role, and they are configured in several ways. The specific combination depends on how the solar arrays are connected to the inverter. Some typical configurations are shown in Fig. 8 and include a central inverter, string inverter, multi-string inverter, micro inverter, and DC module. Several factors, including power rating, voltage level, size, sustainability, cost, and reliability, determine a specific configuration for a given plant.

Comprehending inverter control and grid architecture is required to offer supplementary services for frequency control. Hence, a detailed analysis of these inverter configurations and their controller systems can be found in Ref. [44].

3. Frequency control methods for PV systems

This section gives a hierarchical structure and an overview of frequency control methods employed by PV systems to support grid

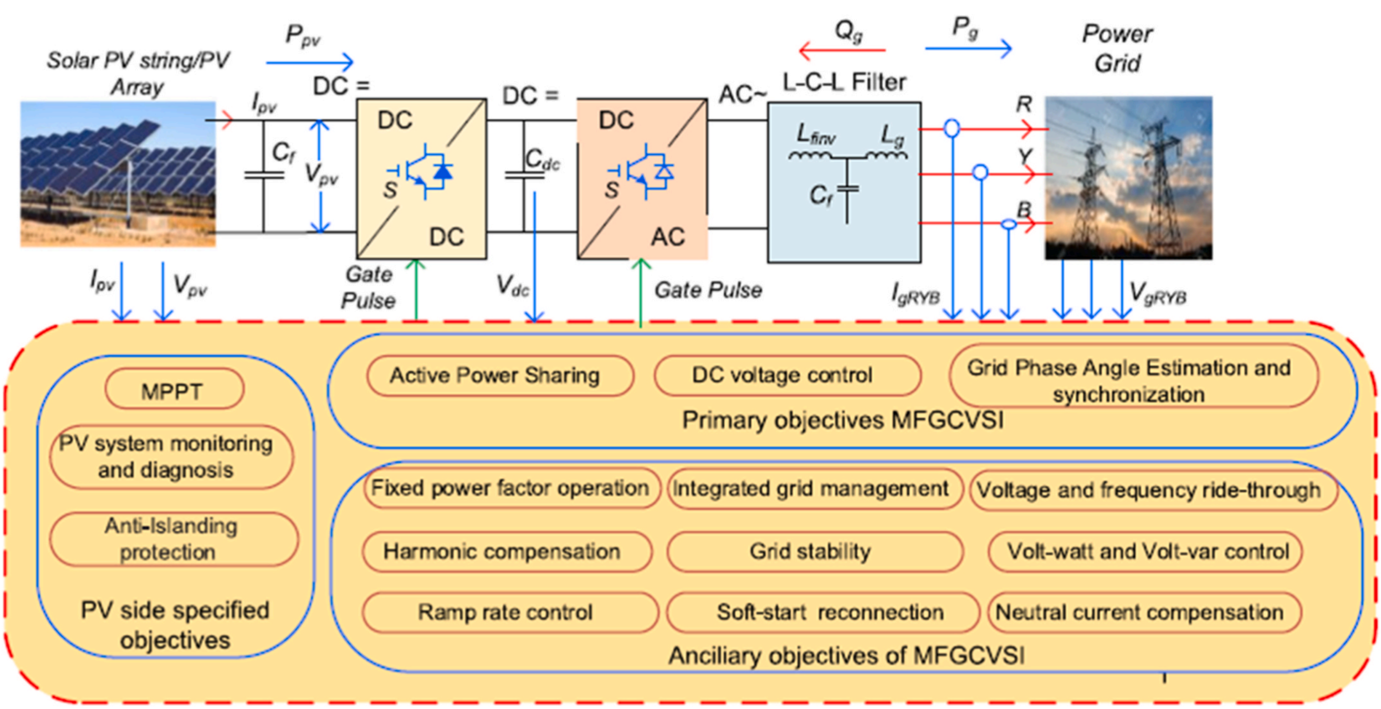

Fig. 7. A general structure of grid-connected PV system with controller functions [44].

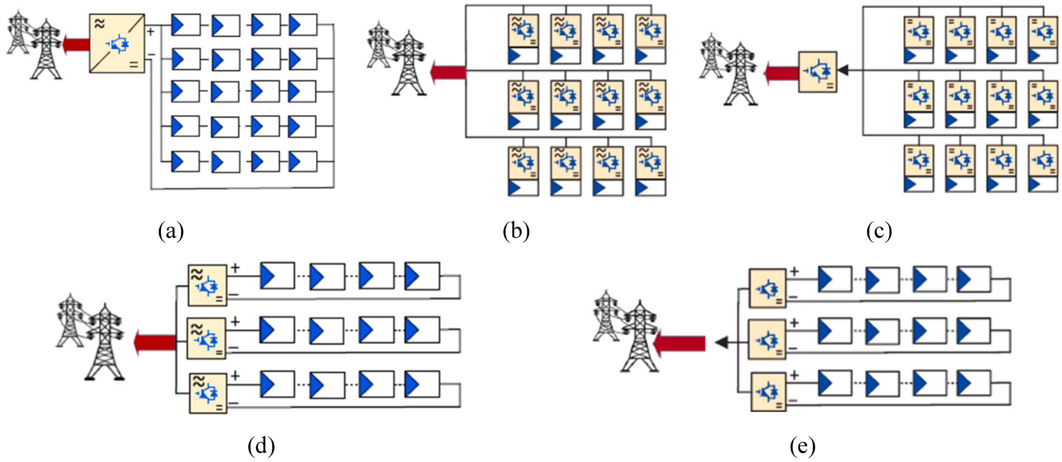

Fig. 8. Solar PV Inverter Configurations (a) Central, (b) Micro Inverter, (c) DC Module, (d) String, (e) multi-string.

stability. Generally, the methods used to provide frequency response for renewable energy systems without energy storage devices (particularly PV) are called Active Power Control (APC) methods. The primary goal of these methods is to control the active power of PV to make a power reserve that may be utilised later to provide frequency control. These have been used interchangeably in the literature, such as Power Reserve Control (PRC), an umbrella term encompassing de-loading, curtailment, and delta power control. However, some key differences have been discussed in the following sections. Fig. 9 shows the control areas of different active power control schemes for grid-connected PV systems, where area 1 indicates the regular MPPT operation. After implementing a PRC method, the power reserve has been generated in area 2, followed by the power ramp rate control and constant power generation in areas 3 and 4, respectively. The sequence concludes with a return to regular MPPT operation despite the lack of inertia in the solar PV system to sustain frequency regulation; these control techniques can enhance the frequency response. The basic concept is to provide the VI by controlling the output of PV systems or inverters. By adjusting the PV system's output power, the control system can mimic the inertial response of conventional SGs and detect frequency deviations in the grid [7].

The following techniques are used for frequency stabilisation of grid-connected solar PV systems.

- DC-Link Capacitor
- Power Ramp Rate Control (PRRC)
- Constant Power Generation Control (CPGC)
- Delta Power Control (DPC)
- PV Curtailment Control
- De-loading
- Soft Computing Techniques

The subsequent sections provide a critical review of each listed technique, including relevant research studies from the literature and a comprehensive summary table comparing their characteristics at the end of each section. This methodical approach provides readers with a concise and easily comprehensible summary, assisting them in making well-informed decisions and directing future research by pointing out gaps, limitations, and promising directions in the literature. Fig. 10 shows how reviewed papers are categorised according to their control methods.

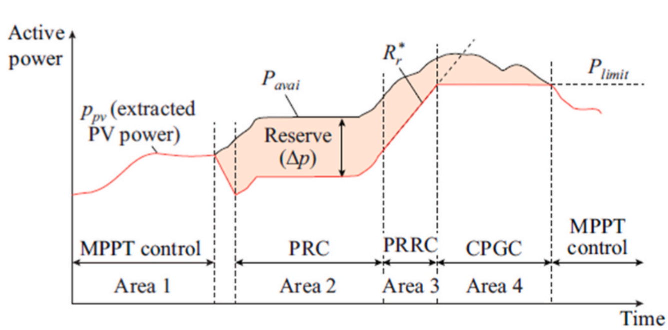

Fig. 9. Different APC schemes for grid-connected PV systems [51].

3.1. DC-link capacitor

The Grid-Connected Converters/Inverters (GCC) can simulate the VI through the DC link capacitor, eliminating the detrimental effects of inertia emulation on the energy efficiency of autonomous grids. This technique can offer primary frequency support during a disturbance by emulating inertia using the stored electromagnetic energy in the DC link capacitor [52]. To improve the transient control performance of an autonomous RE microgrid [53], proposed a VI-based control strategy employing DC-link adjustments by charging and discharging over a predetermined range for damping slight frequency oscillations and PV generation adjustments to accommodate remaining demand for inertia emulation. They integrated the proposed strategy with a gradient-based distributed coordination algorithm and tested the strategy on 6-bus renewable microgrid and it can be extended to other renewable energy generators with DC-link. Their system was stable despite a considerable power setting update time of 0.3s. On the other hand, a 5 % load change resulted in maximum frequency deviation of 0.08 Hz which was further improved to 0.01 Hz in islanding mode with the aid of inertia emulation through integrating their proposed solution with previously developed distributed gradient-based coordination algorithm. The DC-link capacitance (C_{dc}) (electromagnetic energy) of the grid-connected inverter system was utilised by Ref. [54] to simulate the inertial response and was selected by tuning the damping ratio (ζ) within its optimal range of 0.40–0.80. The block diagram of the simulated power system incorporating VI control with a DC-link is shown in Fig. 11.They analysed how C_{dc} can affect the dynamic performance of GCC providing virtual inertia and also the impact of the PV converter system on frequency deviation and RoCoF was examined using a small-signal model of VI produced from the grid-connected inverter's DC-link capacitance. The DC-link emulated inertial response is expressed by (8),

$$\Delta P_{DC} = \frac{C_{dc} V_{dc_{ref}}^2}{VA_{rated}} \frac{dV_{dc}}{dt} = 2H_c \frac{dV_{dc}}{dt} \tag{8}$$

Where C_{dc} is the capacitance of the DC-link, V_{dc} is the DC-link voltage, $V_{dc_{ref}}$ is the reference voltage for the DC-link, VA_{rated} is the inverter

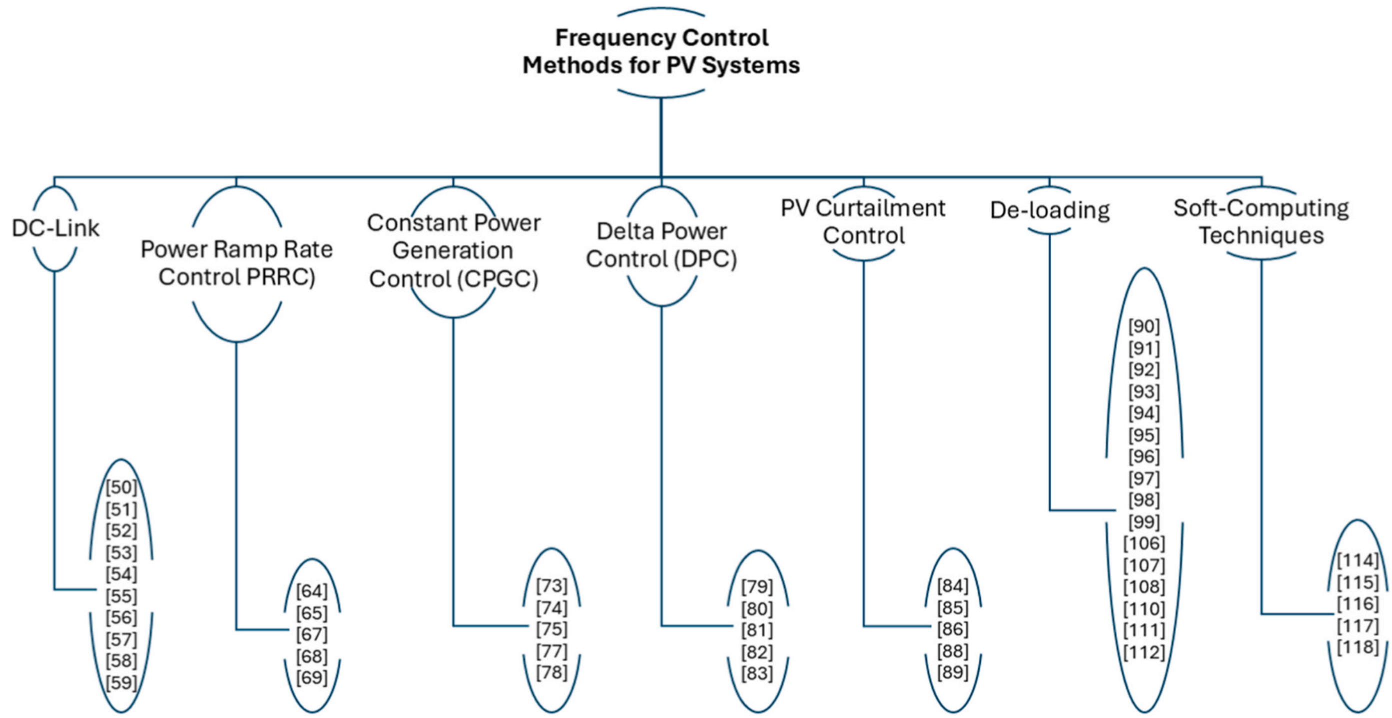

Fig. 10. Categorisation of reviewed papers based on PV control methodology.

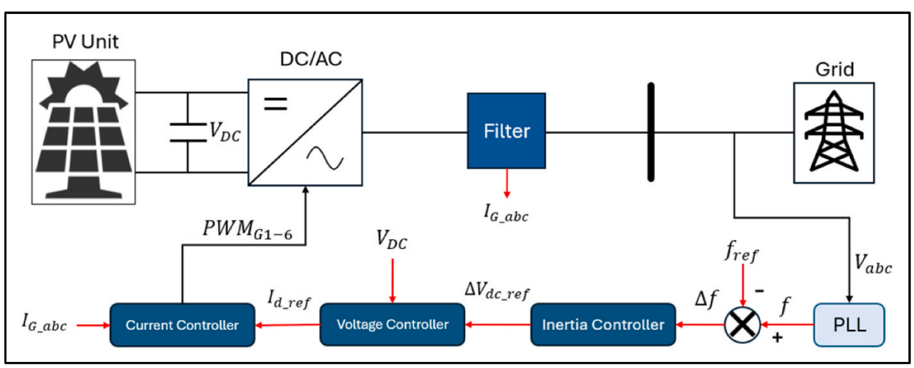

Fig. 11. Block Diagram of Power System Incorporating Inertia Control with DC-link capacitor.

system's rated power, and H_c is the emulated inertia or the inertia constant of the DC-link capacitor.

They used the swing equation to describe the dynamics of a synchronous generator, and after taking extra power from GCC, the inertia constant H of the power system increases to $H + H_{vi}$ and represented by (9),

$$\Delta P_M - \Delta P_D - \Delta P_L = 2(H + H_{vi})\frac{d\Delta f}{dt} \tag{9}$$

Where Δf is the frequency deviation, ΔP_M, ΔP_D and ΔP_L are changes in mechanical, demand, and load power per unit.

It was concluded that size of C_{dc} can directly affect the settling time. As a result, a balance VI support and settling time was achieved with C_{dc} of 2.7 mF resulting in 20s of settling time but the corresponding damping was not clearly mentioned. Conversely, they stated if $C_{dc} = 2.9$ mF and $\zeta = 0.40$, a satisfactory dynamic response was observed based on the given parameters. These values may not be suitable for a system with a different parameter values.

By focusing on the DC-side component of large-scale PV plants and from an electromechanical (EM) oscillations perspective [55], proposed an Active Power Modulation (APM) technique which utilised the energy stored in the DC-link of large-scale PV inverters. The stored energy in the DC-link of PV inverters was effectively utilised to improve the damping of EM oscillations by detecting and reflecting them to the DC-link voltage. Their Peak-to-Peak Power Oscillation (PPPO) analysis as a function of V_{dc} and oscillatory component ratio (λ) with $V_{dc} = 1500$ V and $V_{dc} = 1000$V revealed that the PPPO of the DC-link is more sensitive to λ at high voltage levels. The high voltage levels have voltage fluctuations that can cause power oscillations in the DC-link. They claimed that the proposed technique can enhance the damping ratios of interarea electromechanical modes and improve the power system's overall small-signal stability. The suitability of their proposed controller was verified with interarea EM modes damping, where it was observed that increasing proportional gain can enhance the system's small-signal stability.A saturation term with ±300 V was incorporated to prevent the DC-link voltage from large amplitude fluctuations, limiting the technique's contribution to the system's stability enhancement after severe faults. Case study 1 (two-area four machine system) with 3 EM modes at 0.93 Hz, 0.97 Hz, 0.43 Hz and 0.191, 0.081, 0.033 damping ratios with 5.3 % PV penetration reveals that mode 1 with 0.191 at 0.93 Hz is more robust to the change in load from 0 to 150 MW. While the case study with the IEEE 39-bus system revealed that the Mode 9 tuned with the pole-placement method stabilises the system simulated with a 5 MW load increase, but the damping ratio of this mode is not explicitly defined.

On the other hand, considering the high RESs penetration from a two-area interconnected power system [56], proposed a High Voltage Direct Current (HVDC) link-based Virtual Inertial Control (VIC) frequency control strategy along with a Virtual Synchronous Generator (VSG) scheme, which improves the dynamic frequency performance of future power systems. Their proposed VIC 1 presents a virtual rotor, and VIC 2 presents a virtual router and frequency control loops, enhancing stability. Their proposed VSG emulates the characteristics of real SGs. Particle Swarm Optimisation (PSO) was used to tune the parameters of their proposed VSG optimally. The max. overshoot of VIC 1 was 0.099 p.u and 0.113 p.u for Area 1 and Area 2 respectively, while VIC 2 had 0.090 p.u in Area 1 and 0.087 p.u in Area 2. On the other hand, the max. undershoot for VIC 1 was 0.042 p.u and 0.014 p.u for Area 1 and Area 2, respectively, while VIC 2 had 0.035 p.u and 0.013 p.u. This shows that the proposed VIC 2 had superior performance with 16s (Area 1) and 15s (Area 2) of T_s when compared to conventional and proposed VIC 1. Moreover [57], outlined the process for simulating the inertia response from DC-link capacitors in PV power converter systems. Simulation studies were used to quantify the impact of VI on the system security. The capacitor voltage was adjusted in response to system frequency changes to reduce the strain on other conventional units and prevent potential outages. The outcomes show that the suggested strategy improves the frequency deviation of 49.86 Hz (12.5 % deviation) and RoCoF of 0.075 Hz/s (50 % improvement). The tripping limit of 1 Hz/s for protection relays safeguard the power system from large disturbances. The min. DC-link voltage deviation was 376 V and which stabilised around 22 s at 387 V. Despite to their benefits like high efficiency and long cycle life, their application is restricted due to the high cost and low energy density, which prevents them from maintaining output for extended periods of time.

A dual-mode fast frequency control for a 9.15 kW PV with 10 kW of VSG acting as a power grid was presented by Ref. [58] to overcome the challenges of efficient coordination of power reserve between the PV panel and DC-link, as well as the restoration of voltage after inertia provision. The first mode was called Virtual Inertia Mode (VIM), where the DC-link capacitor and PV provide VI, while in Frequency Damping Mode (FDM), PV provides damping, whereas the DC-link was charged for voltage restoration after a frequency nadir event. According to the case study, the proposed technique increases the PV's grid-support capability by effectively utilising the grid-support resources. The DC-link voltage change rate is necessary to deal with the cascaded frequency events, as the restoration time depends on the capacitor charging power (P_{ch}), if P_{ch} is small, the restoration will take time, while if it is large, the PV power will suddenly reduce. Therefore, a 10 % PV reserve for P_{ch} is being used. The diagram of their entire coordinated control system is shown in Fig. 12. Within the 300 ms, the maximum RoCoF with proposed FFC was −0.738 Hz/s when compared to fixed inertia (−0.795 Hz/s), fixed inertia & damping control (−0.808 Hz/s) and fixed damping control (−0.868 Hz/s). In total a maximum of 15 % improvement was made for RoCoF reduction. The f_{nadir} for the proposed method was 49.47 Hz with steady-state frequency deviation of 49.68 Hz.

Likewise, to replicate the inertia for Inverter Interfaced Distributed Generation (IIDG), full state feedback via a robust Linear Quadratic Regulator (LQR) was used by Ref. [59] to find the optimal inertia and damping coefficients. These coefficients are used to assess how much more power a VSG needs to provide inertia emulation. Additionally, to improve the performance index in LQR, a Bacterial Foraging Optimisation (BFO) algorithm was proposed to select optimal parameters (weights Q and R) in the problem search space. The BFOA tuned VSG has max. undershoot of 0.13 Hz with RoCoF of 0.15 Hz/s, on the other hand, the max. overshoot was 0.138 Hz with RoCoF at 0.35 Hz/s when a 50 kW of step change in load was applied. The max. RoCoF was limited to ± 2 Hz/s and maximum frequency deviation of ± 2 Hz. More penetration of the IIDG is possible with the proposed method, as it improves the VI dynamics and quickly restores the frequency to the nominal value. To explore the concept of Distributed Virtual Inertia (DVI) [60], a new control technique was proposed for a 3.5 kW two-stage PV system by considering the DC bus capacitors that can act as energy buffers to mimic mechanical inertia in traditional power systems. A deadband of ± 0.01 Hz helps to prevent the need for a frequency controller during steady-state significant frequency variations. The frequency stabilised at its nominal value of 50 Hz in 8 s. The droop control damping effect causes the frequency to stabilise more quickly than in the initial istance, and it has the best frequency nadir above 49 Hz.

On the other hand, the Super Capacitors (SC), also known as Electric Double Layer Capacitor (ELDC) or ultra-capacitors, have also been used to provide frequency services due to their high-power densities, burst power handling capability, fast response, and longer life cycle. In light of this, the authors of [61] presented a novel PV-SC Cascaded Topology (PSCT), which integrates a low-voltage SC operating as a voltage source with a high-voltage grid-connected PV system as an economical way to simulate Synthetic Inertia (SI). To simulate dynamic inertia and enable a broader range of RoCoF to be serviced with limited storage capacity, the goal was to cover PFR and Synthetic Inertial Response (SIR) using the proposed Droop-Inspired (DI) method with an adjustable inertia constant. Similarly [62], introduced a Fuzzy Logic-Based Emulated Inertia Controller (FL-EIC) for an inverter connected to the formed SC based Inertia Emulator (IE-SC). The controller used the RoCoF and frequency deviation to determine the necessary inertial power. The FL-EIC accomplishes inertia emulation by proportionally connecting the grid

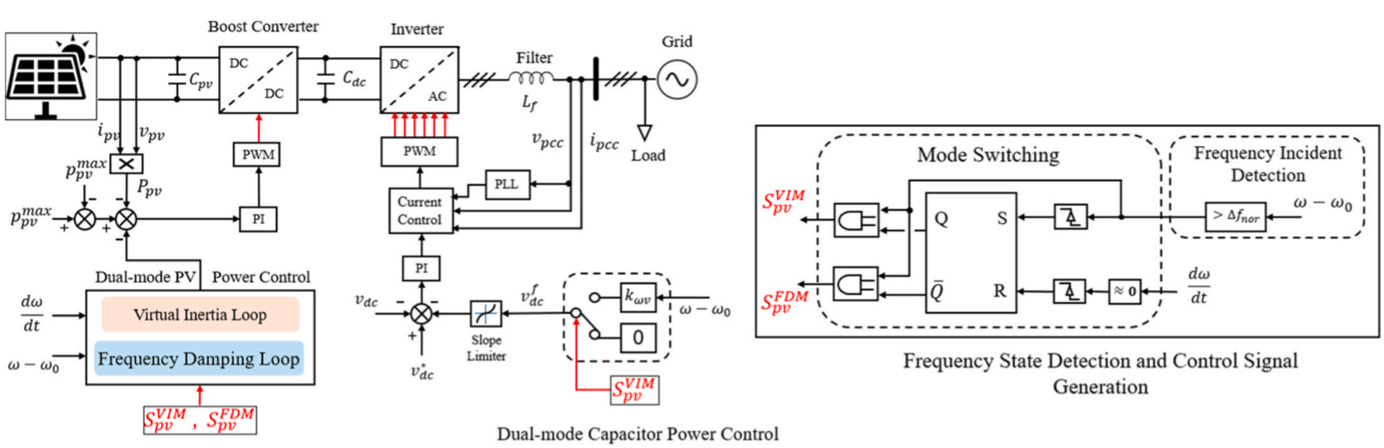

Fig. 12. Coordinated control of dual-mode FFC.

frequency's time derivative and frequency deviation to the IE-SC's active power reference. In contrast to traditional EIC, the proposed method restricted the f_{nadir} during under frequencies events at 49.85 Hz. With a step decrease, power oscillations were dampened in rapid load shifting, and the frequency overshoot was restricted to 50.176 Hz. On the other hand, the f_{nadir} was halted at 49.71 Hz during the irradiance drop.

In summary (Table 1), the reviewed studies indicate that DC-link-based inertial emulation is a viable strategy for improving PV systems' capacity for frequency response and can provide inertia support during contingencies by using the stored energy in the DC-link. These methods have fast response and higher efficiency, which is a crucial element in frequency regulation; however, their application is restricted to their high cost and low energy density, which prevents them from maintaining output over extended periods and is best suited for high-speed frequency events. Some works [53,58] have used the combination of DC-link with PV de-loading, which can complicate the control system, while some have considered the hybrid approach [63,64] with ESS for frequency control that can result in higher costs.

3.2. Power ramp rate control (PRRC)

In active power control, PRRC is presented to eliminate voltage/power fluctuations that can create frequency deviations. The fundamental idea is that because of the fluctuating irradiance, the output power that increases with PPRC cannot exceed a specific ramp-rate limit. Extensive geographical dispersal of PV systems is thought to mitigate these variations [65]; however, in Ref. [66], it was shown that a 1.6 MW PV system might exhibit output power swings that surpass 50 % of its rated capacity in less than 10 s. Therefore, the Transmission System Operators (TSOs) from small to large-scale power systems have started to demand PRRC capabilities from PV generators. Table 2 lists the power ramp rate limitations for various standards and grid codes [67,68].

Typically, PRRC mode is triggered, and the actual power ramp rate (RR_{pv}) is regulated to the intended limit when RR_{pv} exceeds the desired ramp rate (RR_{res}). If not, continuous activation of the MPPT mode is permitted for optimal power extraction. The mathematical expression for the change between modes is given by equation (10).

$$RR_{pv} = \begin{cases} RR_{pv}, \quad RR_{pv} \leq RR_{des}, MPPT\ Mode \\ RR_{des}, RR_{pv} > RR_{des}, PRRC\ Mode \end{cases} \tag{10}$$

The power ramp rate is given by equation (11),

$$RR_{pv} = \frac{dP_{pv}}{dt} \tag{11}$$

Where, dP_{pv} refers to the difference in the sampled power, and dt is the difference to the sampling interval [69]. Notably, the effectiveness of the PRRC can also be impacted by the ramp rate measuring windows (dt). The primary reason for this is the MPP searching (e.g., P&O MPPT algorithm), which typically causes the operating point to wobble in steady state. As a result, even with constant solar irradiance, the measured ramp rate of the PV power will not be zero [50]. Fig. 13 illustrates PRRC on the P-V curve. The controller uses MPPT operating mode and takes the maximum power from the PV array when the power ramp rate falls below the permitted level (R_{lim}) is shown by path A to B. Besides, reducing power should be the first step in lowering the ramp rate if it is over the limit. Consequently, as shown in the figure, the operational path is from point B to point C (left of MPP) or point D (right of MPP).

To perform PRRC, it is evident that the PV power ramp rate needs to be measured first. Therefore, different PRRC algorithms were classified by Ref. [51] as constant ramp rate control (PRRC 1), static and dynamic PRRC (PRC 2 & 3). PRRC 1 is a basic algorithm to control high power ramp rates, where only the MPPT algorithm is modified instead of the controller attached to the PV string. This algorithm needs a forecasting technique to regulate the power ramp-down rate; otherwise, the system must typically run at a sub-optimal operating point other than MPP.

On the other hand, PV systems unconditionally reduce ramp rate with PRRC 2, and no ramp rate constraints are considered. Its drawback is solved with PRRC 3, which does not consider the length of a temporary condition. The ramp rate limits and power oscillations have been considered in this procedure. However, it has slowed the dynamic response. A detailed analysis can be found in Ref. [51] with a comparison table and flowcharts of these PRRC algorithms.

The ESS is typically utilised to smooth out fluctuations and implement PRRC. It is classified into two types: gradient and filter-based methods. However, these methods are complex, data-dependent, ESS-intensive, and susceptible to irradiance changes [3]. A Ground-based Sensor Forecasting System (GBSFS) based PRRC method by developing a dynamic spatio-temporal ramp (DSTR) was proposed in Ref. [70] and has the potential to eliminate the need for ESS. They named it forecasting-based active power curtailment (FAPC), which included the power ramp rate control limits. Fig. 14 illustrates the basic idea of the FAPC approach, where P_{pv1} and P_{pv2} are available powers at high and low irradiance respectively. The GBSFS effectively identifies 95.8 % of ramps over the course of a year, with an annual nMAE of 6.2 %. These outcomes confirm the efficacy of the suggested DSTP predictions and guarantee the operation of the subsequent PRRC methods. The FAPC is a cost-effective option as it reduces power before solar irradiance drops significantly and requires either less or no ESS.

Nevertheless, the reduced energy loss in PV systems causes the self-consumption to decrease without storage. The advantages of lower equipment expenses could occasionally be outweighed by the financial losses brought on by a power outage [3]. Besides, a Flexible Power Point Tracking (FPPT) based ramp rate control was proposed by Ref. [71], which handled both ramp-up and ramp-down events by shifting the operating point away from MPP and operating around an optimal point provided by the operator. The three simulated cases with different ramp rate limits (3 W/s, 2 W/s, and 3 W/s) and ramp-rate changes in irradiance (6 W/s, 6 W/s, and 3 W/s) have shown the good performance in managing both ramp-up and down rates. The results have also been verified by experimental results which confirms the ramp-rate regulation below 3 W/s. The proposed method has some challenges under rapid weather conditions. Additionally, the shading scenarios were not considered. Furthermore, to obtain the fast dynamics [68], proposed an adaptive FPPT-based PRRC strategy. To identify abrupt irradiance changes and quickly determine the power ramp rate, the proposed algorithm does an extra measurement amid each computing step at $(m-0.5)T$, which aids in differentiating PV power fluctuations caused by voltage perturbations and irradiance variations. Due to fast irradiance change detection, the proposed method was able to maintain the ramp-up rates, but it has a limitation in maintaining the ramp-down rate. A storage-less and sensor-less PRRC approach for grid-connected PV was presented by Ref. [67], where the PV power was a controllable parameter rather than voltage. The novelty lies in the control of PV power for PRRC application. A curve-fitting algorithm was used for the MPP estimation, which resulted in adequate power ramp-rate limit tracking. The comparison of their technique with another technique available in the literature through simulation and hardware-in-loop simulation validates its performance.

Moreover, a few research studies [72–74] have proposed ESS-based PRRC techniques and validated their performances. The issue with this approach is the increased overall cost and the control complexity. A ramp-rate control of PV-battery system incorporating the control of time-varying loads was presented by Ref. [72], where the regulation strategy considers the power consumed by the loads, thus mitigating the overall ramp-rate of the PV and loads. Because the control method considers both PV and load fluctuations, it is considered grid-friendly. Furthermore, because some of the necessary active power is now borrowed from the loads, these control methods reduce the size and quantity of batteries, often considered in conjunction with PV systems. To further reduce the battery usage and offer innovative ancillary

Table 1
Summary of the reviewed DC-link techniques.

Ref.	Technique	Power Reserve Source	Control Type	Shading Scenarios Considered?	Method Evaluation	Key Contributions	Limitations
[53]	DC-link & PV Generation Adjustments with Gradient-based Distributed Coordination Algorithm	DC-link & PV	Algorithm in Conjunction with PI controller	No, only under Uniform Irradiance	Simulation Results	• It is ideal for autonomous microgrids with excess renewable generation, prioritising transient performance over energy efficiency. • The basic idea can be extended to other renewable generators with a DC-link. • The ramp-up and down rates are fixed at 0.4 MW/s. • The maximum frequency deviation with a 5 % load increase is around 0.08 Hz. • The frequency deviation in islanding mode is reduced to 0.01 Hz. • The system is stable even with a significant update time (0.3s) of the power setting.	• The energy efficiency of the system is reduced. • It limits the flexibility and responsiveness of power electronics-based microgrids. • Coordination of the DC-link with PV generation adjustment can complicate the control system.
[54]	Small-Signal Model-Based DC-link Capacitance Selection for Virtual Inertia	DC-link	Proportional and PI Controller	No	Simulation Results	• . • The optimisation of DC-link capacitance for virtual inertia is based on small-signal stability, and a selection approach for DC-link capacitance is presented based on the damping ratio. • Results confirm the effects of DC-link capacitance on the dynamic performance of GCCs, providing virtual inertia. • The C_{dc} of 9.0 mF resulted in a settling time of 30s; therefore, a balance between virtual inertia support and settling time (20s) is achieved with C_{dc} of 2.7 mF. • .	• There is a trade-off between virtual inertia support and the settling time of the grid frequency. • The damping ratio with C_{dc} of 2.7 mF is not mentioned. • The f_{nadir} Increases as capacitance decreases. Therefore, a study on finding optimal capacitance is required. • Simulated settling time might be too low for transient instability.
[55]	ESS Independent Active Power Modulation (APM)	DC-link	PI Controller and Dynamic Compensation with Washout Filter Feedback	No, only under Uniform Irradiance	Simulation Results	• Cost-effective compared to a solution utilising ESS. • It is possible to reduce inter-area oscillations of the power system without adjusting the current power system stabilisers. • The variations in DC-link power oscillations as a function of V_{dc} with $C_{dc} = 5\ mF$, N = 1, $f_{osc} = 0.5\ Hz$ and $\lambda = 0.3$ resulted in PPPO of 8.4 kW, 18.52 kW, and 32.42 kW for $V_{dc} =$ 1000 V, 1500 V, and 2000 V, respectively. • Case study 1 with 3 EM modes at 0.93 Hz, 0.97 Hz, 0.43 Hz and 0.191, 0.081, 0.033 damping ratios with 5.3 % PV penetration reveals that mode 1 with 0.191 at 0.93 Hz is more robust to the change in load from 0 to 150 MW. • Dynamic adjustments to power generation-based grid frequency.	• Periodic updates and coordination of multiple units make it complicated. • DC-link low energy density • Increased switching losses due to rapid adjustments. • The PV plant's ability to improve stability following serious faults may be limited by the saturation term used for the DC-link. • Effectiveness might be limited in shading scenarios.

(continued on next page)

Table 1 (*continued*)

Ref.	Technique	Power Reserve Source	Control Type	Shading Scenarios Considered?	Method Evaluation	Key Contributions	Limitations
						• Distributed coordination allows effective load sharing among multiple RE units. • Robustness against tie-line impedance variations and performance improved as the inter-area damping ratios are improved with increasing no of PV units.	
[56]	VIC-based High Voltage Direct Current (HVDC) link VSG scheme	DC-link	PD and PI Controller with PSO	No	MATLAB/Simulink Simulations	• Enhanced frequency stability • Incorporation of virtual frequency control loops enhances the robustness. • Comprehensive evaluations are carried out by testing proposed strategies with and without high RE penetration. • Results shows that the proposed VIC 2 is better than VIC 1 in providing a smooth frequency response, which is superior to the conventional VIC strategy. • Max. overshoot (p.u) for Area 1 and Area 2 by VIC 1 are 0.299 0.289 and max. undershoot (p.u) for both areas are 0.299 and 0.448, respectively. • Max. overshoot (p.u) for Area 1 and Area 2 by VIC 2 are 0.161 and 0.159 and max. undershoot (p.u) for both areas are 0.421 and 0.442, respectively. • By employing PSO, VIC 2 has achieved the minimum objective function of 1.440 in all testing scenarios.	• The effectiveness of the proposed technique depends on accurate mathematical modelling. • The proposed strategy might be compromised in a real-time environment due to its inability to capture critical non-linearities of the systems. • The DC voltage variations in HVDC link are practically limited, allowing it to stay within ±15 % to ±30 % of the nominal value, which brings a gap b/w theoretical possibilities and practical constraints.
[57]	Distributed Power System Virtual Inertia	DC-link	Proportional and PI Controller	No	MATLAB/Simulink Simulations & Hardware Implementation (dSPACE Controller)	• Cost-effective solution as no additional hardware is required, and no modifications to the existing infrastructure are required. • Filled the gap of the exact relationship b/w DC-link capacitance and virtual inertia. • Reduce frequency deviations by 12.5 % and achieve a 50 % improvement in RoCoF.Fast response • Kind of adaptive solution with self-tuning algorithms.	• The DC-link size limits the virtual inertia. • It has potential complexity in control algorithms. • The effectiveness can vary in operating conditions, such as load change or variable irradiance. • The performance of virtual inertia under extreme grid conditions has not been extensively tested.
[58]	Dual-Mode FFC with Inertia Emulation	DC-link & PV	PI Controller	No	MATLAB/Simulink Results	• A dual-mode FFC scheme is proposed, which increases the PV's grid-supporting capabilities. • Rapid DC-link voltage restoration is achieved without reducing the inertia provision performance. • The main objectives of this approach are to reduce RoCoF, maximum, and steady-state frequency deviation. • The max. RoCoF is −0.738 Hz/s within 300 ms	• 10 % PV reserve is allocated for the DC-link charging power, but it can also contribute to economic losses. An adaptive solution for this would be suitable for such applications. • The specific power reserve control technique is not addressed, which can help to maintain the reserved PV power. • Over-frequency events are not considered.

(*continued on next page*)

Table 1 (*continued*)

Ref.	Technique	Power Reserve Source	Control Type	Shading Scenarios Considered?	Method Evaluation	Key Contributions	Limitations
						indicating maximum of 15 % improvement. • The effect of varying triggering thresholds is minimal. • The f_{nadir} was 49.47 Hz with steady-state frequency deviation of 49.68 Hz indicating a 31.9 % improvement for steady-state frequency deviation. • The wide application of the proposed method in practical scenarios is expected, as it is essentially a bang-bang control.	• Shading scenarios are not considered.
[59]	BFO Algorithm Tuned LQR-Based VI Emulation for IIDG	DC-link	PI Controller	No	MATLAB/Simulink Results LINMOD function for linearization	• The frequency and power oscillations are damped with optimal system inertia in a multi-machine power system. • BFO in the outer loop determines how much power IIDG needs to supply. • The ability of the proposed approach to reduce oscillations and the RoCoF is effectively demonstrated. • An improved inertia responise is achieved with RoCoF of −0.35 Hz/s and 0.15 Hz/s. • The max. overshoot with step change of 50 kW is 0.138 Hz. • Simulation results show that this approach outperforms conventional VSG-based PI controllers regarding settling time, overshooting, rise time, and oscillations.	• Obtaining full state feedback is challenging in practical power systems due to sensor limitations, which may limit the applicability and robustness of this approach in real-world scenarios. • Shading scenarios are not considered. • The performance heavily depends on the correct tuning of BFO. • This linearised model may not capture the nonlinearities inherent in power systems.
[60]	Distributed VI Control-Based Synthetic Inertia Emulation	DC-link	Controller-Based Approach	No, constant irradiance is tested	MATLAB/Simulink Results	• Similar studies have been done, but the proposed approach brings the droop control, which has additional advantages. • Finding the capacitor discharge current aims not to increase the no. of sensors required. • During steady-state insifnificant frequency varitions, a deadband of ±0.01 Hz helps to avoid the use of frequency controller. • The frequency stabilised within 8 s at its nominal value of 50 Hz. • Simulation results show that the proposed approach decreases the frequency nadir to 49.05 Hz with H = 50 and $K_{drop} = 2000$, preventing the load shedding.	• During $\Delta f < 0 \,\&\, \frac{\partial f}{\partial t} > 0$ or $\Delta f > 0 \,\&\, \frac{\partial f}{\partial t} < 0$, the inertia response of the system resists the droop control, which is not required. • Variable weather conditions are not tested. • The capacitor size might not be convenient for a practical application.
[61]	PV-Super Capacitor Cascaded Topology-Based Synthetic Inertia Emulation	Super Capacitor	PI Controller	No, Step Drop in Irradiance is tested	MATLAB/Simulink and OPAL-RT Real-Time Simulator	• Topological innovation: it does not require a high-gain complicated isolated SC Power-Processing Stage (SC-PPS) converter, making it a novel approach to connecting a low-voltage SC to	• A defect in the drive circuit of switches might cause one or both Semi-Controlled Inverter (SCI) switches to cease receiving the gate pulses, which could result in an over-voltage fault in SC-PPS.

(*continued on next page*)

Table 1 (*continued*)

Ref.	Technique	Power Reserve Source	Control Type	Shading Scenarios Considered?	Method Evaluation	Key Contributions	Limitations
						a medium/high voltage PV system. • Innovation in Control: The proposed Droop-Inspired method emulates dynamic inertia as a function of RoCoF. Additionally, the operation of SC as a voltage source is achieved by a single PI-based decoupling method, which sets apart the control of two-level SC-PPS. • Methodology: a novel three-point linearization method for PFR and a droop-inspired method for SIR are used to size SC and its PPS. • With a range of 2–9 s, the proposed approach can effectively provide variable synthetic inertia. • The variable inertia emulation flexibility allows to handle wide variety of RoCoF up to nearly 2 Hz/s, with the aid of ramping capability that allows for limited storage of up to 2 kW.	• The SCI stage always stays active when there are no frequency events, even though SC is not dealing with any active power, which can result in extra running losses. • Over-frequency events have not been considered.
[62]	Fuzzy Logic Controller-Based Emulated Inertia Controller	Super Capacitor	PI Controller	No, tested with 200 W/m^2 and 500 W/m^2 step change in irradiance	MATLAB/Simulink and OPAL-RT Real-Time Simulator (OP 5700)	• The super capacitor-based inertia emulation is formed, which is based on Mamdani fuzzy logic. • The proposed technique limits the frequency nadir in under-frequency events at 49.85 Hz compared to conventional EIC. • The frequency overshoot is limited to 50.176 Hz, and power oscillations have been damped in rapid load shifting with a step decrease. • During the irradiance drop, the frequency nadir is arrested at 49.71 Hz. • Hardware testing shows that the proposed method effectively handled sudden load and PV variations by limiting the frequency nadir to 49.86 Hz and a frequency rise to 50.18 Hz.	• Performance depends on the appropriate identification of fuzzy rules. • The proposed method is not commercially appealing as SC has low energy density, which allows it to provide power for limited periods, and when it discharges, the voltage decreases gradually and increases linearly when it charges.

Table 2
Power ramp rate limits by various grid codes.

TSO	Country	Ramp-Up Limit	Ramp-Down Limit
HECO	Hawaii	2 MW/min	2 MW/min
		1 MW/min	1 MW/min
German TSO	Germany	10 %/min	10 %/min
Denmark TSO	Denmark	100 kW/s	100 kW/s
PREPA	Puerto Rico	10 %/min	10 %/min
EIRGRID	Ireland	30 MW/min	10 %/min
ENTSO-E	Europe	No requirement	No requirement
National Standards	China	10 %/min	No requirement

services, a ramp-rate control based on a VSG was initially proposed in conjunction with load control. Bi-directional PV-VSG and load adjustment both further reduce the (dis)charge from 13 to 3. This allows for the addition of a modest capacity battery for ramp rate control with a longer lifespan. Because of active load correction, the suggested technique successfully decreased more high frequency dynamics. A novel predictive dynamic smoothing PRRC strategy was presented by Ref. [73], which is validated based on the real one-year solar irradiation data from the Coto Laurel PV power plant located in Ponce, Puerto Rico. The real-time hardware testing validates the performance and indicates that the proposed method has considerably reduced the levelized storage cost.

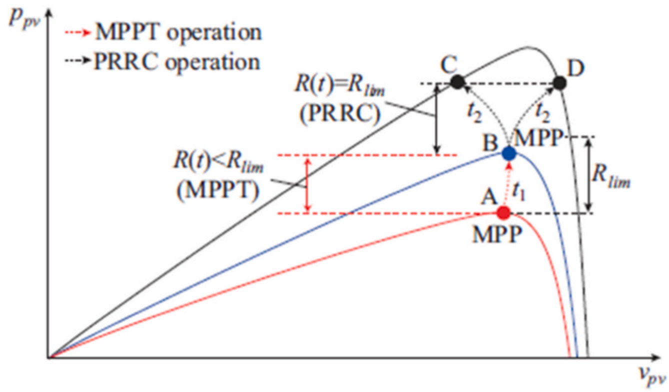

Fig. 13. PRRC concept on the P-V curve of the PV panel.

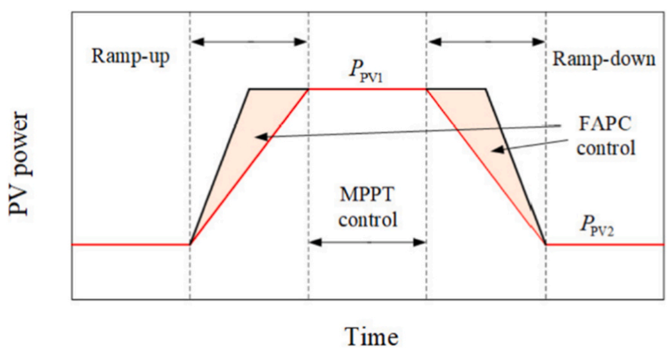

Fig. 14. FAPC fundamentals by [70].

On the other hand [74], proposed a ramp-rate method for PV using energy storage, which was also available for storing extra power or countering voltage increase. To reduce the fluctuations during the ramping event, energy storage was controlled based on an inverse relation with the ramp rate of PV. In addition, compared to Moving Average (MA) methods, the ramp rate can be regulated regardless of historical PV output performance. Simulation results based on the Australian distribution system verify the approach's effectiveness. Using the ageing model, the smooth performance of five distinct ESS-based and two distinct APC-based PRRC approaches was compared by Ref. [75], which shows that the MA and Enhanced Linear Exponential Smoothing (ELES) methods have a longer battery life expectancy than other methods.

Furthermore, the FAPC approach has a low power loss, and efficiency might reach 98.59 % with an RR of 10 %/min when the predicting error is excluded. The Levelized Cost of Energy (LCOE) of FAPC does not vary significantly in the ramp-rate range from 20 %/min to 5 %/min, as the power loss only makes up a tiny percentage of the total power generated. Additionally, with a ramp rate of 10 %/min, the LCOE of MA and ELES is almost double that of FAPC. The FAPC technique is more economical because of the slight power loss, even if the MA and ELES methods can lower the battery's cost using less capacity. Table 3 summarises the reviewed articles. In general, the battery-based solutions are effective for smoothing both upward and downward ramps; their key limitation lies in significant capital cost, finite energy capacity, and efficiency losses associated with battery charging/discharging. Conversely, storage-less methods, which leverage the inverter control for active power reduction, present a more cost-effective solution but are fundamentally limited in mitigating ramp-down limits.

3.3. Constant Power Generation Control (CPGC)

The purpose of CPGC, also known as Power Limiting Control (PLC) or absolute active power control, is to control PV panel output power (P_{PV}) to a predetermined reference value (P_{ref} *or* P_{limit}) that maintains a constant power output from the PV system regardless of grid frequency fluctuations. Generally, this method focuses on regulating the inverter to deliver a steady stream of power even as the irradiance changes throughout the day, incorporating ESS or controlling the active power of PV. The PV operates in the MPPT mode until the PV output power (P_{PV}) falls below the power set point (P_{limit}). When P_{PV} exceeds P_{limit} and the PV system is still operating at the P_{limit}, considered as Constant Power Point (CPP) as shown in Fig. 15. The value of the reference voltage V_{PV}^{*} can be calculated by (12), which is the modification of the conventional P&O algorithm [76].

$$V_{PV}^{*} = \begin{cases} V_{MPPT}, & P_{pv} \le P_{limit}, \\ V_{PV} - V_{step}, & P_{pv} > P_{limit}, \end{cases} \tag{12}$$

Where V_{MPPT} is the MPPT voltage, V_{PV} is the measured PV voltage, and V_{step} is the voltage step size.

During fast irradiance changes, the PV power suddenly increases/decreases, resulting in overshoots/undershoots that were reduced by (13), and power losses were reduced by (14) and (15).

$$Irradiance\ Condition\_inc = \begin{cases} 1, & when \quad P_{PV,m} - P_{limit} > \varepsilon_{ir\_inc} \\ 0, & when \quad P_{PV,m} - P_{limit} \le \varepsilon_{ir\_inc} \end{cases} \tag{13}$$

$$Irradiance\ Condition\_dec = \begin{cases} 1, & when \quad P_{PV,m-1} - P_{PV,m} > \varepsilon_{ir\_dec} \\ 0, & when \quad P_{PV,m-1} - P_{PV,m} \le \varepsilon_{ir\_dec} \end{cases} \tag{14}$$

$$OP_{previous} = \begin{cases} CPG, when \left|P_{limit} - P_{PV,m-1}\right| < \varepsilon_{om} \\ MPPT, when \left|P_{limit} - P_{PV,m-1}\right| \ge \varepsilon_{om} \end{cases} \tag{15}$$

Where, $P_{PV,m-1}$ is measured power at the previous sample, $P_{PV,m}$ is measured power at the current sample, ε_{ir_inc}, ε_{ir_dec} and ε_{om} are criteria for determining fast irradiance increase, decrease, and CPG operating mode, respectively.

The CPGC based on power, current, and P&O for a 3 kW PV was covered in Ref. [77]. A slow-changing trapezoidal solar irradiance profile is adopted for the experiments, where three different power limits (20 %, 50 %, and 80 % of rated power) are used to verify the feasibility of the CPGC strategies. The proportional-integral (PI) controller receives the direct reference power commands in power control CPGC rather than the reference voltage command, which can be calculated using the following expression (16). The power control approach is shown in Fig. 16 (a).

$$P_{PV}^{*} = \begin{cases} P_{MPPT}, & when \quad P_{MPPT} \le P_{limit} \\ P_{limit}, & when \quad P_{MPPT} > P_{limit}, \end{cases} \tag{16}$$

Rather than tuning to the reference voltage signal, the PI controller is tuned to the reference power signal. Tracking inaccuracy is decreased, and the power control CPG mode offers a greater dynamic response. Furthermore, the steady-state responsiveness and stability of P&O-based CPG are superior. Controlling the PV output current i_{pv} It can also limit the PV power to a specific limit. According to PV array characteristics, V_{PV} varies in a small range on the right side of MPP during irradiance change. PV current is highly dependent on irradiance level; therefore, limiting the current to i_{limit} can effectively curtail PV output power. The current limiting strategy is depicted in Fig. 16 (b). During this operation, to calculate the PV reference current, the reference current from the MPPT i_{MPP}^{*} is limited and the i_{limit} is calculated by $\frac{P_{limit}}{V_{PV}}$ which is given to the saturation block. On the left side of MPP, PV current is primarily constant and higher than MPP's. Therefore, only the PV system can use the right side of the MPP when current is employed as the control variable. The results show that the modified P&O algorithms show the highest robustness and achieve minor tracking errors when operating on the left side. On the other hand, the current limiting method cannot ensure robustness under fast-changing irradiance conditions, while the power

Table 3
Summary of the reviewed PRRC methods.

Ref.	Technique	Control Type	Operating Side of MPP	Shading Scenarios Considered?	Method Evaluation	Key Contributions	Limitations
[67]	Novel Storage & Sensor-less PRRC Technique	PI Controller with PRRC algorithm	Right Side	No, tested under various irradiance levels	MATLAB/Simulink and C-HIL (PV emulator (*Typhoon HIL402*) & Control System (*Opal-RT 5600*))	• The curve-fitting algorithm (problem solved by Levenberg-Marquardt method using MATLAB function *lcqnonlin*) is used to estimate MPP and power reserve in real-time, and it does not require temperature or current sensors. • The plant model is obtained from system identification using sample data, which avoids the linearization process. • The control of PV power allows the PV system to react inherently during irradiance changes to maintain power reference, and the ramp rate is effectively tracked. • The ramp rate is never exceeded as the PV power is regulated every moment, and the power reference is changed according to the maximum power ramp-rate limit. The delay in ramp-rate measurement is minimised with a filtering parameter (n = 1). • A low or zero reserve is utilised to reduce energy waste, while a high reserve is used for shorter periods to limit the ramp-down rate.	• The effectiveness highly depends on the estimation of the MPP. • The curtailment power command (power reserve creation) is not adaptive, which can add to the financial costs. • The ramp-down rates are not limited due to a lack of available power reserve. While with 20 % reserve, the ramp-down rate is limited, it is associated with the curtailment costs.
[68]	Adaptive FPPT-Based PRRC	Algorithm Based	Left & Right	No, only tested in different irradiance levels	MATLAB/Simulink and Hardware (Regatron TCACS 4-quadrant grid simulator & Regatron TopCon Quadro Programmable DC Power Supply as PV simulator) Testing	• The proposed method detects irradiance change quickly and has fast dynamics. • It can detect the power-ramp rate in one control time $(m-0.5)T$ and mT steps compared to available solutions, which require several control steps. • It can measure and constrain the ramp rate at the beginning of the rapid changes in environmental conditions. • An adaptive step size is utilised, which is based on PV operating point and calculated power limit, and a large voltage step is adapted when the ramp rate is away from the limit, resulting in fast dynamics. • Hardware and Simulation testing reflect the effectiveness of the proposed approach in fast detecting irradiance change and maintaining the ramp-rate.	• During irradiance decrease, the ramp-down rate is not maintained. • In hardware testing, the dynamic performance of the proposed method is limited due to hardware limitations and the proposed PRRC sample time step, which is designed per inner loop voltage and current controllers.

(*continued on next page*)

Table 3 (*continued*)

Ref.	Technique	Control Type	Operating Side of MPP	Shading Scenarios Considered?	Method Evaluation	Key Contributions	Limitations
[70]	GBSFS-based PRRC with Power Curtailment	Dynamic Spatio-Temporal Ramp (DSTR) Forecasting Algorithm	N/A	Dynamic Shading (Cloud Movements)	Simulation and Hardware Testing	• The proposed DSTR forecasting algorithm enhances the prediction of power ramps. • It provides a dynamic control that can adapt to varying environmental conditions. • The proposed FEC strategy reduces the ESS power capacity size to a quarter. • It can effectively participate in frequency regulation. • The GBSFS effectively identifies 95.8 % of ramps over the period of 1 year which confirms the efficiency of the proposed DSTP predictions.	• The effectiveness is highly dependent on the forecasting algorithm. • The deployment of a GBSFS incurs initial costs, which may be a barrier for some operators. • The limited forecasting horizon breaks the state of charge equilibrium. • It is effective for the ramp-up rate but not for the ramp-down rate. • The performance of the forecasting algorithm can be affected by rapid weather conditions.
[71]	FPPT-based PRRC	PI Controller Based	Left & Right (Depending on Irradiance Movement)	No, only rapid irradiance changes	Simulation and dSPACE Hardware Testing	• The proposed technique has no additional hardware costs and is suitable for ramp-up and ramp-down events detected by the proposed ramp-rate measurement method, which is simple and more effective. • Details of three common ramp rate measurement methods and how they are calculated are given. • It can effectively reduce the power fluctuations in the ramp-down event by managing the ramp-rate limits in simulation which are below 3 W/s. • Experiment results show that the proposed method can effectively regulate the ramp rate under 3 W/s, corresponding to 5 % of the rated PV power per minute. • The flexible selection of operating points can enhance the stability and optimise the performance under varying conditions.	• The effectiveness of the method hinges on precise real-time power ramp rate measurement. Any measurement error can compromise control performance. • Did not consider the shading scenarios. • The variability in weather conditions can affect the effectiveness.
[72]	A Novel Load Compensation and VSG-Based RR Mitigation Strategy	PI Controller Based	Left side	No, tested for time-varying irradiance	MATLAB/Simulink	• A novel RR mitigation strategy incorporating a load compensation method curtailed PV acting as VSG (uni-directional and bi-directional) to reduce dependency on BESS in the gentle case. • Numerical simulations demonstrate significant reductions in battery capacity requirements and charge/discharge cycles (31–13 as depth of (dis) charge reduce from 76.6 % to 19.6 %), directly affecting battery lifespan and system cost. • With both load compensation and bidirectional PV-VSG the (dis) charge further reduce	• The optimisation of the battery's cost and profit is not considered. • The strategy could face constraints in actual deployment unless coupled with smart load management systems or incentives. • The simulation scenarios are based on idealised or specific load/PV profiles. The robustness of the control strategy under diverse, unpredictable, or extreme weather conditions is not thoroughly evaluated. • The dependency on batteries is reduced, but residual capacity requirements still depend on system constraints, as it

(*continued on next page*)

Table 3 (*continued*)

Ref.	Technique	Control Type	Operating Side of MPP	Shading Scenarios Considered?	Method Evaluation	Key Contributions	Limitations
						to 3 from 13. Due to this a small capacity battery can be added for ramp rate control with prolonged lifetime. • The proposed method effectively reduced more high frequency dynamics due to active load compensation. • The VSG-based control allows the PV-BESS system to contribute to frequency regulation, aligning with grid codes and operational needs. • The time-varying load and irradiance are used for simulations, and results indicate that the proposed method can reduce the depth of (dis)charge and the number of (dis)charge cycles using PV-VSG, which also allows the improvement in frequency robustness from a grid operating standpoint.	relies on the initial assumption that some battery capacity is always available for emergencies or critical conditions.

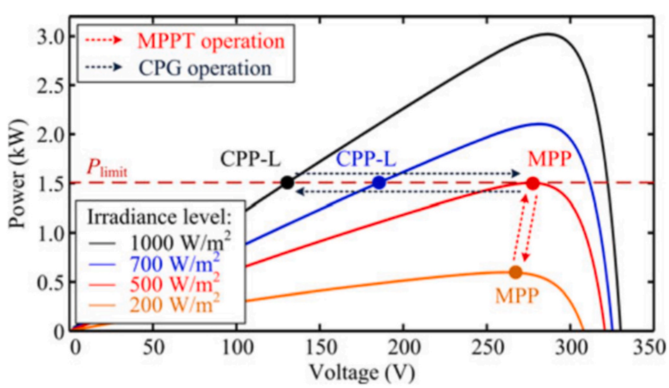

Fig. 15. Operation Principle of CPG based on P&O Algorithm [76].

control method has a significant tracking error.

A comprehensive evaluation of various CPGC algorithm techniques was conducted by Ref. [51]. They classified two methods of CPGC: i) CPGC based on PV voltage/power control, ii) CPGC based on direct computation of voltage reference. Later, the algorithms of these two methods are described in detail. To improve the dynamic response and tracking error of P&O-based CPGC [78], proposed a CPG scheme based on Error-Based Active Disturbance Rejection Control (EADRC) and conventional P&O. The flowchart of their proposed CPG method is presented in Fig. 17. Besides, to achieve the optimal performance, they used Double Quantum Chaotic Social Spider Optimisation (DQCSSO) due to its better searching accuracy. The results show that their proposed CPG has the fastest dynamic performance in the transient state and minimum power oscillations in the steady state compared to P&O, PI, and P&O-Linear Active Disturbance Rejection Control (LADRC) proposed by Ref. [79]. In terms of search accuracy and speed, the SSO outperforms a conventional swarm intelligence system. An existing power plant can readily use the suggested method without having to replace the entire control units. Its settling time was 0.019 s with minimum tracking error of 0.21 %.

A model-based MPPT with CPGC was proposed by Ref. [80], which is based on a new formulation where the effect of temperature and irradiance is considered to improve the system reliability and reduce its cost. In addition to assisting power regulation strategies in PV systems, a CPGC scheme was integrated with the developed MPPT. The switching frequency was mitigated by employing a weighting factor technique. The system's transient behaviour was enhanced by adding an adaptive DC-link controller, and the effects of partial shading were tested to improve the system's transient response. Moreover, the exchange of active and reactive power with the grid was managed by Finite Set MPC (FS-MPC). An Extended Kalman Filter (EKF) was employed to estimate grid voltage, resulting in the reduce dependency on the voltage sensors. In CPG, ABC current THD of 3.90 % were achieved with no weighting factor. On the other hand, implementation of CPG as a secondary control reudeces the dependency on the BESS as well. Similarly, a multi-mode strategy was presented by Ref. [81], which calculates the PV voltage reference and does not require modification in the DC-DC controller. This technique can also be implemented in both single-stage and double-stage PV systems. To provide a quick dynamic response and low-power oscillation in steady-state, a hysteresis band controller is proposed that modifies the time step of the algorithm and voltage increments between voltage steps. By controlling the operating point to left or right, robust power regulation was accomplished, allowing it to avoid instability on the righr side and excessibe converter stress on the left side. Because the controller reconfiguration was not necessary, it can be retrofitted on existing MPPT solutions.

Based on the review summary of articles given in Table 4, generally, the P&O algorithm is used for CPGC operations, while the only drawback of this method is oscillations around the MPP, which can be reduced with a smaller step size, but there is a trade-off between stability and fast dynamics. Therefore, a study is required to find the optimal step size for CPGC applications. Some methods [78,80] have tried to reduce the steps, but the adaptiveness of this method is preferable. Furthermore, the study reveals that the quantum chaotic algorithm is better than the particle swarm algorithm due to its better search speed and accuracy, which effectively avoids problems of premature convergence and local extremum. However, SSO cannot meet demand for industrial

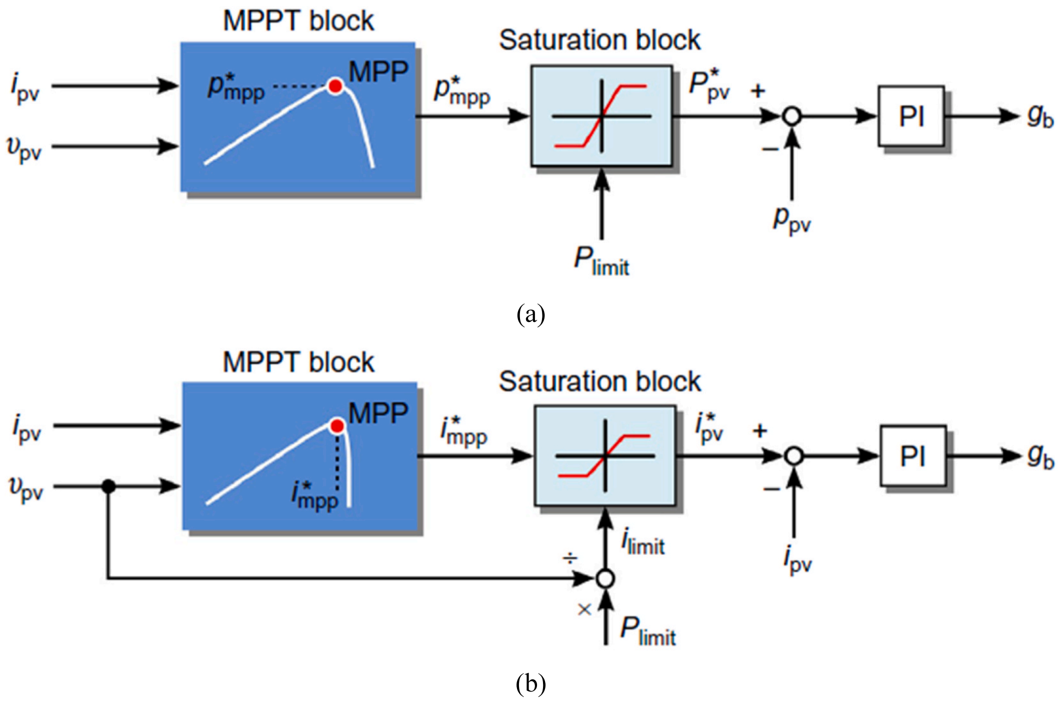

Fig. 16. Control Structure of DC-DC converter: (a) with direct power control, (b) with current limiting control [50].

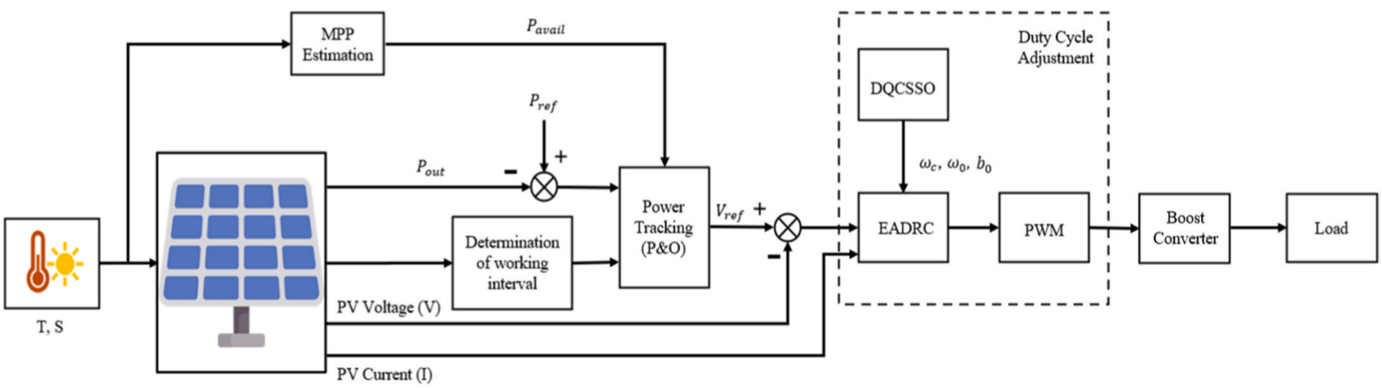

Fig. 17. Flowchart of the DQCSSO-Based EADRC CPG scheme.

applications because of the influence of randomisation and the low ability to find high-quality solutions.

3.4. Delta power control

Delta Power Control (DPC) is typically achieved with the combination of MPPT and CPGC, where specific sets of PVs (master) are operated in MPPT mode while other sets (slave) are limited to one point to provide the constant power regardless of irradiance level. The master PV estimates the total power and then sends a delta-power command to slave PVs, which are then curtailed to a setpoint according to the delta power constraint [52]. Delta power can be adjusted by the operator or computed as a function of grid frequency deviations. In Ref. [82], a DPC approach for multistring grid-connected PV systems was presented, which is shown in Fig. 18, where a 3 kW single-phase two-stage PV system with a trapezoidal solar profile and a power reference of 200W is developed. Moreover, the effectiveness of the proposed DPC is also validated by experiments with real-world operating conditions, which show that the proposed system can maintain the power reserve in all operating conditions. Similarly, a storage-free-master-slave based power reserve control strategy for PV systems was proposed by Ref. [83], in which a small-rated PV module of a few Watts served as the master. Besides, to quickly convert the power to a voltage command for connecting the DC-DC converter, a unique adaptive voltage control mechanism (inner-control) is developed. Furthermore, an inertial and damping control method with active power reserves is implemented in response to system demands. The cost and complexity of any control mechanism are contingent upon the precision of the sensors employed to calculate the MPP. This model estimates the MPP without irradiance sensors, in contrast to existing approaches. The proposed method was used to verify the frequency control for a three-area power network and the updated two-area four-machine test system referred as Kundur's system. When tested for 0.01 p.u load variation, frequency and tie-line deviations were decreased by 70 % and 60 %, respectively. Despite not utilising BESS and irradiance sensors, this method is not financially viable for large-scale PV systems due to the additional cost of setting up the slave PV strings for delta control.

A master-slave technique for LFC of a hybrid interconnected power system was proposed by Ref. [84], where the master PV was using FOPID tuned by Salp Swarm Algorithm (SSA), and slave PVs were tuned by MPC, which forms a strategic controller. The effectiveness of the proposed technique was tested on the IEEE New England 39-bus test

Table 4
Summary of the reviewed CPGC methods.

Ref.	Technique	Control Type	Operating Side of MPP	Shading Scenarios Considered?	Method Evaluation	Key Contributions	Limitations
[76]	High Performance P&O-CPG	PI Controller with modified P&O Algorithm	Left	No, tested under sudden irradiance drop	Hardware Testing using 3 kW PV Simulator	• An advanced and simple P&O-based control strategy that maintains a fast dynamic response by operating PV at a set point. • It has stable operation across varying irradiance conditions by operating on the left side and avoiding stability problems typical of single-stage systems. • A constant voltage applied accelerate the tracking speed resulting in minimum power losses.The overshoots and power losses are effectively reduced using adaptive step size, and a smooth transition between CPG and MPPT mode is ensured.	• The designing of the parameters like $\gamma, k, \varepsilon_{ir\_inc}$, ε_{ir_dec} and ε_{om} is not explicitly described. • There is a lack of elaboration on the robustness against faults like grid disturbance, partial shading, or inverter faults, which are critical in real-world applications.
[77]	Current, Power, and P&O-Based PLC	PI Controller Based	Left & Right	Dynamic shading and different operating conditions	Hardware Testing using 3 kW PV Simulator	• Three power limits (20 %, 50 %, 80 %) were used to verify the feasibility of the proposed method. • P-CPG and I-CPG have fast dynamics during rapid changes in irradiance. • P-CPG and I-CPG have minor tracking errors for both cloudy and clear day scenarios. • P&O CPG is only stable in operating conditions on the left side. • The control structure of I-CPG is simple. • P&O-CPG is suitable due to its robustness and feasibility for future grid codes.	• P&O has large power overshoots during MPPT to CPG transition, resulting in a significant tracking error while operating on the right side. • The proposed current limiting method is not robust in fast-changing irradiance conditions. • P-CPG and P&O CPG can cause instability while operating on the right side. • The control structure of P-CPG and P&O-CPG is complex.
[78]	Error-Based Active Disturbance Rejection Control (EADRC)	PID Controller Based with Optimisation Algorithm (DQCSSO)	Left & Right	No, tested for different irradiance levels	Simulation Results	• Substantial flexibility in operating points and operation mode ensures flexible and stable power output. • The EADRC simplifies the control process as it does not need a time derivative within a dynamic time range in outer loop control, making it more robust to noise. Moreover, the tracking error is selected as a state variable rather than the output value. • Proposed DQCSSO improves the algorithm's spatial traversal and local search ability compared to SSO. • The SSO is better than a traditional swarm intelligence algorithm regarding search speed and accuracy. • The proposed method can be easily applied to an existing power plant without replacing the whole control device. • It has a minimum tracking error of 0.21 % and the settling time is 0.019s.	• Applying DQCSSO to a system that requires prompt reaction is challenging. Besides, in real-time applications, these metaheuristic algorithms can be computationally complex. • This kind of solution needs validation on physical PV systems or HIL setups because real-world disturbances and non-ideal hardware can pose a challenge. • The efficient and rapid tuning of parameters is required for efficient performance, as ADRC can be sensitive to measurement noise and model uncertainties. • Due to its operating speed limitations, DQCSSO is challenging for a system that requires timely feedback. • The proposed method in a single-stage PV system is a future research direction. • The step size for P&O is a key parameter in CPGC; therefore, an optimal or adaptive step size is required

(*continued on next page*)

Table 4 (*continued*)

Ref.	Technique	Control Type	Operating Side of MPP	Shading Scenarios Considered?	Method Evaluation	Key Contributions	Limitations
							to reduce the oscillations and fast dynamics further.
[80]	Model-Based MPPT with CPGC	Adaptive DC-link controller with FS-MPC Algorithm	Right	Yes	Hardware Testing – Voltage & Current sensing module (*USM-31V*), dSPACE DS1202 MicroLabBox, smart gate driver module (*GDA-2A2S1*), HIL (*RT Box CE*) for European standard test (*EN50530*)	• A new formulation is derived and explained to estimate the loci of MPP considering irradiance and temperature effects. The irradiance is estimated mathematically, hence eliminating the irradiance sensors. • The existing voltage and current sensors are used to estimate the irradiance. • The CPG is added as a secondary objective, which does not require any storage device for operation. • Adding an adaptive DC-link controller has removed the DC-link deviations (offsets) caused by dynamic PV power fluctuations. • FS-MPC is utilised for active and reactive power exchange with the grid, and a weighting factor approach to reduce the switching frequency in DC/AC conversion is used. • The Extended Kalman Filter (EKF) is implemented to estimate the grid voltage, removing the grid voltage sensors. • Proposed inverter control without a weighting factor has abc currents THD of 3.90 % in CPG mode.	• The approach is based on simplified models of the PV system, which might not capture the complexities of real-world conditions. • As it aims to reduce the dependency on irradiance sensors, it is still required for calibration purposes. Otherwise, it might not perform optimally, especially in partial shading without environmental data. • The instantaneous efficiency of the proposed MPPT is reduced to a low value in step-down response. • The PV current has large overshoots in CPG mode while operating on the right side. • PV voltage has a high undershoot due to reduced current on the right side of the operation. • Solutions to tune the weighting factor are required, as it can increase the THD of currents. • The proposed method gets stuck at the global and local peaks for two different static partial shading scenarios, but has low oscillations. • The proposed method failed in dynamic partial shading. • The effect of ageing of PV and its impact on this model-based method should be investigated.
[81]	P&O-Based Multi-Mode CPG	Hysteresis Band Controller with modified P&O	Left & Right	No, tested with an irradiance profile	Simulation and Hardware Testing	• This strategy can be implemented for both single-stage and double-stage PV systems. • The time and voltage steps for CPG mode are calculated using a hysteresis band controller, which results in the controller's fast dynamic response. • Robust power regulation is achieved by regulating the operating point to the left or right, which enables it to avoid instability (on the right side) and prevent excessive converter stress (left side). • The controller reconfiguration is not required, which makes it an add-on to existing MPPT solutions.	• The decision on the operating side is pre-defined externally. It lacks an adaptive strategy to decide the optimal side based on grid conditions or system state. • The fixed threshold parameters may limit the performance across different environmental conditions. • The voltage/reactive power support and frequency supports/deviations are not considered, which are crucial for grid code compliance for large PV plants. • Hardware testing is limited to a 1 kW setup; scalability to large PV systems is not demonstrated.

system with a fault analysis. The multi-area system consists of thermal, wind, and PV, where PV was kept at 45 %, resulting in a high RE penetration effect. During the overall interconnected hybrid system, the high penetration is done in the thermal power system, and the deterioration effect on frequency is considered. By maintaining a settling time of 1.09 s for area-1 and 0.87 s for area-2 and achieving a settling time of 1.4 s under a fault scenario, the MS controlling mechanism has demonstrated its supremacy and efficient adjusted to the unforeseen circumstances in the power system.The stability and control of a master/enslaved person micro-grid architecture using frequency-based power management was studied by Ref. [85], where a current-controller grid-connected inverter was employed rather than

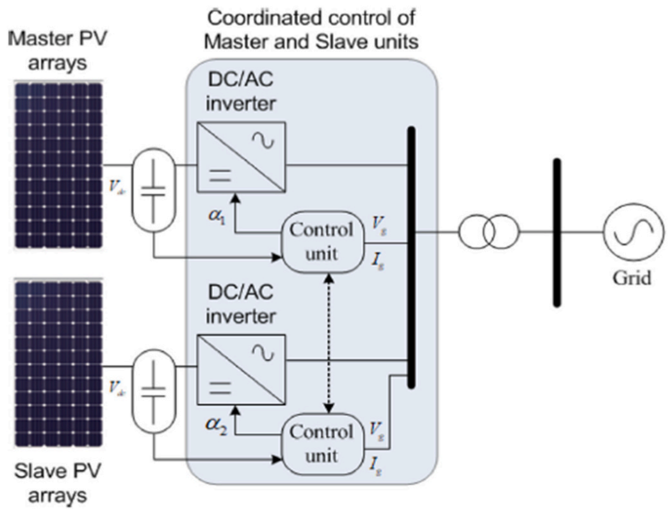

Fig. 18. Dpc strategy for PV system.

traditional droop-controlled systems to regulate power flow in low-voltage grids with high RE penetration, as shown in Fig. 19. To minimise reverse power flow and improve grid stability, the master inverter can indirectly control the power output of distributed sources by modifying the grid frequency in response to overload circumstances. The PLL dynamics stability analysis indicated that it is a crucial parameters and system instability can be resulted from inverter's inability to swiftly track freuquency changes if the PLL's bandwidth is limited.

The further extension of the master/slave approach for stabilising frequency in a microgrid with the integration of a storage element was presented by Ref. [86]. A novel quasi-master/slave control framework for PV-storage independent microgrids was proposed, where the PV units acted as slaves (current control sources) and the storage acted as master units (voltage sources). The master units maintain the system frequency stability, while slave PVs maximise the energy extraction and contribute to grid support through droop-based power control. It addressed the limitations of conventional peer-to-peer and master-slave control frames in PV-storage microgrids. The ESS is controlled by active power droop (17) and proposed adaptive reactive power droop (18).

$$\omega_i = \omega^* - m_i(P_i - P_{i_a}) + \left(K_{Pi} + \frac{K_{Ii}}{s}\right)\left(u_{dci} - u_{dci}^{ref}\right) \tag{17}$$

Where, P_{i_a} is available active power of the i-th PV is given by a feed-forward controller. K_{Pi} and K_{Ii} are proportional and integral coefficients of the i-th PV, respectively. u_{dci} and u_{dci}^{ref} is the DC-side capacitor voltage and reference voltage, respectively.

$$V_i = V^* - n_i Q_i \tag{18}$$

Where, n_i is an adaptive droop coefficient and represented as $n_i = \frac{V_{max} - V_{min}}{Q_{i,a}}$, $Q_{i,a} = \sqrt{S_{rate}^2 - P_i^2}$, $Q_{i,a}$ is the available reactive power of the i-th distributed generator, which is calculated according to rated apparent power and available active power. Table 5 comprises a summary of the reviewed DPC article.

3.5. PV curtailment control

Curtailment is usually referred to as an intentional, controlled reduction of PV output below its maximum capacity (operating below its MPP and explained in section 3.6). This reduction is typically prescheduled or mandated by grid operators, often driven by strategic planning and market-based decisions/mechanisms to manage congestion and voltage issues or reserve capacity for ancillary services like frequency support. Curtailment may be viewed as a reactive strategy responding to the above-listed issues. According to Ref. [87], PV plants modifying their active power output can offer ancillary services and contribute to frequency regulation. Their proposed strategy is shown in Fig. 20, which has two modes: frequency droop control to provide PFR, and emergency mode, which prevents excessive generation tripping after a fault by preventing system frequency collapse.

Using an optimal unit commitment scheduling model considering forecasted PV and electricity power output [88], evaluated the impact of scheduled curtailment control at 30-min intervals on reducing curtailed PV power output, compared to a fixed curtailment control. The impact of ramp rate control of curtailed PV was further examined using an energy supply-demand model to prevent the abrupt shift in grid frequency driven by a step change in curtailment. This study assumed the plant parameters based on the Japanese power system models developed by Japan's Institute of Electrical Engineers (IEE). When curtailment is necessary, the cumulative PV power supply can be raised by 2 %, as opposed to when it is applied with predetermined upper limits. Depending on the requirement, a novel real-time non-linear least square curve fitting-based PV power curtailment strategy was developed by Ref. [89], which allows the operation on both sides of the MPP of the PV curve. Their control structure is shown in Fig. 21. An affine parameterisation is applied to tune the compensator in terms of the robustness and stability of the closed-loop system. Generally, the curtailment of the PV results in energy wastage, but their approach has created a reserve that can be dispatched during frequency deviations. This technique is referred to as "de-loading," which is discussed in section 3.6 with more detail. Their control methods allow the operation on the left-hand side of

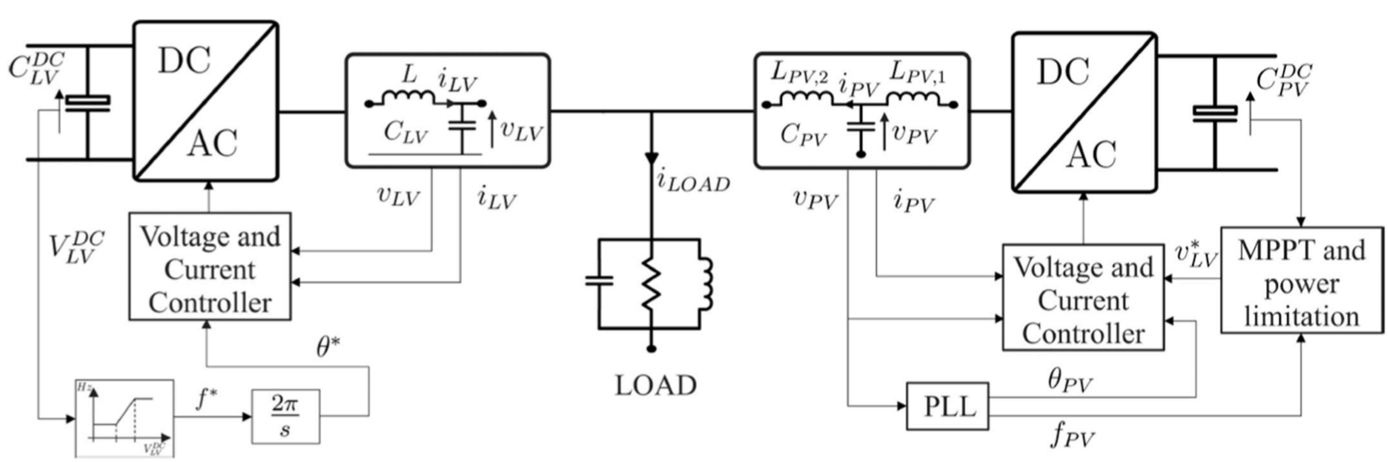

Fig. 19. Block diagram of control with master inverter and PV converter.

Table 5
Summary of the reviewed DPC methods.

Ref.	Technique	Control Type	Operating Side of MPP	Shading Scenarios Considered?	Method Evaluation	Key Contributions	Limitations
[82]	Master-Slave DPC	P&O algorithm and PI controller	Left	No, tested under three irradiance levels	Simulation (PLECS/ Simulink) and Hardware testing	• A hybrid approach for a PV system that eliminates the need for irradiance sensors and storage devices, reducing the system complexity and cost. • This can be seamlessly integrated into residential/ commercial PV systems without hardware modifications. • The functional efficiency of a 3-kW single-phase PV system under dynamic and grid frequency deviations is presented through simulation and hardware testing.	• The power reserve generation is highly dependent on MPP estimation from the master PV. • This strategy assumes the exact characteristics of PV strings, but mismatched panels or ageing may degrade the performance. • The adaptive ΔP is required for more flexible control. As constant operation below MPP inherently sacrifices energy yield. • The implementation on a large scale may face challenges in communication latency. • The discussion on the failures, such as DC-link voltage variations, has not been done.
[83]	A Self-Adaptive Voltage Tracking-Based DPC	Inertia & Damping Controller with TLBO Optimisation Algorithm	Left	No, tested under varying irradiance and temperature	Simulation Results	• A novel master-slave approach where a small-rated PV of a few watts accurately serves as a master for a large PV plant. • A single time-intensive curve-fitting application is used, which does not require temperature and irradiance sensors. • MPP variables are calculated using a perturbation-free method from a single measurement sample. • The frequency control for a three-area power network and the revised two-area four-machine test system (Kundur's system) is verified using the proposed method. • Frequency and tie-line deviations are reduced by 70 % and 60 % respectively, under testing for 0.01 p.u. load variation.	• The factors involved in selecting the size of the curtailment power command were not considered. • A single measurement can be noisy and uncertain, especially in rapid irradiance changes. • The system's dependence on the grid operator to determine reserve power highlights its lack of autonomy. • Irradiance and temperature estimations from master PV assume that it operates in the same environment as slave PVs. Any environmental differences can lead to inaccurate estimations, thereby impacting performance. • The estimation of MPP from masters requires all slaves' PVs to be of the same rating, which might not be an optimal solution.
[84]	A Novel Master-Slave (MS) Strategy for a Hybrid Inter-Connected Power System	FOPID (master) and MPC (slave) Controllers with Salp Swarm Algorithm for master tuning	N/A	No, tested in varying irradiance	MATLAB/ Simulink and HIL	• The high penetration level of 45 % PV is considered in a multi-area power system. • The proposed MS effectively combined the rapid convergence and zero steady-state error feature of FOPID with the low overshoot and improved transient response of MPC, resulting in more robust and adaptive control. • The proposed technique is robust against abrupt load changes and faults, indicating improved robustness compared to traditional controller designs. • Resilience to fault and load variations enhances its practical utility, especially in systems with critical stability margins. • The high penetration levels are considered crucial for modern power systems,	• The two-tier control structure involving FOPID tuned via SSA and MPC might introduce computational overhead, which could be a concern in real-time large-scale applications. • The control design assumes accurate system modelling and parameter knowledge, which might be challenging in real systems where uncertainties and parameter variations can degrade the effectiveness. • There is a lack of an adaptive mechanism for tuning the controller parameters.

(continued on next page)

Table 5 (*continued*)

Ref.	Technique	Control Type	Operating Side of MPP	Shading Scenarios Considered?	Method Evaluation	Key Contributions	Limitations
						offering insights into managing RE integration impacts on system stability. • Under fault scenario, settling time of 1.09 s for area 1 and 0.87 s for area 2 were achieved, verifying the supremacy and efficiency of MS controlling mechanism.	
[85]	Master-Slave Based Micro-Grid Stability Analysis using Current-Control Grid-Connected Inverter	PI Controller Based	N/A	No	MATLAB/ Simulink with PLECS Toolbox and dSPACE	• A frequency-based power management approach for master/slave micro-grids does not require specialised inverter control modifications, making it compatible with existing commercial equipment. • This technique can be applied in a smart transformer distribution grid. • The indirect control of power by the master converter effectively prevents the reverse power flow and grid overloading. • The stability analysis focused on PLL dynamics reflects that it is a critical parameter. If the bandwidth of the PLL is low, the inverter may not track frequency changes quickly, making the system unstable. • The simulation and experimental tests highlight the practical feasibility and effectiveness in real-world scenarios.	• The micro-grid stability heavily depends on the bandwidth and dynamic response of PLLs. Improper tuning of the PLL can make the system unstable, especially in rapid frequency changes. • The master converter should be adequately sized as it is responsible for grid voltage and frequency regulation; under-sizing could compromise the entire micro-grid. • Effectiveness relies on the grid-connected inverters' ability to detect frequency changes rapidly.
[86]	A Novel Quasi-Master/Slave Control Frame for PV-Storage Independent Microgrid	PI Controller Based	N/A	No	Simulation and Hardware (Prototype) Testing	• A novel quasi-master/slave framework that blends aspects of peer-to-peer and conventional master/slave systems eliminates the need for extensive communication and PLLs, enhances system reliability, and reduces complexity and cost. Moreover, it enhances the adaptability and plug-and-play capability. • It facilitates high PV penetration by flexibly arranging PV as slaves and storage as the master. • The islanding and grid-connected mode offers a versatile microgrid operation, which is advantageous in deploying autonomous and grid-interactive systems. • The MPPT-based power droop with adaptive reactive power regulation maintains voltage and grid stability and optimises PV energy. • Load fluctuations are addressed swiftly with a response time of 0.2s due to adaptive droop. • The simulation and practical experiments support the potential for real-world implementation due to their feasibility and robustness.	• Microgrids with small units are addressed, but the stability and control coordination may become complex as the number of PVs and storage increase in large systems. • The assumption of ideal voltage source and inverter behaviour may affect the real-world performance due to inverter non-linearities, measurement noise, parameter uncertainties, and ageing effects. • The detailed analysis of power quality issues under severe disturbances remains unexplored, crucial for ensuring power quality standards. • Adaptive tuning during gradual system changes is not addressed, which is essential for persistent microgrid operation.

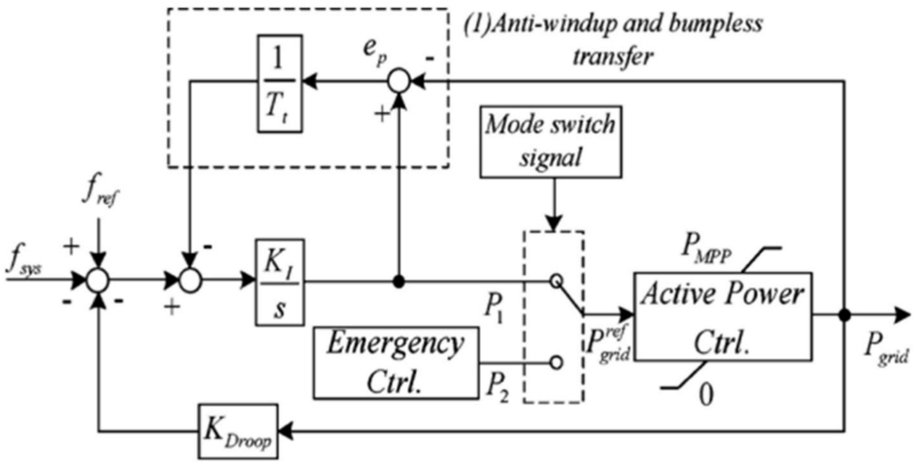

Fig. 20. Virtual frequency droop controller for PV systems [87].

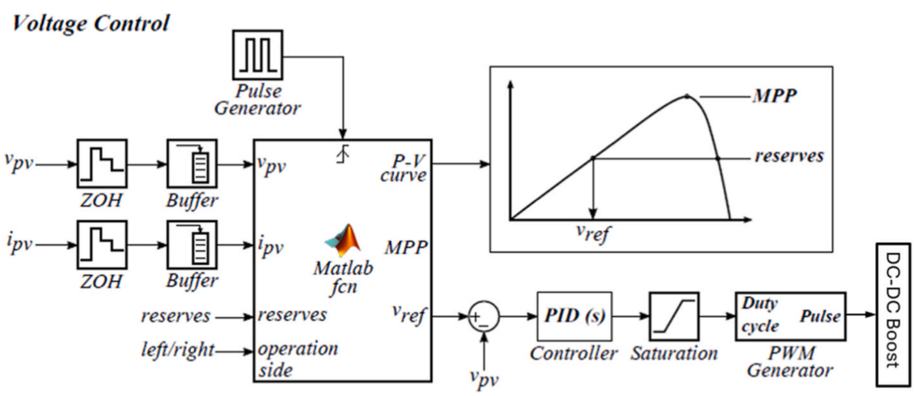

Fig. 21. Control structure of least squares curve fitting-based curtailment.

MPP during fast irradiance changes, while the right-hand side is used when curtailment is prolonged enough to cause a temperature change. The inherited ripple used for reducing power and voltage fluctuations is low when the power reserve levels are 90 %.

PV curtailment with decentralised energy storage has also been utilised in hybrid power systems by Ref. [90], but they considered the over-voltage protection, which reduced to 0 % from 53 % with 100 % RE integration for end-users. Furthermore, a method to improve the accuracy of PV curtailment for grid stability in North Sulawesi and Gorontalo power grid was presented by Ref. [91], where the largest PV plant is Likupang PV with 15 MW, followed ithby Isimu PV with a capacity of 10 MW. The simulations were divided into two parts, first wh 73.79 % of the MAP was tested to mimic the intermittency of up to 11.62 MW in normal conditions while second had under curtailment with 7.08 MW drop. During normal conditions, the intermittency caused a frequency drop of 49.71 Hz while with curtailment mode, it dropped to 49.8 Hz which indicated the stable and normal operation. Analysis of the relationship between changes in demand impacting frequency and variations in multiple PV is the first step for PV curtailment. The Pearson correlation coefficient was employed to ascertain the strength of the correlation between these variables. The function of the influence of PV power variations on frequency deviations is understood through data mining (the data science trajectory method is used), and this function can be used to determine the operating limits of PV to achieve the desired frequency response. The role of curtailment in providing frequency response and ancillary services was explored by Ref. [92], which focused on developing frequency-watt (FW) curves that enable PV systems to participate actively in grid stability. The FW configurations were designed to find the most economical and effective curve. Due to its versatility across a range of PV penetration levels, it is scalable and applicable to multiple grid scneraios. The FW curve that will yield the greatest savings was found by optimisation using Sequential Quadratic Programming (SQP); nonetheless, the outcomes for SQP and Latin Hypercuve Sampling (LHS) were the same. The results of the second optimisation, known as the interiror point approach, were marginally superiror to those of SQP and LHS data for 70 % and 120 % penetration, respectively. A summary of the reviewed articles is given in Table 6.

3.6. De-loading

Like PV curtailment, de-loading also refers to operating the PV below its MPP, which creates a reserve for grid support services like frequency support. Both methods are conceptually similar, but the key differences are timing (milliseconds to seconds) and control methodology. The de-loading is a proactive approach implemented before a problem occurs and focuses on control schemes used during regular operation, often through power curtailment, which is implemented dynamically through inverter controls (real-time, automatic) to reserve power for immediate ancillary services. Typically, PV units operate at their MPP at a specific temperature and irradiance, which ensures maximum efficiency. Moving away from the operating point (OP) of MPP can create a constant reserve that can later be used for frequency regulation. The flexible shifting of the operating point is referred to as Flexible Power Point Tracking (FPPT) and can be done either on the left or right side of MPP. As shown in Fig. 22 at two different voltage levels ($V_{mpp} - V_{deload}$) and ($V_{mpp} + V_{deload}$), same amount of power can be extracted from PV.

De-loading is particularly prominent and has attracted significant research interest due to its potential to provide substantial power

Table 6
Summary of the reviewed PV curtailment methods.

Ref.	Technique	Control Type	Shading Scenarios Considered?	Method Evaluation	Key Contributions	Limitations
[87]	Frequency Droop Curve-based Active Power Adjustment	Integral Controller Based with modified NQI algorithm (Curve fitting)	No, only tested for different irradiance levels	Simulations Results	• It provides an essential primary response by adjusting the PV power based on the frequency of the droop curve. • The active power control algorithm at NQI-based active power control provides rapid adjustments to reference power and a rapid response to frequency deviations. • The control scheme is decentralised, which is suitable for large-scale PV plants. • The proposed control strategy can be implemented for various types of PVs with distinct inverter topologies. • The derivative of the system frequency after the low-pass filter is used to avoid frequent or delayed triggering of the frequency signal. • The frequency is limited to 50.14 Hz after a 10 % load drop, while a 45 % drop resulted in 49.90 Hz.	• Highly dependent on the PV operating conditions (irradiance and temperature) • The immediate power curtailment in emergency mode can lead to excessive output reduction. • There may be a delay before the system returns to regular operation after emergency mode, affecting stability. • Ignoring the dynamic of internal resistance can lead to suboptimal performance, increased oscillations, and overshoots or undershoots due to sudden load changes or grid disturbances.
[88]	Optimum Unit Commitment Scheduling Model-based Curtailment Control	High-level scheduling and limiting based on forecasts and pre-planned intervals	No	MATLAB/ Simulink Results	• The upper limit ratio (r_c^h) is calculated by dividing the curtailed accumulated power by the total capacity of PV, as, from a pragmatic perspective, each PV should be notified of r_c^h as a relative value to rated capacity rather than predicted PV output. • The 10 %/min ramp rate control limits the steep change in system frequency. • The cumulative PV power supply can be increased by 2 % on a day when curtailment is required as opposed to when it is implemented using a set upper limit. • A feasible control scheme is presented considering the operational limitations of large-scale PV systems. • The combined approach of forecasting, scheduled control, and ramp-rate limiting provides a comprehensive technical technique for integrating high PV capacity.	• The generalizability of findings to other grid systems with different characteristics may be limited, as this approach relies on specific regional power system data. • There is a lack of empirical validation because managing a large PV capacity (up to 100 GW) in real-time presents significant technical challenges like synchronisation and robustness against communication failures. • The effectiveness of scheduling relies heavily on accurate short-term PV output forecasting. • Inadequate consideration of control system limitations, such as response time and measurement accuracy, is not addressed.
[89]	Real-Time Non-Linear Least Squares Curve Fitting Based on PV Power Curtailment	PID controller with affine parameterisation	No, tested in varying irradiance	MATLAB/ Simulink Results	• Depending on the requirement, a curtailment strategy that allows PV to operate on both sides of MPP offers enhanced control depending on grid conditions and improves system stability in transient events. • Despite the discharge level, the proposed method performs efficiently when irradiance and required reserve are varied, keeping the temperature constant. • The operating sides shifted without altering the available reserve, mainting a constant support by PV. • The non-linear least squares (NLS) allow the accurate real-time estimation of P-V curve and MPP, which is facilitated by the inherent ripple in PV voltage/current, reducing the need for additional ripple control. It simplifies the	• Authors reported that curve fitting cannot accurately estimate temperature on the left side since it substantially impacts MPP and system behaviour. This might limit the method's application in rapid environmental changes. • NLS is susceptible to measurement noise, especially in low irradiance or high fluctuation. • The approach simplifies the hardware, but the computational complexity involved in curve fitting in real-time may impose processing demands. • This approach lacks experimental validation. • Operation stability on the right side under rapidly changing conditions remains a concern.

(continued on next page)

Table 6 (*continued*)

Ref.	Technique	Control Type	Shading Scenarios Considered?	Method Evaluation	Key Contributions	Limitations
					hardware and reduces the cost. Comparative performance analysis with the existing method demonstrates better residual in curve fitting and comparable tracking of power reserves, highlighting the method's effectiveness.	
[91]	Pearson Correlation-Based PV Curtailment	Algorithm-Based Supervisory Control (Data-Driven Algorithm)	N/A	DigSILENT and Site Experiments	• A Pearson coefficient determines the correlation strength between affecting frequency changes, such as changes in demand and PV. • Depending on this correlation, the target PV for curtailment is selected. • The MAP curtailment is applied at the final stage when all generators have responded through primary and secondary control. • With PV initially contributing 7.58 % of the 330 MW daytime peak load, this approach provides a framework for managing higher renewable shares as demand grows. • The max. frequency deviation in curtailment mode is 49.8 Hz which indicates a stable system operation.	• The Pearson analysis relies on historical PV and demand data, which may not fully capture future grid dynamics or extreme weather events. • Designed for a low-stiffness system, it might not translate well to stronger grids or distributed solar networks. • The proposed approach's economic effects (e.g., revenue losses from reduced generation) should be evaluated as it is implemented on two actual PV systems. • Curtailment amount is again based on the correlation between variables; it would be good to consider adaptive curtailment to reduce revenue losses.
[92]	Frequency-Watt Curve Design for Frequency Regulation and Impact on Curtailment	SQP and Interior Point Method for Optimising FW curve	N/A	MATLAB and PSLF Simulations	• It demonstrates that carefully designing Frequency-Watt (FW) curves can lead to significant economic benefits and enhance grid stability simultaneously. • Using Latin hypercube sampling allows for efficient parameter space exploration, making the optimisation process robust. • It is scalable and relevant for various grid scenarios due to its adaptability across different PV penetration levels. • The Sequential Quadratic Programming (SQP) is used for optimisation to find the FW curve that will give more savings, but the results for SQP and LHS are identical. • The second optimisation routine, named the interior point method, was employed and resulted in slightly better results than SQP and LHS data for 70 % and 120 % penetration. • As penetration increases, the amount of curtailment increases, which can compensate for variability and fluctuations, smoothing out the power supply.	• Poorly designed or inflexible curtailment schemes may lead to unnecessary energy loss or insufficient grid support. • There are inconsistencies in SQP, LHS, and Interior Point methods due to the low sensitivity of the cost model to changes in deadband and droop. • Future work should focus on refining and validating the cost model.

reserves for frequency control; therefore, this is the more focused section of this review paper. According to Ref. [1], it has been proven that the de-loading approach is more feasible and cost-effective for frequency regulation for utility-scale PV systems of 1 MW or more than employing a BESS with a shorter life cycle. However, regardless of the system's ancillary requirements, which change over time, it necessitates continuous, constant PV power curtailment; therefore, it is not the best course of action. Identifying the best de-loading option that will also work in non-uniform shading scenarios is necessary and currently under focus by researchers. As the P-V curve in this case contains multiple peaks, as shown in Fig. 25 (b), conventional methods cannot be satisfied. Thus, by merging algorithms, hybrid controllers, and soft computing techniques, researchers have implemented numerous techniques and are working on optimal and adaptive solutions.

A multi-area power system of twelve PVs with two conventional generators without any BESS was presented by Ref. [93] to provide frequency support, wherein the percentage of de-loading each PV to its MPP was equal to 18 %. To distribute the frequency control capabilities equally throughout the system, they ensured PV with more reserve capacity would participate more than those with low reserves. The calculation of $V_{\mathrm{dc\_ref}}$ considering power reserve from PVs can be expressed as (19).

$$V_{dc\_ref} = (V_{MPP} + V_{deload} - V_{dc}) - \left(\Delta f^{*} \Delta V_{reserve}{}^{*} K_{p2}\right) \tag{19}$$

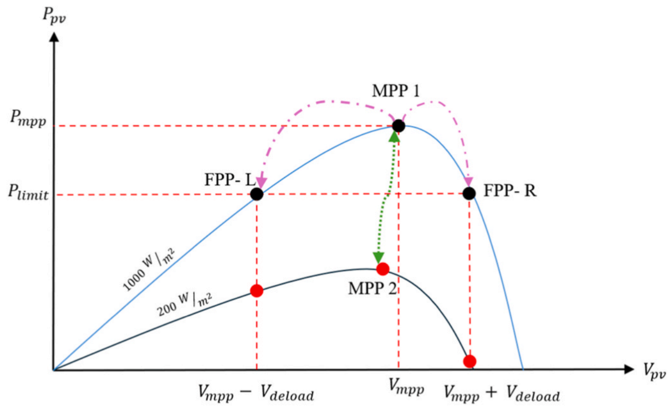

Fig. 22. P-V Curve of a de-loaded PV with Implementation of FPPT.

Where, V_{deload} is the voltage to be changed corresponding to the power reserve needed to be provided, V_{dc} is the DC-link voltage, which is proportional to Δf, $\Delta V_{reserve}$ change in the power reserve voltage and K_{p2} is the proportional gain.

According to the cost study, the investment cost of a battery with a 444.44 kW capacity and a PV with a 1 MW reserve was equal, which supported the use of de-loaded PV.

An adaptive de-loading strategy for 500 kW grid-connected PV was developed in Ref. [94], which utilises three different controller loops: droop, Active Power-Voltage Matching (APVM), and vector controller. These extra loops help quickly adjust the PV output power for frequency regulation. They used linear regression to solve the transcendental implicit equation of PV to derive a polynomial that can predict the V_{dc} and used the R-squared criterion to determine a range where the proposed APVM is accurate.

In [95], the de-loading technique was presented in conjunction with using a DC-link capacitor for a two-stage three-phase PV system. The frequency regulation ability was dynamically adjusted depending on de-loading using a variable droop method to meet the effects of changing environmental conditions. To confirm the efficacy of the proposed control technique, case studies were conducted using a microgrid system integrated with a diesel generator and solar panel. The linear proportional relationship between DC-link voltage and system frequency can be expressed as (20), where K_{in} is proportional gain, f_0 and V_{dc0} are the nominal system frequency and DC-link voltage, respectively. To prevent excessive voltage variations, the DC-link voltage was constrained within 0.86–1.14 p.u. and $C_{dc} = 30,000\ \mu F$ and $K_{in} = 10$ by trial-and-error method to achieve a satisfactory transient response. The derivation for this term can be find in the [95], which is based on the dynamics of SG and DC-link.

$$V_{dc} = K_{in}(f - f_0) + V_{dc0} \tag{20}$$

To account for environmental uncertainties, the de-loading was divided into two parts attributed to irradiance and temperature, as shown by (21), which calculates the required increase in DC bus voltage, where ΔV_{dc_I} shows an increase in DC bus voltage with varying irradiance and constant temperature (25 °C), ΔV_{dc_T} shows the increase in DC bus voltage by varying temperature and constant irradiance (1000 W/m^2), and ΔV_{stc} indicates the increase in DC bus voltage for de-loading control under STC.

$$\Delta V_{dc\_bus} = \Delta V_{dc\_I} + (\Delta V_{dc\_T} - \Delta V_{stc}) \tag{21}$$

Since accurate MPP estimation is necessary for de-loading, several approaches have been used in the literature. These include measurement-based methods, including curve fitting approximations, hybrid operation with MPPT and CPGC in one PV system, and empirical methods. A comprehensive review of the PRC algorithms was conducted by Ref. [51], where these algorithms are classified. The comparison tables have been provided, which state that PRC 6 [96] is effective with a swift dynamic response, low tracking error, low computational complexity, low steady-state fluctuation, and efficient and reliable operation under environmental changes. This algorithm is shown in Fig. 23, which uses a modified version of the P-V curve (Fig. 24(a)) to achieve the monotonic relationship between power and duty cycle. Mathematically, it can be obtained as equation (22):

$$P'_{PV} = \begin{cases} P_{PV} & V_{PV} \geq V_{MPP} \\ 2P_{MPP} - P_{PV} & V_{PV} < V_{MPP} \end{cases} \tag{22}$$

Where P_{PV}, V_{PV} and V_{MPP}, P_{MPP} are the power and voltage at the actual operating point and MPP, respectively, whereas P'_{PV} is the modified power. When the operating point shifts to the left side, this modified power is fed to the PI controller, which exhibits a strong negative error that allows the operating point to move back to the right. It has been claimed that this is the first method in the literature to use SDM for MPP and a five-parameter model in de-loading mode.

On the other hand, an event-triggering VIC-based MPPT-PRC strategy to switch PV between different operating modes was presented by Ref. [97]. Again, a monotonic technique was adopted to operate the PV to the left side of the MPP. The modified power can be obtained by equation (23), and the modified curve is shown in Fig. 24 (b). The P&O-based MPPT-PRC is computationally efficient and does not require sensors or curve-fitting algorithms. The event-triggering signal effectively coordinates between MPPT-PRC and VIC.

$$P'_{PV} = \begin{cases} P_{PV} & V_{PV} \leq V_{MPP} \\ 2P_{MPP} - P_{PV} & V_{PV} > V_{MPP} \end{cases} \tag{23}$$

Similarly, a PV voltage variation-based PRC for a 100 kW system with two modes, the first for MPPT and the second for providing power reserves without employing irradiance and temperature sensors, was presented by Ref. [98]. This PRC provided VIC and primary frequency control with a second synchronous generator technique to address the lack of rotational inertia.

A power tracking control based on the curtailment power-current curve was proposed by Ref. [99], which can automatically track the given reserve ratio in any environmental conditions. When inverter-based PV and wind systems are coupled to a deficient grid infrastructure, frequency changes can be minimised by application of Grid-forming Control (GFC) techniques [5]. Therefore, a model-free GFC for a two-stage PV system was presented by Ref. [100]. In addition to avoiding the estimation of MPP, it has a current limiting scheme that ensures that the current overshoots during faults are contained. The operating mode is selected on the right of MPP to allow the entire power range, but the proposed solution introduces disturbances when operating under transient conditions due to cloud movements. In Ref. [101], a Sliding Mode Control (SMC) based Adaptive Power Point Tracking (APPT) for bidirectional primary frequency regulation (BPFR) of an AC micro-grid was proposed. This technique provides an adaptive power reserve to limit frequency variations by adaptively regulating the sliding mode surface based on locally measured frequency of the microgrid, which does not require any communication channel, a detailed PV model, irradiance sensors, or MPP estimators. A frequency regulation control strategy for single-stage PV was proposed by Ref. [102]. To improve the dynamic and steady-state performance of the PV power tracking process, they proposed an ideal step-size calculation approach based on a flexible power tracking evaluation function that is suitable for left-side operation for creating power reserves. A small-signal model was used to assess the system response, and simulation and experimental analysis confirm the accuracy and efficacy of the suggested primary frequency regulation and step calculation method.

3.6.1. De-loading under partial shading

Partial shading (PS) is more common in building-integrated PV systems in metropolitan environments. It occurs when some parts of a PV

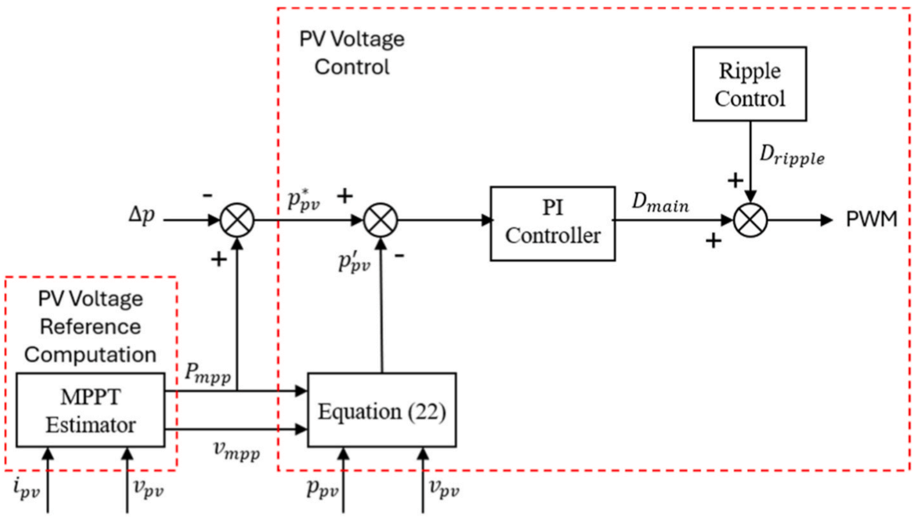

Fig. 23. PRC 6 with modified P-V curve [51].

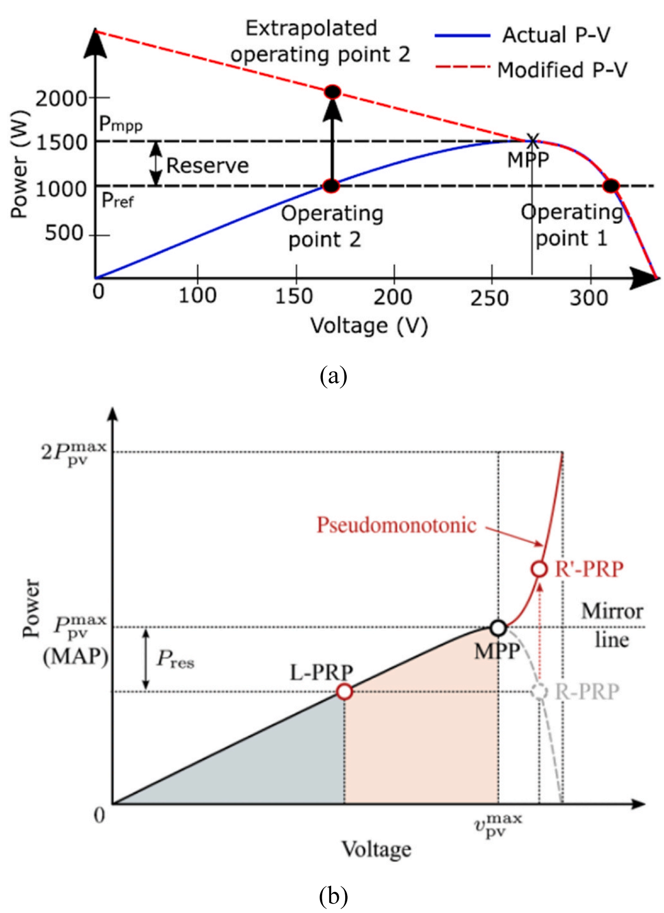

Fig. 24. Modification of P-V curve (a) to operate on the right side [96] (b) to operate on the left side [97].

array receive less sunlight due to obstructions like trees, buildings, or other objects. It is divided into two sub-groups: 1) Static, 2) Dynamic. Static shading is when a specific shadow remains fixed on the PV array for an extended period, like dust accumulation, dirt, bird droppings, etc. Meanwhile, dynamic shading involves shadows that move over the PV array due to changing conditions like cloud movements, swaying branches of trees, etc. When partial shading occurs, the modules in the same array achieve varying irradiance values, which trigger the bypass diodes connected among the modules. This activation produces a staircase I-V waveform, diverting the current from the shaded module. As a result, P-V curves show several peaks rather than just one, as shown in Fig. 25. However, the amount of irradiance levels determines how many peaks are in the P-V curve [103]. Bypass diodes are crucial components to avoid partial shading; if not used, the output power of modules is affected. Another way is to use a microinverter with each module or modify the MPPT of the central inverter. Furthermore [104,105], provided a detailed overview of the effects of partial shading on the power output of different PV arrays. A detailed analysis of MPPT methods used for PS was conducted in Refs. [106–108]. Where [106] classified methods as MPPT optimisation, hybrid algorithms, new modelling approach, and converter topologies. In Ref. [107], four evaluation criteria were used: tracking accuracy, duration of voltage variations, convergence time, and transient efficiency when locating the global MPP. In Ref. [108], these methods were classified as conventional, soft computing, and hybrid techniques. The tracking speed, algorithm complexity, and dynamic tracking under partial shading were critically analysed for each solution.

Different optimisation approaches, such as the Fibonacci series technique [109], ANN techniques, and adaptation of P&O algorithms, were used in these systems. Studying irradiance patterns and hill climbing modification is one of the most current approaches to global MPPT [110]. For the PV system operation on the right or left side of MPP in a multi-peak P-V curve (shown in Fig. 25 (b)), a reserve generation algorithm has been proposed in Ref. [111]. Reference voltages are used in this control to examine the left and right regions of the P-V curve. The number of shaded and unshaded cells in an array determines the generation of these reference voltages. Following inspection of these regions, the system stores multiple MPP values. If Global MPP is located on the right peak region, II is selected for LPPT operation; otherwise, region I is selected. The choice of these areas guarantees operation throughout a broad range of reserve percentages.

In [112], the voltage region was divided into manageable subregions by taking voltage samples from the P-V curve, and the P&O technique was then used to find the precise global MPP value, which reduced the search space for global MPPT. It calculates an upper limit for the array power in each subregion by using a simple curve to approximate the I-V curve of that subregion. The search region of Global Maximum Power Point (GMPP) is then constrained by comparing the observed absolute power values with the estimated upper limits, and the neighbourhood of GMPP is identified using a set of predetermined criteria. A novel global FPPT (GFPPT) was proposed by Ref. [113] to provide constant power control and power reserve control in partial shading conditions. The

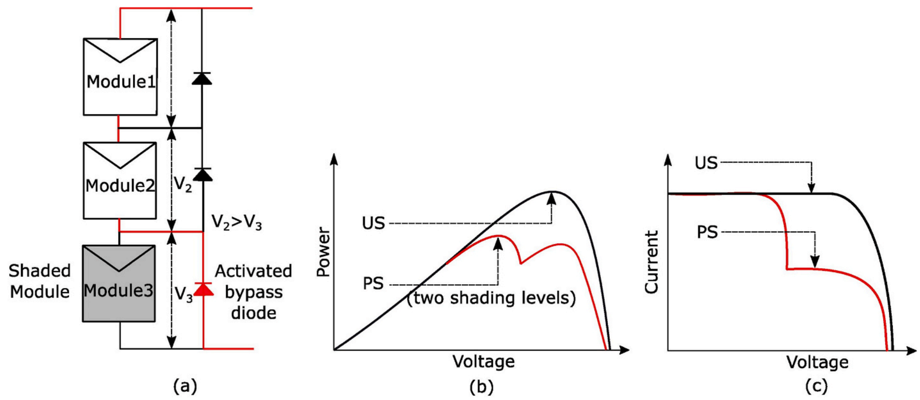

Fig. 25. (a) PV array with shaded module, (b) P-V curve under partial and uniform shading, (c) I-V curve under partial and uniform shading.

study aimed to obtain faster dynamics after detecting any environmental changes, which is achieved by modifying the conventional GMPP to adapt to the proposed GFPPT.

Apart from the problem of local peak blockage, a metaheuristic approach-based solution of dynamically selecting multiple equilibrium points in FPPT was proposed by Ref. [114]. The main control element is the metaheuristic-based optimisation called metaheuristics-assisted efficiency maximising (MAEM) control algorithm. The method consists of nine intricate logical blocks that can operate the system in the right-side region of the global maxima. The control only operates when a PS is detected; otherwise, the system is controlled by an adaptive step enumeration-based control under normal irradiance conditions. Besides, to control the duty cycle of the DC-DC converter for PV under partial shading [115], proposed a control scheme by extending the work of [96]. The converter's duty cycle was controlled by comparing the reference power with the modified power. They extended the pseudo-P-V curve for multiple peaks as shown in Fig. 26.

The least squares (LSQ) curve fitting method estimates the MPPs and inflection points. In this case, the PV curve has four points of interest: MPP1, Inflection Point (IO), MPP2, and the open circuit (OC) point. Depending on the reference power command, the operating point for the necessary power reserve could be between MPP2 and OC or MPP1 and IP. The final curve is selected based on the following equation (24):

$$P'_{PV} = \left\{ \begin{matrix} P_{mod\,1}, (P_{ref} > P_{mp2}) or \ (P_{mp1} > P_{mp2} \ and \ P_{ref} > P_{ip} \ and \ V < V_{ip}) \\ P_{mod\,2}, Otherwise \end{matrix} \right\} \tag{24}$$

Moreover, a de-loaded control approach for a 100 MW PV plant (25 PV units of 4 MW) under dynamic shading was proposed by Ref. [116]. A method based on fractal geometry was used to create the stochastic movement and distribution of clouds and the irradiance over the PV power plant. A compensated P-V curve scan approach was employed to track the MPPs of the de-loaded PV units, which mitigates the natural

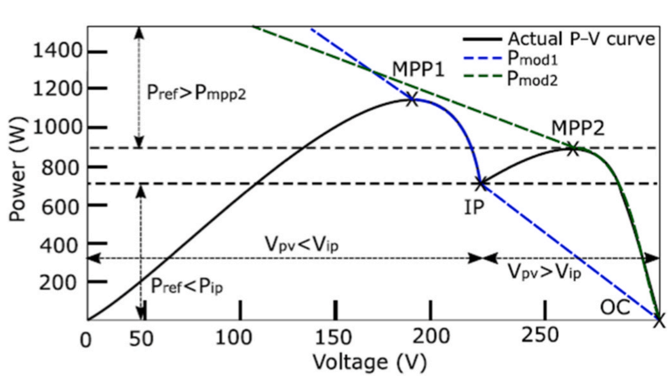

Fig. 26. Modified P-V curve for partial shading scenario [36].

power fluctuations caused by a traditional P-V curve scan approach. The proposed control was efficient and performed well under various cloud coverings. As the irradiance variations can introduce errors in the de-loaded power reference and estimated MAP of the array, the power reference (P_{ref_PV}) as a function of error can be expressed as equation (25).

$$P_{ref\_PV} = P_{ref\_real} - (1 - D_{PV})P_{error\_mpp} \tag{25}$$

Where, D_{PV} is the de-loading factor, P_{mpp_error} is the estimated MPP error, and $P_{ref\_real} = (1 - D_{PV})P_{mpp}$ is the de-loaded power reference without error. As P_{error_mpp} caused by irradiance variation can affect the power margin requested by the system operator, resulting in a difference between real (ΔP_{real_mar}) and estimated (ΔP_{est_mar}) power margins. Therefore, ΔP_{est_mar} as a function of ΔP_{real_mar} and MPP error (ΔP_{error_mpp}) can be expressed as equation (26).

$$\Delta P_{est\_mar} = \Delta P_{real\_mar} - D_{PV} {}^* P_{error\_mpp} \tag{26}$$

A dynamic reserve power point tracking (RPPT) was proposed by Ref. [117], which combines FPPT and MPPT simultaneously. It extracts the MPP information and calculates and regulates the amount of PV reserve power. The effectiveness is demonstrated under grid frequency deviations, changing irradiance, and partial shading conditions. A summary of the methods that were reviewed is given in Table 7.

3.7. Soft computing techniques

This section covers the power reserve strategies that use Artificial Neural Networks (ANN) and fuzzy logic. Some approaches have recommended combining ANN and fuzzy techniques for conducting power reserve in PV systems, while others have only used fuzzy or ANN techniques. In Ref. [119], a novel ANN-based adaptive predictor-corrector MPPT mechanism was employed to track the MPP at different irradiance and temperature levels for a diesel-PV-fuel cell-based hybrid AC microgrid. The $P_{MPP} - V_{MPP}$ The curve in this method is created for a range of temperature values. It is impractical to utilise a single curve to represent a specific temperature because many polynomial equations must be considered to anticipate the MPP precisely. For this reason, the nonlinear mapping of P_{MPP} versus V_{MPP} at different temperatures has been carried out using an ANN. The Levenberg-Marquardt back propagation algorithm is used to train the ANN. The training data consists of six temperature changes and twenty irradiance level changes. Twenty hidden neurons, two input layer neurons ($\frac{P_{PV}}{P_{MPP}}$ and temperature) are inputs, one neuron (V_{MPP}) is the output. Fig. 27 shows the ANN structure. In comparison to the P&O, the proposed method has a shorter tracking time (~0.05 s) which is independent of variations in irradiance.

Furthermore, a neural network-based two and three-peak handling control under partial shading conditions, which is the modification of

Table 7
Summary of the reviewed de-loading methods.

No.	Technique	Control Type	Operating Side of MPP	Shading Scenario Considered?	Method Evaluation	Key Contributions	Limitations
[93]	Storage-less Reserve Generation for Hybrid PV-Rotating Machine	PI-Based Control	Right	No, tested under one low irradiance, but the irradiance level is not mentioned.	Simulations (*on a multi-bus system in IEEE Standard 399–1997 and modified with 12 PVs*) in Power Factory Software	• Considering PV with a large power reserve for frequency regulation is insightful, as PV with less capacity will reach its MPP faster and cannot contribute to frequency regulation. • The PVs considered in the study are 5.385 MW. • The proposed method results in low or little ramping up of the generator for frequency regulation during high irradiance and low load changes, as frequency is stabilised with PVs with more reserve. • During high irradiance change and high load change, the PV reserve is consumed, allowing generators to participate in frequency regulation. • The cost analysis states that the investment cost of PV with 1 MW reserve and battery with 444.445 kW battery is the same, which advocates the usage of de-loaded PV. • The two modes are defined, one with high irradiance where de-loading is fixed, and the second mode, where de-loading varies due to low irradiance.	• The fixed 18 % power reserve can account for more wastage in energy, contributing to increased operational costs that are not considered in the cost analysis. • Their method requires additional PVs to provide the reserve of 1 MW, which resulted in an additional cost of $2,240,000. • In mode 2, the varying de-loading is based on the fixed power reserve required under low irradiance. An approach for adaptive de-loading size is required for more cost-effective operation.
[94]	Active Power-Voltage Matching (APVM) Technique	Controller-based with linear regression and R^2 criterion	Left	No, only tested for irradiance from 800 to 1000 W/m^2	PSCAD/EMTDC Simulation Results	• It can derive the easiest polynomial that predicts V_{dc} using linear regression. A transcendental implicit equation is computationally intensive to solve. • R-squared criterion adoption to determine P_{PV} makes APVM more accurate. • The proposed 3-layer control provides the online adaptive PV active power response to frequency fluctuations. • The APVM technique has a minimal error when observing the corresponding change of the P_{PV} and V_{dc} during frequency fluctuations under 1000 W/m^2.	• During changing irradiance and temperature, the PV mathematical model needs modifications that can be more complex, time-consuming, and require more computational effort. • The proposed approach is prone to errors when non-uniform irradiance occurs because the P-V curve is calculated inaccurately. • The development of APVM for a shaded PV system is for future work. • The testing under real-world scenarios remains to be thoroughly tested. • Under 800 W/m^2, the APVM is not accurate and P_{PV} and V_{dc} fluctuates, and it has a long steady state time.
[95]	Variable Droop Control and DC-link Based De-loading	PI-Based Control	Right	No, tested under varying irradiance and temperature from Lookup Tables	DIgSILENT/Power Factory Simulation Results	• The combination of DC-link control and de-loading control unleashes the full power of the PV system to support frequency deviations. • The additional reserve from de-loading helps to decrease. f_{nadir} which improves the microgrid's ability to maintain power balance and prevents load shedding. • The variable droop control strategy dynamically adjusts the frequency regulation ability under various working conditions, as real-time active power and reserve capacity vary dynamically.	• Secondary frequency control is not considered due to its ability to reschedule active power set points in a relatively long time. • Using a lookup table consumes much memory, especially if it has fine-grained coverage of many input parameters. • The efficiency will be affected due to extrapolation issues where the operating conditions are outside the lookup table data, as the behaviour on those new operating points is unknown. • A study for adaptive de-loading percentage based on frequency deviation is required, as

(*continued on next page*)

Table 7 (*continued*)

No.	Technique	Control Type	Operating Side of MPP	Shading Scenario Considered?	Method Evaluation	Key Contributions	Limitations
						• The simulation results show that the proposed DC-link method helps reduce f_{nadir} from 49.292 Hz to 49.335 Hz. The simultaneous control also performs better with f_{nadir} improving from 49.317 to 49.496 Hz while maintaining DC-link voltage and frequency.	a fixed 10 % de-loading is currently implemented. • The inertia support is limited due to the limited capacity of the DC-link.
[96]	A Monotonic Curve-Fitting-Based Power Reserve	PI-Based Control with Levenberg-Marquardt Algorithm (for curve-fitting)	Right	No, Tested Under Different Irradiance Levels	MATLAB/Simulink and Hardware Testing with JTAG Emulator (TMS320F28335) by Texas Instruments, for data transfer	• The least square curve-fitting on non-simplified SDM is applied on voltage and current measurements to obtain real-time MPP voltage and power while operating at a suboptimal point. It estimates MPP and the five parameters of SDM, providing all PV properties (P-V and I-V curves). • It allows for maintaining power reserve from nearly 0 % to 100 % of MPP, providing the entire operating range. • The reference parameters are calculated using the explicit method [118] on a measured I-V characteristic obtained through a curve scan. • A single PI controller regulates power rather than voltage to operate at the desired power value given by an external command. • A ripple control method controls the power fluctuations at appropriate levels (less than 1 %), facilitating the curve fitting under any condition by ensuring an appropriate measurement window. • The MPP efficiency is greater than 99 % at MPP with a ripple level of 2–3 % during rapid environmental conditions and noise, which are adequate. • The stability is analytically assessed, and simulations for a 2 kW PV system were carried out, which advocates the effectiveness under normal and varying irradiance conditions.	• The curve scan is required once per month or year for crystalline PV modules, and it might be different for some other types. • The proposed method might have limited handling of non-monotonic regions during partial shading conditions. • The full SDM model parameter estimation via curve-fitting can be computationally intensive for real-time embedded systems with limited processing power, possibly affecting responsiveness. • The approach assumes that the device can handle the ripple control perturbations without adverse effects; this might not always be true in all hardware configurations. • The scalability from 2 kW to a large-scale system might introduce complexity in controlling and have an increased impact on measurement noise, affecting the effectiveness by reducing the efficiency of MPP estimation. • Frequency stability using the proposed approach is not considered.
[97]	Event-Triggering VI Control with Power Reserves	PI-Based Control	Left	No, Tested Under Different Irradiance Levels	StarSim Real-Time HIL	• A P&O MPPT is adopted to measure the maximum available power, and event-triggering avoids heavy computational algorithms like curve-fitting or empirical models. • It does not require hardware modifications, enhancing its widespread adaptation feasibility. • During the MAP measuring, P&O-MPPT generates transient power pulses, which have been dampened by transient power damping control (TPDC) implemented in DC-link voltage control. • The event-triggering enhances the stability and responsiveness of virtual inertia	• The MPPT-PRC assumes that during cycle transition, irradiance does not change drastically, which can affect the accuracy of the MAP calculation. • Despite event-triggering, rapid or frequent switching might cause control instability, primarily if frequency disturbance occurs near the trigger threshold. • The TPDC smooths out the PV power output, but it can cause fluctuations in the DC-link voltage. • The speed of MAP measurements and control switching inherently limits the VI emulation response. • Scalability to large systems with multiple units can cause synchronisation and

(*continued on next page*)

Table 7 (*continued*)

No.	Technique	Control Type	Operating Side of MPP	Shading Scenario Considered?	Method Evaluation	Key Contributions	Limitations
						provision by switching between operating modes. • The power reserve operation and frequency support are decoupled, which prevents conflicts and potential instabilities. • The hardware-in-loop validation demonstrates the strategy's real-time performance and robustness.	communication challenges, particularly in VI emulation.
[98]	A Novel PRC with Hybrid Inertia Response	PI Controller Based	Right	No, Tested Under Different Irradiance Levels	MATLAB/Simulink	• A monotonic P-V curve is used to limit the operation on the right side of the MPP. • A novel PRC method employing voltage variations without additional sensors to manage power reserve. • A droop gain-based primary frequency response is employed, common in some PFC research and hydropower plants. • The hybrid approach considering SG with VIC represents a significant step toward restoring the grid's inertial characteristics lost due to high PV penetration. Moreover, it can facilitate the retrofitting or gradual system upgrades. • The strategies are tested in different grid configurations (interconnected and isolated), increasing versatility for various deployment contexts. • The simulation results validate the proper operation, fast response, and efficiency of generating power reserves.	• The cascaded frequency disturbance events, which can arise due to transient states, are not considered. • PRC technique relies on PV voltage variation detection; any measurement noise or latency can significantly affect the control precision, leading to undesired switching or power fluctuations. • A further investigation is required for mode switching, which might induce switching transients and harmonics affecting power quality. • A fixed power reserves of 10 % and 20 % are used in test scenarios; approaches for adaptive reserve generation may be more feasible.
[99]	Curtailment P-I Curve Tracking Algorithm	Algorithm Based	Right side of P-I Curve (left side of P-V curve)	No, variable irradiance conditions verified	RT-LAB Semi-Physical Simulation	• The proposed PRC method has a max tracking error of 0.008 and tracking time of 0.16s, which shows good tracking accuracy and speed when T and I are fixed, and the reserve ratio varies. • When T is fixed and the reserve ratio and I are varied, the max tracking time is 0.21s, and the steady-state error is 0.0014. • When T, I, and reserve ratio are varied, the system showed a maximum steady-state error of 0.013 and tracking time of 0.2s. • When the PV plant participates in frequency regulation, the maximum frequency deviation is 0.19 Hz, and the RMSE is 0.0891 Hz. • Overall, the control strategy is reliable, fast, and accurate.	• The proposed method verified the results in changing irradiance conditions, but the system may have limitations during shading conditions. • The validation for a large-scale PV system can be done, as a small-scale system might not have the same level of complexity. • The steep nature of the P-I curve can make the control process susceptible to noise, particularly under high irradiance conditions. • The steep nature of P-I can lead to stability issues in current tracking. • In rapid environmental conditions, the accuracy of power reserve estimation may be challenged.
[100]	Model-free GFC with Current Limitation Mechanism	PI Controller Based	Right	No, tested for irradiance from 500 to 1000 W/m^2	MATLAB/Simulink Simulations (Electromagnetic Transient (EMT) simulation mode	• The proposed GFC techniques do not require real-time estimation of MPP by using the P&O algorithm and make optimal use of the limited power reserve. • The control strategy works in two modes: i) GF mode (de-loaded PV), where the DC-link voltage is regulated, and ii) Limited GF mode, where MPPT is executed to extract maximum power from PV. It is activated	• The proposed schemes introduce disturbances resulting from cloud movements. • The impact of partial shading was not considered, but it can enhance credibility and reliability under all scenarios. • Dynamic interaction between GFC and GFL inverters and the rest of the power system at

(*continued on next page*)

Table 7 (*continued*)

No.	Technique	Control Type	Operating Side of MPP	Shading Scenario Considered?	Method Evaluation	Key Contributions	Limitations
						when the operating point overtakes the MPP. • The current limitation schemes incorporated in the GFC method effectively reduce current overshoots, reducing the risk of damage to the inverter. • The proposed strategy works with different converter sizes and voltage levels if a two-stage system exists. • The proposed method has been tested for various generation mixtures with GFC and GFL inverters at the WSCC 9-bus testbench. • The modelled PV plant is 105 MW nominal capacity, with 30 MW of power reserves. • The simulations used future-dominated power systems, where SMs (a detailed 7th-order model) and GFC were used on the testbench WSCC 9-bus. • Replacing SMs with GFC improved frequency profiles during load disturbances due to fast response from PV.	various sizes and generation mixtures is a future work. • An appropriate ratio of GFC and GFL in converter-dominated power systems is required, which would be very useful.
[101]	SMC-based Adaptive Power Point Tracking	PI Controller Based	Right	No, tested under varying irradiance	MATLAB/Simulink (Electromagnetic Transient (EMT) simulation mode)	• The proposed method provides both up and down regulations (bi-directional regulation) during disturbances by analysing the P-V and $\frac{dP_{pv}}{dV_{pv}}$ characteristics of the PV array. • No mathematical models, sensors, or MPP estimators are required; it only relies on the local frequency measurements, simplifying implementation. • The droop curve based on $\Delta S - f$, where ΔS is the regulating term on the sliding surface for creating reserve, is used for adaptive frequency regulation. • The conventional droop adjusts the output within a known power adjustment range based on frequency measurement, while the proposed droop control adjusts the ΔS based on frequency variation, which affects the PV output power. • Two factors determine the value of ΔS: i) the amount of reserve when the system frequency is within the dead zone of the nominal frequency, and ii) frequency deviation from the nominal frequency to mimic droop characteristics. • When $\Delta S = 0$, MPP operation, and when $\Delta S < 0$, power reserve mode. • Generally, their strategy allows the system to operate in power reserve mode when the frequency fluctuates between f_{min} & f_{max} to provide frequency regulation. • The local control eliminates the need for a central system operator, improving	• An improved strategy to track the global MPP can be adopted for partial shading scenarios. • The effectiveness heavily relies on the accurate frequency measurements, which can be challenged under fast transient conditions. • The proposed method needs improvement to more effectively regulate output power in response to frequency deviations, as p_{pv} vs $\frac{dP_{pv}}{dV_{pv}}$ It could have different characteristics based on irradiance and temperature, making it challenging to create an adequate power reserve. • Implementing real-world scenarios may still present challenges, particularly in varying environmental conditions.

(*continued on next page*)

Table 7 (*continued*)

No.	Technique	Control Type	Operating Side of MPP	Shading Scenario Considered?	Method Evaluation	Key Contributions	Limitations
						reliability and reducing single-point failure risks. • Small-time-step EMT simulations are adopted instead of extensive steady-state simulations to reflect the actual physical system performance. Moreover, instead of averaged models, detailed switching models are adopted. • The tests were conducted with 30.23 %, 46.43 %, and 72.22 % power generation from PV out of the total generation capacity of the microgrid. • The proposed APPT has the same frequency regulation performance in irradiance and load changes.	
[102]	FPPT-based Optimal Step Size Calculation Method	Algorithm Based (Variable Step Size Tracking Algorithm)	Left, but can operate on the Right	No, different irradiance levels are tested.	MATLAB/Simulink Simulation (to verify FPPT strategy and system stability) Experimental Validation (dSPACE)	• The fitted function using Linear regression accurately predicts the minimum DC voltage. • The variable step-size tracking algorithm enhances the tracking speed. • The system can quickly adjust to power demand and environmental conditions, improving stability and efficiency. • The proposed method applies to both single and two-stage PV systems. • The system response time is 0.3s–5s.	• Does not provide low-frequency regulation support. • The responsiveness under rapidly changing conditions may be affected by longer tracking times than the right-side operation. • The proposed control strategy can be affected by local shadows.
[111]	P-V Curve Scanning-Based Deloading Strategy for Power Reserves under PS Conditions	PI Controller and Reserve Generation Algorithm Based	Left & Right	Yes	MATLAB/Simulink (*solver: variable step, ode 23 t,* max *step size: 1e-4, relative tolerance: 1e-3*) and hardware setup using dSPACE DS 1104. MECO 9009 Solar Module Analyser (to get multiple peak P-V curve	• To provide power reserve in Partial Shading (PS), this approach only scans over the generated reference point, avoiding the blind scanning of the whole P-V curve, and it is tuned to work on both the left and right sides of MPP. • This method indicates the operating region on P-V before the occurrence of PS, which is detected using the PV voltage. The shaded module has a lower voltage than the other, and PS is detected when the difference between the two PV modules' voltage exceeds a threshold value. • The location of the last operating point was detected by PV voltage, if $V_{pv} < 0$ last operating point was on the left, and vice versa. • The proposed steps to trace the MPP of left and right peaks help reduce scanning time and energy losses. The left and right peaks are identified by comparing their voltages. Higher voltage means right and vice versa. This comparison is summarised in equation (2). • GMPP is traced by comparing the power values of both MPPs; the existence of GMPP decides the region of de-loading. If dP exceeds the set threshold, GMPP changes, and then GMPP tracking reoccurs.	• The strategy is designed for only two peaks and might be ineffective if the P-V curve has more than two. In a large-scale system, there must be many peaks, so handling those peaks would be challenging. • The fixed reserve commands of 20 % are used, which are not suitable for PS scenarios. An adaptive reserve generation based on frequency droop may be more beneficial, especially when considering large-scale implementations. • The control for reserve generation assumes that PV has static shading, and a fixed reserve percentage is given, which is unsuitable for PS. • Upon detection of PS, GMPPT is located by scanning the P-V curve, which generates oscillations. Without first scanning, the detection of local and global peaks is impossible. A more robust solution is required to find the global and local MPPs. ANNs can be used, but they need accurate data, which can increase the cost by installing new sensors. • Frequency stability is not considered in this approach.

(*continued on next page*)

Table 7 (*continued*)

No.	Technique	Control Type	Operating Side of MPP	Shading Scenario Considered?	Method Evaluation	Key Contributions	Limitations
						• The root locus diagram analyses the stability of the PI controller. • The overall simulation results indicate the effectiveness of the proposed strategy for generating power reserves in PS conditions.	
[112]	I-V Curve Approximation Based on GMPP Tracking	PID & PI (*for single voltage loop control*) Controller with Proposed GMPP Algorithm	Left (*during the search process*)	Yes	Simulation (*PV module is YL70P-17b 1/2*) and Experimental (*ARM Cortex-M4 32-bit processor-based control unit*) Results	• A GMPPT approach is presented, which is based on dividing the voltage range into subregions and then approximating the I-V curve of the array in each subregion using a simple curve. • The modified I-V curve approximation is below the constant current curve, which takes less time to get the GMPP (3–4 samples) and has a smaller upper power limit than the constant current curve, which takes longer to get the GMPP. • This method does not assume that the peaks are at integer multiples of V_{oc} orI_{sc} as some studies have claimed, it is robust against non-uniform shading patterns and module mismatch, a common challenge in the PS condition. • The search regions for GMPPT are named candid subregions, which are limited by a condition when the upper power limit is greater than the maximum power. • The algorithm guarantees that GMPP is located within known voltage intervals by analysing the search space and defining candid subregions. • The simulation and experimental results show that the proposed method pinpoints GMPTT with 0.42 s tracking time, with a small margin of error, and with total energy loss of 81 J.	• The search region is defined based on V_{oc} which makes the method insensitive to module mismatch, but inaccuracy in measuring V_{oc} can limit the effectiveness. • The method is based on a static shading pattern; effectiveness might be reduced during rapid changes in shading or a new shading pattern. • While the method is insensitive to module mismatch, its applicability to large-scale PV systems is uncertain. • The frequency regulation is not considered. • The method reduces the sample count, but dividing the voltage range into subregions, approximating them, and estimating the upper bound can introduce computational overhead.
[113]	Global FPPT Strategy for Power Reserve	Algorithm Based	Left and Right (*Based on the sign of the slope*)	Yes	Experimental Results (*Regatron TCACS 4-quadrant Grid Simulator, Regatron TopCon Quadro Programmable Power Supply as PV simulator)* dSPACE 1006	• The proposed approach is the combination of constant power control and PRC, which can be implemented to PV arrays with any no. of local MPPs. • This method does not rely on any optimisation or intelligent algorithms; it is easier to implement and offers computational superiority over existing solutions in real-world systems. • A conventional search-skip-jump GMPPT is modified to find GMPP in partial shading conditions. • This method is implemented on a two-stage system, but can be implemented on a single stage, where the proposed GFPPT calculates a voltage reference for the DC-link of the inverter. • When moving the operating points from GMPP to below Local MPP, a flag is used to help the algorithm not get stuck at the	• A constant voltage step is employed, which can take longer to track GMPPT. An approach to implement an adaptive or variable voltage step is required. • The stability and robustness in highly variable environments or system faults remain potential challenges that have not been tested. • The paper mentioned that the proposed method can be implemented for many peaks, but the scalability to large arrays with complex shading patterns needs further validation.

(*continued on next page*)

Table 7 (*continued*)

No.	Technique	Control Type	Operating Side of MPP	Shading Scenario Considered?	Method Evaluation	Key Contributions	Limitations
						section divider (left local peak). The sign of R (slope) is changed at this point, and the algorithm will oscillate around this point if the flag is not used. • The experimental analysis using a 2.5 kW system validates the adaptability of the proposed method during PS conditions.	
[115]	Least-Squares Curve Fitting-Based Active Power Reserve for PS	PI Controller-Based (Power Control)	Right (*referred to as downhill points*)	Yes (for three peaks by monotonic relation)	MATLAB/Simulink & Experimental Tests (2kW *PV System*)	• The least-squares curve fitting algorithms (*using Levenberg-Marquardt)* have been employed on voltage and current measurements to estimate MAP and shading conditions that do not rely on irradiance and temperature sensors. • A multipeak P-V curve is modified to allow the power PI controller to track power setpoints quickly and effectively. • A P-Q control is applied to maintain a constant DC-link and proper energy flow to the grid. • The sampling and ripple control are used to limit the oscillations around the operating point, and a notch filter is used to filter the voltage and current to get the non-oscillating values, which are used in the new curve ripple metric and in the central control for tracking reference values. • The MPP scan per shading event reduces the spikes in power, which are more apparent in the MPPT algorithm performing frequent MPP estimation. • When the shadow extent crosses a specific limit, a curve scan is done, one per shading event, because currently, its intensity is unknown, so a wider range of variations around operating points is done to capture the entire P-V curve. • The robustness and effectiveness of the proposed strategy are tested on a 2 kW PV prototype. • Results show that the proposed algorithm works well even in fast changes in irradiance and shading conditions, and the grid-side power does not have noticeably high-frequency ripples.	• The monotonic relation derived does not count the power conversion losses, even though they are small; they can have an impact while maintaining reserves. • The proposed method is designed for two irradiance levels; hence, future work will be focused on three or more irradiance levels with more complicated shading scenarios. • The reserves have been generated, but their utilisation for the ancillary services is left as a future research topic. • A more sophisticated approach for smoothing the short-term spikes in power output.
[116]	Compensated P-V Curve Scan	Algorithm Based	Left & Right (de-loaded mode)	Yes, Dynamic Shading	Non-linear time-domain Simulations on MATLAB/ Simulink (*ode 23s solver, step size of 0.01*) & Hardware Testing	• One of the multiple innovative contributions is defining the reference power for de-loaded PVs as a function of the de-loading factor. • The control stages of the proposed method make it more accurate and robust for estimating MPP under cloud movements. • The irradiance variations have been identified by measuring the PV array voltage of unloaded PVs.	• They did not consider frequency regulation; they focused only on estimating the MPP in cloudy conditions to create an appropriate reserve. • The proposition and assessment for frequency and voltage control approaches for large PV power plants operating under dynamic shading is future work. • Fractal-based cloud modelling and per-unit MPP tracking require significant processing

(*continued on next page*)

Table 7 (*continued*)

No.	Technique	Control Type	Operating Side of MPP	Shading Scenario Considered?	Method Evaluation	Key Contributions	Limitations
						• Robust MPP estimation achieves a root-mean-square error of the proposed method that is less (169.55 MW, <2 %) than that of the conventional DPC technique (446.73 MW, 8 %). • Using a fractal-based approach to generate stochastic solar irradiance allows for a more realistic simulation of cloud movements and their impact. • The capacity to provide ancillary services associated with active power regulation was assessed using a stochastic power reference signal.	power. Scaling to plants with >100 PV may be challenging in real-time control systems. • The performance of two-stage systems, common in distributed generation, remains untested. • Aggressive de-loading with single control can destabilise the DC-link voltage control loops.
[117]	Dynamic Reserve Power Point Tracking (RPPT) – A Curve Scanning Approach	Controller Based	Left & Right (Dynamic Curve Scanning)	Yes, Partial Shading	Simulation & Hardware Testing	• The proposed method provides power reserve control while injecting the desired power into the grid. • It is the successor of FPPT/MPPT, as it does not require complex MPP estimations or additional sensors. • It can regulate the dispatchable power reserve under all operating conditions, especially partial shading. • It is immune to PV panel ageing and faults as it does not rely on the characteristic model of the PV curve. • The voltage resolution of 1V has less than 2 % error, considering a 60V MPP. • It can easily be retrofitted on existing PV panels.	• High-frequency scanning can cause computational load. • The large scanning frequency size produces more current and thermal stress on the DC-link. • The voltage resolution size can limit the accuracy of MPP determination.

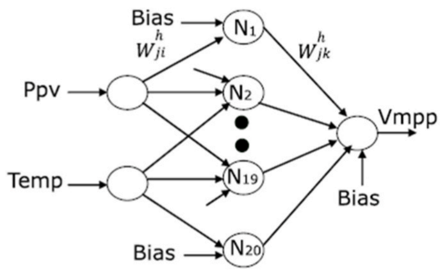

Fig. 27. ANN structure [119].

[111], was proposed by Ref. [120]. The neural network was trained using Lavenberg-Marquardt back propagation algorithm with a sample dataset producing two or three peak and the mean square error analysis assessed the performance. Seventy percent of the 375 dtasets utilised were for training, and 15 % were for validation, and 15 % for testing. The ANN was accurately tuned, as evidenced by the voltage and power error percentages of 1.055 % and 0.6677 %, respectively. After achieving a satisfactory level of training, the network can accurately predict the voltage and power values of three MPPs on the P-V curve (Fig. 28 (b)) based on the irradiance patterns. The system was then operated on limited power points based on the position of the global maxima using these values. Region II and I were chosen in the same manner as previously stated; however, region III was chosen if a global maximum is seen on the middle peak.

A power reserve strategy for a 100 kW two-stage three-phase PV system based on an ANN model using the Newton-Raphson method was developed by Ref. [121] and shown in Fig. 29. Where $I_{PV(k)}$ is I_{PV} in kth iteration, $V_{PV(k)}$ is the V_{PV} in the kth iteration, ΔV_{PV} is the increment. By changing the temperature from 5 °C to 55 °C and irradiance from 50 to 1000 W/m^2, 146 input-output datasets were taken to create the model. The Levenberg-Marquardt algorithm trains the ANN model, with 15 % of the training data reserved for validation and the remaining 15 % for testing.

After using a MATLAB simulation tool to realise and simulate the proposed strategy, the system was tested in various climate conditions to confirm that the proposed strategy produces and ensures the necessary power reserve in various climate conditions without compromising system stability.

In [122], a Neural Network (NN) based FPPT control was developed to create a power reserve for a two-stage PV system. A set of neural network blocks in MATLAB determines the point of operation for FPPT. In this control system, ANNs were trained to provide the regulated reference voltage for the FPPT operation. The simplified control scheme is depicted in Fig. 30, which shows that the temperature, irradiance, and power reserve ΔP were used as inputs to train the ANNs, where temperature and irradiance were measured using sensors and ΔP was calculated using frequency regulation control. To accurately train the ANN, 1000 randomly generated input and output values were used for training. While the output was generated using a simple algorithm, wherein the system was operated on V_{MPP} if the P_{ref} is above the P_{MPP} or operates on V_{ref} otherwise. The proposed frequency control method had response time within 1 s of the contingency.

A novel methodology based on multiple linear regression analysis (MLRA) to estimate the appropriate de-loading percentages for PV systems was proposed by Ref. [123]. They used a fixed incremental de-loading percentage (0.25 %) to create a power reserve, which was decided after several trial-and-error simulations. They also mentioned the different levels of de-loading for different levels of RE penetration because higher penetration results in lower de-loading levels. They went up to 60 % of RE integration and values of variables (RoCoF, f_{nadir}, and de-loading) were in limits. The de-loading percentage was determined to be 9.976 % in the 20 % PV penetration example, and all metrics were within range with the exception of f_{nadir}, which deteriorates when PV support was inadequate. In cases of 30 %, 40 %, 50 %, and 60 % PV penetration, the necessary de-loading was determined to be 7.283 %, 6.536 %, 6.335 %, and 5.694 %, respectively. This indicates that as the overall amount of de-loaded PV support increases, the proportion of de-loading reduces. According to additional validations, the projected de-loading percentage outperforms BESS with the same support size and maintains f_{nadir}, and RoCoF within acceptable range. Table 8 summarises the reviewed methods.

3.8. *PV inverter control strategies*

This section briefly discusses the primary inverter control techniques that have been developed and applied to address these challenges. The specific details of these inverter control strategies are beyond the scope of this paper; their presence and influence on the overall system are implicitly considered in the context of the DC-DC stage methods mainly discussed in the preceding sections. The DC-DC stage's primary job is to extract maximum power from the PV array. The inverter is responsible for converting DC power to AC and plays a critical role in the overall system's stability and grid interaction, particularly in supporting grid frequency. It serves as the interface between the DC-link and the AC grid, and its control strategy plays a vital role in ensuring stable power transfer, high power quality, and compliance with grid codes. Modern power grids are designed to operate within a tight frequency range, and deviations can lead to instability. Consequently, the inverter's control strategy is paramount for providing ancillary services. There are many control strategies, each with its advantages.

For instance, Voltage-Oriented Control (VOC) is a widely used method that provides decoupled control of active and reactive power, making it a robust choice for grid-connected systems. This control is divided into an inner current loop and an outer voltage loop, where the outer voltage loops generate a current reference for the inner current loop, and the voltage is controlled based on the output of this loop. A virtual inertia control with a current controller operating in rotating reference frames (d-q frames) was designed by Ref. [54], where the DC-link capacitor was controlled by employing VOC to provide the virtual inertia. The d-axis current and q-axis current are decoupled,

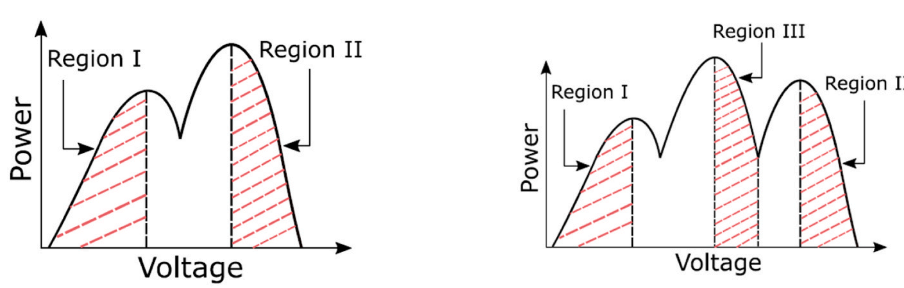

(a) Two Peaks (b) Three Peaks

Fig. 28. P-V curves with multiple peaks under a partial shading scenario [36].

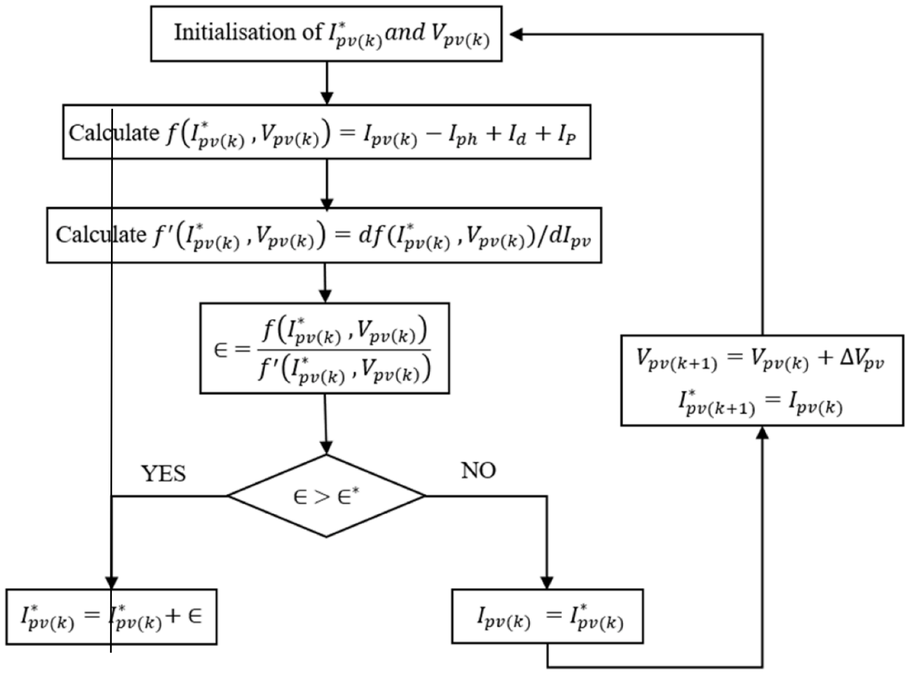

Fig. 29. Newton-Raphson Algorithm for determining the I-V characteristics of a PV.

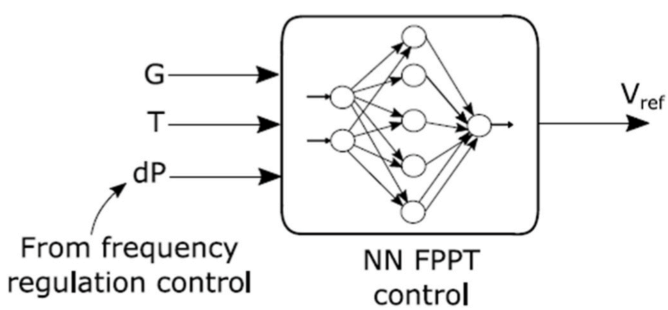

Fig. 30. Simplified depiction of NN-based FPPT control [36].

which allows the inverter to inject the active power from PV and provide reactive power support to help stabilise the grid's voltage. Likewise, a cascaded VOC with dual-capacitor control (as shown in Fig. 12) was utilised by Ref. [58] to control the DC-link capacitor to stabilise the voltage after f_{nadir} event. To achieve the MPPT for a 250 kW PV and inverter control without DC-DC stage a single stage three-phase structure was presented by Ref. [124]. For this purpose, a Fuzzy Sliding Mode Controller (F-SMC) with VOC was designed, where the reference voltage generated by the modified INC-based MPPT was fed as a reference signal to the DC-link controller. This resulted in THD of 2.48 % when using only the L filter and the response time with F-SMC was reduced to 0.01s from 0.12s compared to only modified INC. A frequency domain analytical model was proposed by Ref. [125] to analyse how real and reactive power coupling affect forced oscillations caused by an oscillating power reference (p_{ref}) from the MPPT of voltage-oriented vector control PV inverter connected to weak power grids. Bode plots of the proposed frequency domain model were used to investigate the magnitudes of forced oscillations brought on by various control parameters. Their cascaded control consisted of DC-link control, outer power control loop and inner current control loop in SRF. Fig. 31 represents the block diagram of their proposed strategy.

Direct Power Control (DPC) offers a more intuitive approach by directly controlling the instantaneous active and reactive power without relying on inner current loops. While having fast dynamic performance and simple control implementation when compared to other methods, it may nonetheless result in variable switching frequencies, which may lead to higher Total Harmonic Distortion (THD). A cascaded control comprising DPC and Vector Current Control (VCC-DPC) for three-phase VSI in SRF through active and reactive powers was presented by Ref. [126]. The proposed approach performs better when considering the slow dynamics of PLL since Park transformation and PLL are not present, and it resulted in a lower computational load than the traditional VCC. The synchronisation of the VSI to the grid was achieved by employing direct power computation instead of a PLL, as shown in the control structure of their proposed method in Fig. 32.

To improve the power quality, a dual-topology control scheme was proposed by Ref. [127] where a Simplified Super-Twisting Algorithm (SSTA) with PI was used to extract maximum power from PV and DPC was employed on a three-level neutral point clamped (NPC) inverter. The modified Space Vector Modulation (SPV) and PLL were used with DPC to regulate active and reactive power injected into the grid. Additionally, a Shunt Active Power Filter (SAPF) was integrated into the system to specifically address the power quality issues, such as THD, reactive power compensation, when supplying a non-linear load. The control structure of their proposed technique is shown in Fig. 33. The instantaneous active and reactive power of the system was expressed as (27) and (28) were used to estimate the shunt active filter's control voltages.

$$\frac{dP}{dt} = -\frac{R_g}{L_g} - \omega Q + \frac{U_g^2}{L_g} - \frac{U_g}{L_g}\nu_{ld} \quad \frac{dQ}{dt} = -\frac{R_g}{L_g}Q + \omega P - \frac{U_g}{L_g}\nu_{ld} \tag{27}$$

$$v_{fd}^* = v_{ld}^* + R_f i_{fd} + L_f\frac{di_{fd}}{dt} + L_f\omega i_{fq} \quad v_{fq}^* = v_{lq}^* + R_f i_{fq} + L_f\frac{di_{fq}}{dt} - L_f\omega i_{fd} \tag{28}$$

More advanced methods like Model Predictive Control (MPC) are also being increasingly explored for their ability to handle system constraints and optimise performance across various operating conditions. A decentralised control strategy for PV and BES-based DC microgrids was presented by Ref. [128], which enables cooperation among all sources without the need for communication. The core innovation was a Finite Control Set Model Predictive Control (FCD-MPC) strategy specifically designed for the grid-forming PV units. This approach is tailored

Table 8
Summary of the reviewed soft computing methods.

No.	Technique	Control Type	Operating Side of MPP	Shading Scenario Considered?	Method Evaluation	Key Contributions	Limitations
[119]	ANN-based Adaptive Predictor Corrector MPPT	Neuro Fuzzy Logic Controller	Right	No	MATLAB/ Simulink Simulations	• A significant advancement is using a neuro-fuzzy controller to coordinate PB with other generators (diesel and fuel cells) for transient and steady-state frequency regulation. • The Levenberg-Marquardt algorithm is used to train the ANN. • The adaptive nature of neuro-fuzzy systems during changing conditions improves the response accuracy and robustness over conventional control methods. • The adaptive neural network-based MPPT accurately predicts the MPP across varying conditions and addresses the limitations of static polynomial-based MPPT techniques. • It provides a quick and accurate tracking of the MPP. • The proposed method has a short tracking time (~0.05 s) compared to the P&O method. This tracking time is irrespective of the irradiance changes. • The demand response incorporation broadens the system's flexibility, which allows for enhanced frequency regulation and load balancing without additional storage.	• Implementation of an ANN for tracking may introduce system design and maintenance complexity. • The method required extensive training data for the ANN, which may not always be readily available, especially in varying environmental conditions. • It is highly dependent on the accurate measurement of temperature. • Integrating a neuro-fuzzy controller with a neural network-based MPPT increases the complexity of the overall system. • It mentioned life cycle aspects, but a detailed techno-economic analysis could further substantiate the feasibility and cost-effectiveness of the proposed scheme, especially when scaling up.
[120]	ANN-Based Power Reserve Strategy	PI Controller and Levenberg-Marquardt back propagation algorithm (for training ANN)	Left & Right	Yes, Dynamic Shading	MATLAB/ Simulink & dSPACE DS 1104. MECO 9009 Solar Module Analyser (to get multiple peak P-V curve	• A three-layer feed-forward ANN-based reserve generation technique to handle the dynamic shading is proposed, where the ANN is trained on multiple irradiance patterns by keeping the temperature constant, resulting in two or three peaks on the P-V curve. • The ANN has been used to estimate the system MPPs with various combinations of irradiance, while the reference power is obtained from droop control. • The PS is detected based on the difference between the irradiance of two modules exceeding the threshold level. Voltage values can achieve this, but irradiance values have been chosen for the ANN. • The input layer has four neurons (irradiances), 6, and 30 neurons in the hidden layer, which are decided based on error values attained during the training process. • ANN is trained using the Levenberg-Marquardt back propagation algorithm, which evaluates performance using mean square error analysis. A total of 375 datasets have been used, 70 % of which are used	• ANN is trained by keeping the temperature constant, while temperature also significantly affects PV performance. The proposed technique might not cover the full dynamics during temperature changes. • The efficiency of MPP estimation depends upon the no. of datasets. A large dataset is required to cover more dynamics, which can increase computational costs. • The strategy depends on the assumption that modules are completely shaded. • Due to wide variations in the dataset values, some samples have voltage and power percentage errors of more than 10 %. • A fixed reserve ratio of 20 % is used; an adaptive reserve generation algorithm might be more useful, especially when applied to large-scale systems, as it can count towards the up-regulation cost.

(continued on next page)

Table 8 (*continued*)

No.	Technique	Control Type	Operating Side of MPP	Shading Scenario Considered?	Method Evaluation	Key Contributions	Limitations
						for training, 15 % for validation, and 15 % for testing. • The error percentages for voltage and power are 1.055 % and 0.6677 %, respectively, indicating that the ANN is precisely tuned. • The operating region is selected based on the GMPP location. If it is left, then the left side is chosen and vice versa, but if GMPP is on the middle peak, then the right side is chosen, and reference power point tracking will work until inflection points arrive. • The convergence speed of their strategy is 0.8 s.	
[121]	Newton-Raphson-Based ANN Model for Power Reserve	PI-Based Controller	Right	No	MATLAB/ Simulink	• An ANN-based power reserve strategy for a two-stage three-phase 100 kW PV system. • The Newton-Raphson method is used to determine the I-V characteristics of the PV by using I_{pv} and V_{pv}. • The ANN is composed of three layers, the input layers are temperature and irradiance, and P_{mpp} is the output layer. The hidden layer contains several neurons determined by observing error values during the training process. • The model is formed by 146 input-output datasets with temperature and irradiance variations from 5 ° to 55 ° and 50–1000 W/m^2 15 % of the data has been used for training and 15 % for testing.	• The dataset might not be enough to capture the full PV characteristics, especially during rapid changes and PS scenarios. • Using these models can increase the computational cost, which might not be feasible in practical scenarios. • The fixed de-loading gain of 0.9 can contribute towards the up-regulation cost; therefore, testing the proposed method with adaptive gain might be more suitable.
[122]	NN-based FPPT Control	PI Controller and Algorithm-Based	Left	No	MATLAB/ Simulink Simulations (*Tested on IEEE-13 bus test system*)	• The trained NN control dynamically modifies the PV operating voltage. • It effectively creates and manages power reserves in a grid-connected PV system, and the tolerance for nominal frequency deviations is set to ±0.2 Hz. • The inputs/predictors and outputs/responses are arranged as matrices in the proposed ANN-based FPPT. The predictors matrix is a [1000 × 3] double matrix, and the responses matrix is a [1000 × 1] double matrix. Where inputs are G, T, and the required reserve, and the output is the operating voltage. • The data set consists of 1000 randomly generated values of G and T, and 70 %, 15 %, and 15 % of the data is used for training, validation, and testing, respectively. • The network is created using a sigmoid function in the hidden layer and a linear function in the output layer. The hidden layer has a size of 10.	• The trained NN might have inaccurate results in rapid irradiance changes. • Shading scenarios are not considered. • The effectiveness of the proposed control is contingent upon the quality of training data. • The proposed control needs improvement by training the actual system data to test in real-time operation. • The settling time, steady-state error, and tracking time are not considered. • Testing the method with actual system data and implementation in real-time operation is for future work.

(*continued on next page*)

Table 8 (*continued*)

No.	Technique	Control Type	Operating Side of MPP	Shading Scenario Considered?	Method Evaluation	Key Contributions	Limitations
						• From a neural net fitting application in MATLAB, Levenberg-Marquardt optimisation is chosen to update weight and bias values in the neural network. • The response time of the proposed frequency control is within 1s of contingency.	
[123]	MLRA-Based De-loading Percentage Estimator for Frequency Regulation	PI-Based Controller	Right	No	DIgSILENT Power Factory (*IEEE 39 bus test system to test different penetration levels*)	• A multiple linear regression analysis is used to accurately estimate the de-loading percentage for large-scale PV systems by considering frequency response characteristics (f_{nadir} and RoCoF) as well. • The prediction models for deciding required PV support during contingency are evaluated regarding R^2, adjusted R^2, and Root Mean Square Error (RMSE). • Detailed analysis shows the necessary de-loading percentage at different penetration levels. • They used an equivalent system frequency for the generator tripping event, as multiple synchronous generators run simultaneously in the grid, which can cause small oscillations in frequency. • In the 20 % PV penetration case, all parameters were in range except f_{nadir} which deteriorate when PV support is insufficient, and the de-loading percentage was calculated as 9.976 %. • In 30 %, 40 %, 50 %, and 60 % PV penetration cases, the required de-loading was calculated as 7.283 %, 6.536 %, 6.335 % and 5.694 % which states that with total required de-loaded PV support increasing, the de-loading percentage decreases. • All the MLRA models for each PV penetration level show acceptable goodness-of-fit parameters, predicting satisfactory accuracy. • Further validations confirm that the estimated de-loading percentage keeps f_{nadir} and RoCoF within limits, and outperforms BESS with the same support size.	• The study uses fixed incremental de-loading at first, which may miss the optimal de-loading percentage, which could be between two of the fixed steps. • The PV intermittency is ignored considering the time duration, but this can significantly affect the proposed strategy's performance. • A mechanism for adaptive de-loading percentage is required, which can update in real-time based on frequency droop control. • This study does not consider the variations in the load demands.

to the characteristics of PV sources and eliminates the need for an external PI controller. The FCS-MPC for the PV units work cooperatively with the FCS-MPC for BES units to improve the overall stability and reliability of the microgrid. Furthermore, a Distributed MPC (DMPC) was developed by Ref. [129] for microgrid frequency regulation to overcome the frequency deviations caused by load fluctuations. The mathematical modelling of PV, BESS, and VSI was modelled and implemented in MATLAB/Simulink and shown in Fig. 34. Microgrid stability was tested once with and without the proposed control strategy and their performance was benchmarked against existing methods using Bode plots and dynamic frequency response analysis. The results show that this control strategy effectively optimises performance and limits voltage fluctuations. Specifically, during validation with the base load, the system exhibited minimal oscillations, deviation by only 0.002 Hz from the nominal frequency. This indicates exceptional stability and a deviation of less than 0.005 %.

Moreover, a novel Model-Free Deadbeat Predictive Current Controller (MF-DBPC) was presented by Ref. [130] without needing to know the exact details of the system's components, like resistance and inductance of the filter. In contrast to conventional methods, the

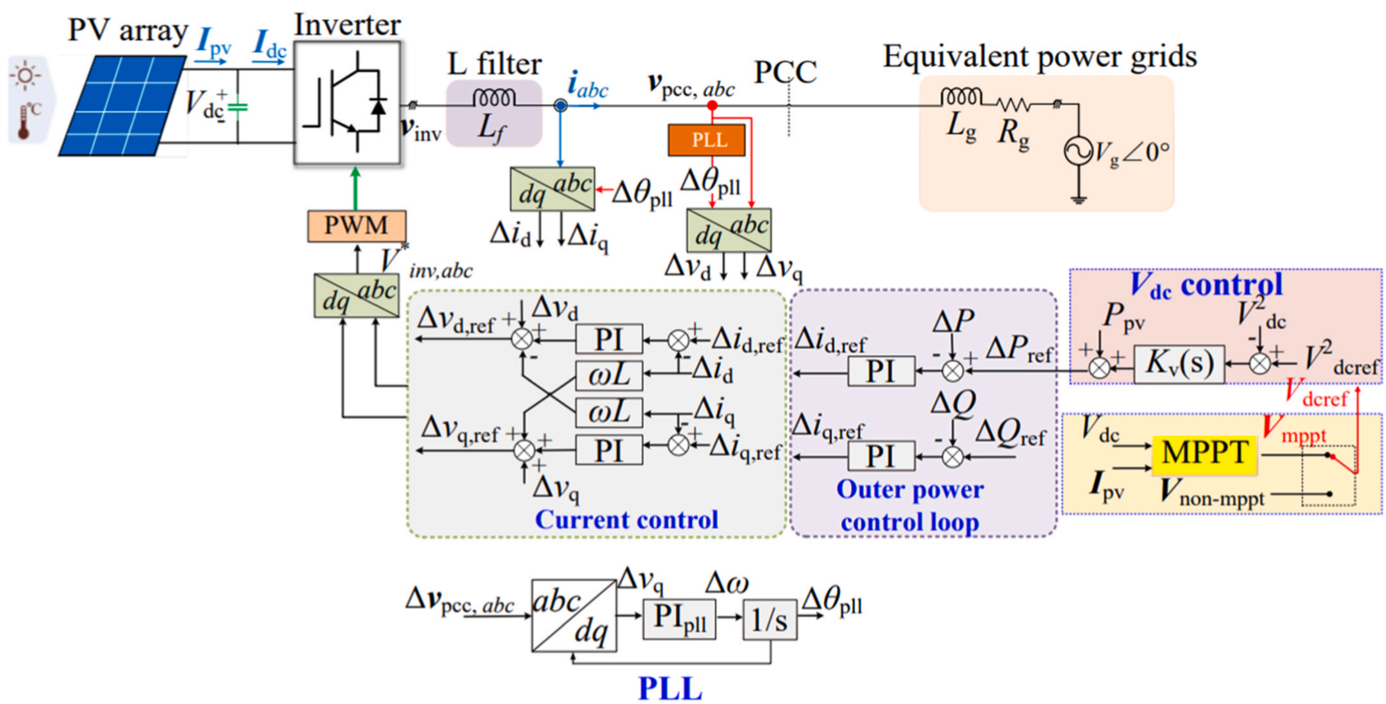

Fig. 31. Control Block Diagram of a Grid-Connected PV Inverter using SRF-VC [125].

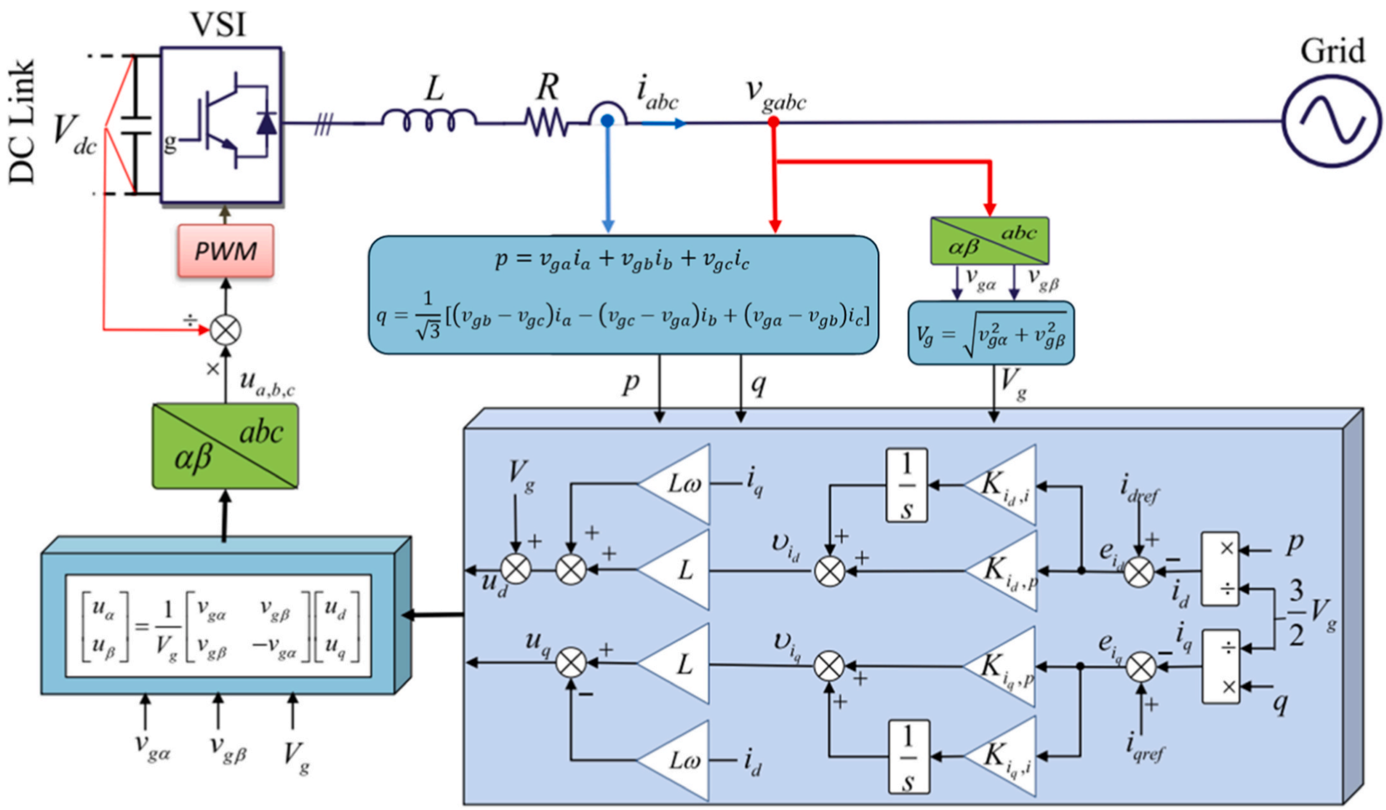

Fig. 32. VCC-DPC-based three-phase VSI control.

MF-DBPC uses a data-driven model based on current and voltage measurements. An Auto-Regressive with Exogenous Input (ARX) model and a Recursive Least Square (RLS) estimator for real-time parameter identification were essential components of the operation. This approach achieved robustness against parameter mismatches inherent in grid-connected inverter systems and provides improved adaptability to dynamic system situations. To illustrate this, two different model-free predictive control strategies, where one is based on the rolling optimisation technique and the other on the deadbeat control principle, were compared, and the results show that the MC-DBPC stands out with

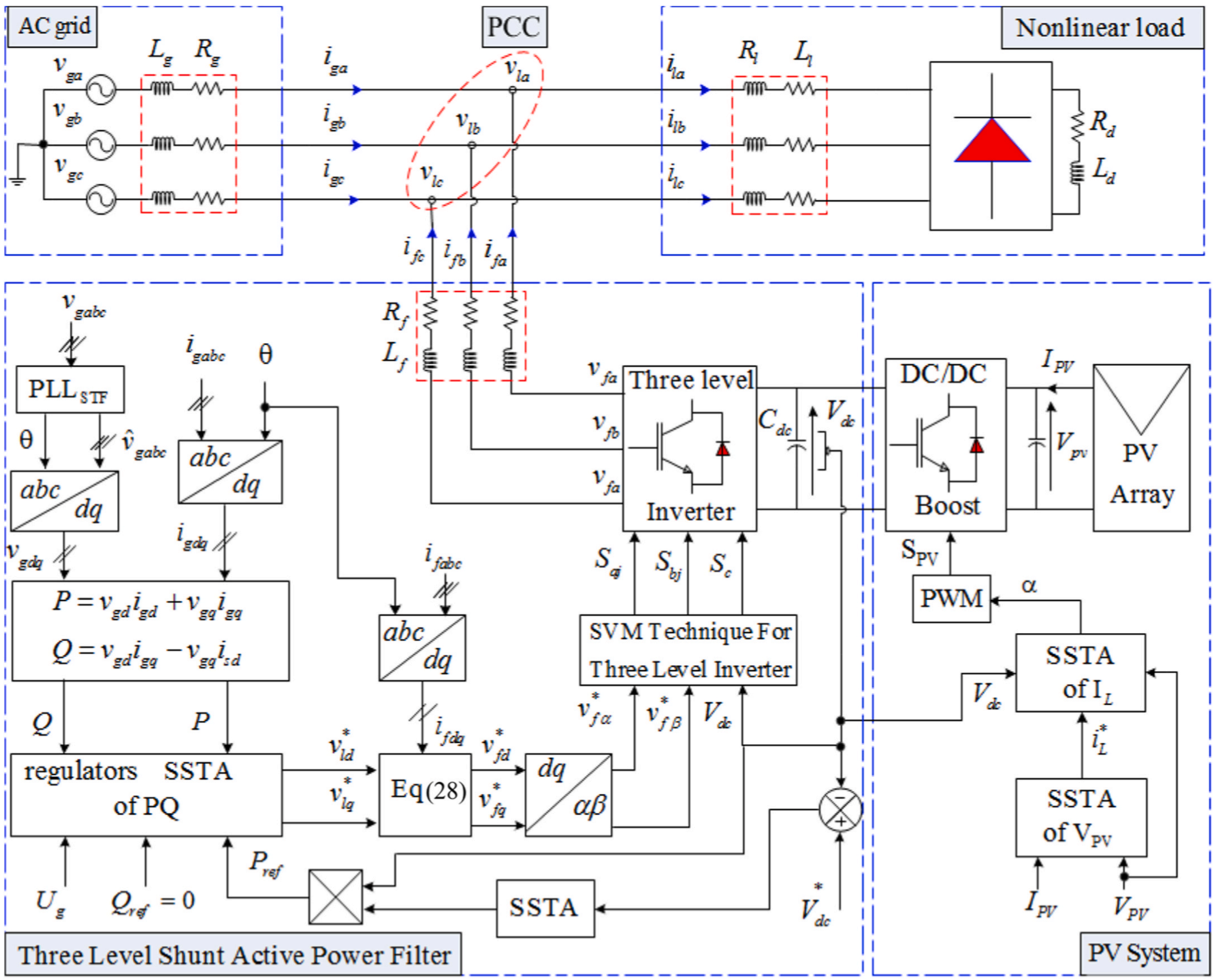

Fig. 33. Control Structure of DPC, SAPF and SSTA based Three-Level PV Inverter [127].

current waveform quality with a sampling frequency five times lower than its rolling optimisation. The effectiveness of the method was further supported by experimental validations across both steady-state and dynamic performance metrics.

Several other types of inverter control strategies shown in Fig. 35 are further detailed in Ref. [131], providing an in-depth analysis of control strategies for grid-connected PV inverters and their corresponding modulation techniques. Furthermore [132], carried out an extensive review of the topologies and control strategies of Multi-Functional Grid-Connected Inverters (MFGCI). Similarly [133], presented an overview of high-power inverter topologies and control techniques in large-scale PV power plants.

3.9. Optimising algorithms for frequency regulation

As discussed earlier, different techniques have been used for frequency regulation. Some have used various controllers and optimisation algorithms to develop a frequency control mechanism. This section gives an overview of different optimisation algorithms used in the literature for frequency regulation.

A Genetic Algorithm (GA) based fuzzy logic controller was designed by Ref. [134] to control the system's frequency with low overshoot and short settling time. The optimality of the PID controllers was determined by Ref. [135] using a GA with Integral Time Absolute Error (ITAE) performance indices as the objective function for hybrid generation including PV, wind turbines, geothermal power plants, and EVs. A combination of GA and PSO was used by Ref. [136] to modify the PI controller parameters for voltage and frequency control for islanded microgrid or load change conditions. The robust PID controller's parameters were optimised using the Imperialist Competitive Algorithm (ICA), and the outcomes demonstrate its superiority over the traditional PI controller that was optimised using NN and GA [137]. In Ref. [138], a shorter convergence time on the global peak under a partial shading scenario and power oscillations was reduced by proposing an adaptive velocity PSO. To improve the LFC in a two-area system, the authors of [139] modified the PI controller using the Bacteria Foraging Optimisation (BFO) algorithm. The findings revealed that BFO outperformed the GA. Similarly, NN-based BFO was proposed by Ref. [140] to reduce the overshoot and adjust the frequency of the hybrid power system. Under mismatching power conditions, NN-BFO outperformed the PID, achieving the lowest standard transit time of 5.20s. Ant Colony Optimisation (ACO), along with super-twisting sliding mode controller (STSMC), was used by Ref. [141] for energy balancing that can effectively handle system nonlinearities and improve the system's responsiveness to uncertainties and variability of RESs and loads. Table 9 provides a short overview of various optimisation algorithms employed

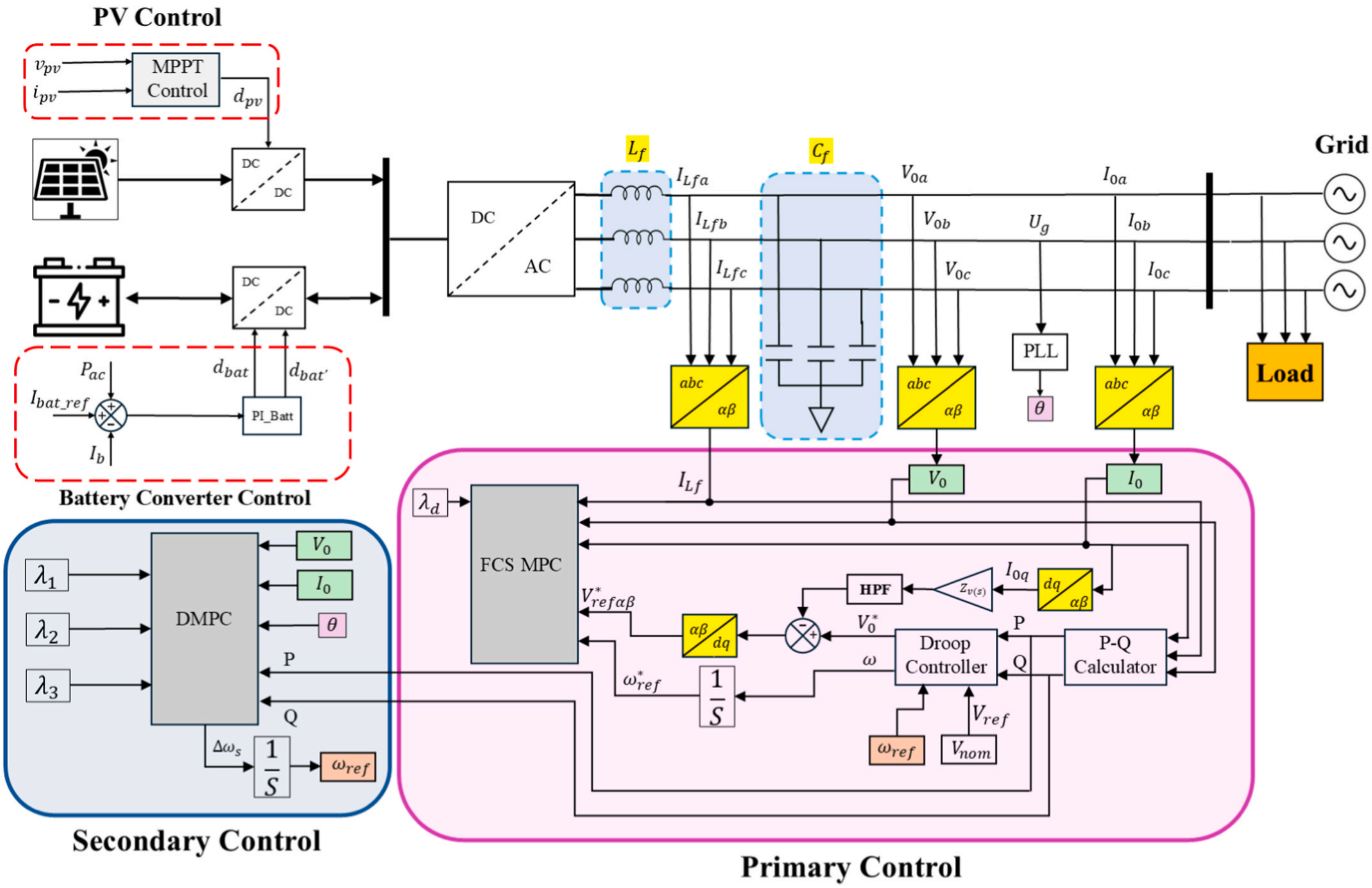

Fig. 34. Control structure of FCS-MPC-based DMPC for hybrid microgrid.

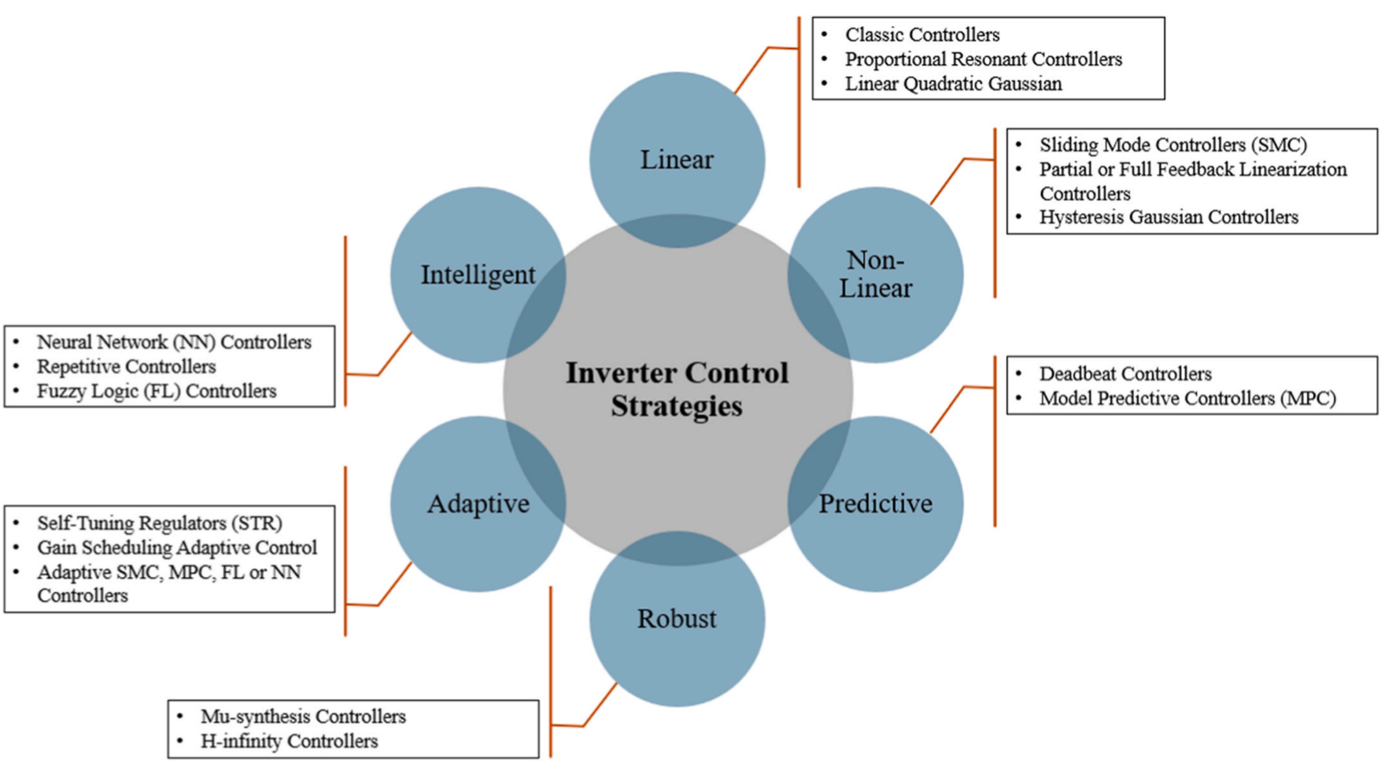

Fig. 35. Types of inverter control strategies.

Table 9
Overview of different Optimisation Algorithms used in Literature.

No.	Ref.	Optimisation Technique	Objective Function
1.	[142]	Differential Evolution Optimisation (DEO)	Integral of Absolute Error (IAE) to minimise the error of the system
2.	[143]	Directional Permutation Differential Evolution Algorithm	To tackle the parameter estimation of several types of PVs
3.	[144]	Firefly Optimisation (FO)	Integral Time Absolute Error (ITAE) of two areas and tie-line power to improve the system response for frequency deviation
4.	[145]	Grey Wolf Optimiser (GWO)	Used for the first time to solve the multi-objective load frequency control problem. Besides, minimum fitness value (ITAE) of 0.1340 is obtained.
5.	[146]	Jaya Algorithm	To minimise the load frequency control deviations
6.	[147]	Barnacle Mating Optimiser	To diminish the frequency rate (5.6s for area 1 & 5.5s for area 2) and tie-line power changes (6.2s)
7.	[148]	Harris Hawks Optimisation	To minimise the voltage and frequency fluctuations in combination with Model Predictive Control (MPC)
8.	[149]	Coyote Optimisation Algorithm	To reduce frequency variations caused by load variations in conjunction with a Proportional-derivative with filter cascaded-proportional-integral (PDn-PI) controller
9.	[150]	Salp Swarm Algorithm	For load frequency control of a multi-area hybrid renewable nonlinear power system, along with a PID controller
10.	[151]	Multi-objective Symbiotic Organisms Search Algorithm	To self-tune the parameters of the PI controller to solve multi-objective issues like voltage overshoot and undershoot, rise time, settling time, and ITAE
11.	[152]	Dragonfly Search Algorithm	To operate a grid-tied PV system in non-uniform weather conditions. It was selected due to its ability to trace global peaks, higher efficiency, and shorter response time.
12.	[153]	Slime Mold Algorithm	To tune the PI controller to enhance the frequency stability in a two-area interconnected thermal and PV generator power grid
13.	[154]	Chaotic-based Atom Search Optimisation	To minimise the ITAE for automatic load frequency regulation of a multi-area, multi-source hybrid power system It avoids premature convergence and getting trapped in local optima.
14.	[155]	Teaching Learning Based Optimisation (TLBO)	To adjust the inertial and damping controller for frequency regulation of the solar-diesel hybrid power system.
15.	[156]	Flower Pollination Algorithm	To address LFC in solar wind-based power systems in conjunction with a fractional order proportional integral derivation (FOPID) controller
16.	[157]	Cuckoo Search Algorithm	Used to tune the PID controller for frequency regulation in microgrids. A cost function is defined by considering stability margin, overshoot, and settling time.
17.	[158]	Water Cycle Algorithm	Used to tune the Cascaded Tilt Integral Tilt Derivative (CC-TI-TD) controller to control the system frequency under load variation for a multi-area interconnected power system
18.	[159]	Memetic Salp Swarm Algorithm	Enhancement of convergence stability under partial shading was achieved by designing a virtual population-based regroup operation for global coordination between salp chains, which resulted in small power oscillations as well. Moreover, employing multiple independent salp chains to simultaneously implement exploration and exploitation which can rapidly search for a high-quality optimum.

in the literature, in addition to these optimisation strategies.

4. Recommendations and outlook

Based on the critical assessment of the reviewed literature, this section outlines recommendations for future research directions to address the identified gaps or challenges.

The methods utilising the DC-link capacitors and ELDC for frequency regulation have been reported in the literature and referred to as inertia emulation methods. These methods offer quick responses and high efficiency but are constrained by high costs and limited energy storage, especially when scaling to large-scale PV systems. PRRC methods struggle with dynamic irradiance changes, and their application in shading scenarios remains under-investigated, while some methods often provide only unidirectional ramp control. Forecasting-based ramp rate methods are cost-effective, but they are highly dependent on the accuracy of the prediction model. Therefore, more optimised and robust PRRC techniques are necessary for diverse grid architectures.

The CPGC is convenient, but the traditional CPGC also requires ESS for a steady stream of power to maintain a specific power reference, and it is not optimal during periods of high frequency deviations. The P&O algorithm is generally used for CPGC operations, while the only drawback of this method is oscillations around the MPP, which can be reduced with a smaller step size, but there is a trade-off between stability and fast dynamics. Therefore, a study is required to find the optimal step size for CPGC applications. Some methods [78,80] have tried to reduce the steps, but the adaptiveness of this method is preferable. On the other hand, as reviewed by Ref. [51], the CPGC based on the power control has a better dynamic response and has less tracking accuracy. CPGC, based on the current limiting control, can effectively curtail PV output power, but it cannot ensure robustness under fast-changing irradiance conditions. Voltage-controlled CPGs have the highest robustness and have minor errors when operating on the left side. DPC is effective and easy to implement, but it depends on the correct MPP estimation from master PVs. Besides, large-scale PV systems are expensive.

The power curtailment methods reduce the system load by temporarily reducing the PV output, but can lead to power quality issues if not carefully managed. Generally, it is a reactive strategy dependent on operator instructions and the scheduling of curtailed limits, which relies heavily on PV output forecasting. Moreover, it might be challenging to shading scenarios that have not been tested as per the reviewed literature.

De-loading on the other side is getting the interest of the researchers, which is a CPG/PV curtailment control, but with a dispatchable power reserve created due to operating away from MPP. It is still an active research area, particularly employing FPPT algorithms, which emerge as promising solutions. It is considered a more economical solution for large-scale power plants as it requires no additional hardware. However, there is a trade-off between the cost associated with the curtailed power, typically called up-regulation cost. To reduce this problem, many studies [123,160,161] have worked on finding an optimal de-loading percentage and have shown that this has helped to reduce the up-regulation cost a bit. Besides, as the required amount of reserve changes by the percentage of PV integration [160], has identified the different de-loading percentages. It was stated that with 30 %, 40 %, and 50 % PV penetrations, de-loading percentages are 6.95 %, 5.93 %, and 4.96 % without load shedding and 14.92 %, 13.3 %, and 12.42 % with load shedding, respectively. On the contrary, this does not count towards the adaptive operation for frequency regulation and can have some challenges under shading scenarios where PV usually gets stuck in the local maxima. This is where FPPT comes in because it allows flexible operation by adaptively shifting the operating points to create power reserves. An overall cost assessment of a de-loaded PV is done by Ref. [162] and is compared with BESS. Moreover, a de-loaded PV is compared with a BESS and synchronous condenser by Ref. [160]. The results from these two studies show that de-loaded PV outperforms considering both technical and economic aspects.

Generally, de-loading/FPPT requires the correct estimation of the MPP, especially under shading scenarios, to determine the amount of power reserve. However, few research studies have avoided estimating MPP and provided the power reserve without it. These methods are efficient under uniform irradiance or shading scenarios but face problems when partial shading scenarios occur. It can be seen from the literature that most of the frequency control methods were efficient under uniform and variable irradiance conditions. A limited number of studies have been reported working on shading scenarios. Therefore, more research is required to develop control strategies that can work effectively and are less susceptible to partial shading conditions. Few studies have used the monotonic techniques to force the PV to operate on either the right or left side. The left side is more stable, has less thermal stress, and has improved efficiency in shading scenarios, but can account for slower response time and less power output. The selection of the operating regions solely depends on the system requirements, and there is a trade-off between grid stability and dynamic response.

On the other hand, different soft computing-based approaches have been reported that provide quick and accurate tracking of MPP, can dynamically modify the operating voltages for creating power reserves, and have short tracking and response times. However, these techniques are highly dependent on the accuracy of the data used to train the ANN models. To overcome this issue, future research should focus on.

- Exploring unsupervised machine learning techniques to allow the PV system to learn independently, potentially leading to improved performance.
- Developing computationally cost-effective, hybrid solutions combining fast responding algorithms with advanced controllers to manage the trade-off between complexity and computational power for real-time large-scale systems.

Integrating frequency regulation with other grid services is a key area for development. Optimal demand response programs can be integrated with these frequency control strategies to overcome the issue of grid stability, addressing the trade-off between user comfort and grid stability, which is a challenging scenario.

Finally, due to the intermittent nature of PV systems, inverter control strategies are crucial for managing power quality, flow, and integration with the grid. Therefore, investigating more accurate and robust control methods is essential for reliable PV integration. The future research can focus on the following.

- Developing control strategies for multi-level intelligent inverters to scale up for high-power applications
- Hybrid topology optimisation
- Multifunctional control (unified ancillary services) for enhanced grid support
- Intelligent modulation techniques with the aid of metaheuristic algorithms to provide high quality inputs to grid for minimising THD, improve efficiency, and enhanced grid support.

5. Conclusion

The equilibrium of supply and demand ensures grid security, and any difference between these two can cause system disturbances. Considering this, frequency is a valuable indicator of the degree of harmony between load and generation compared to other ancillary services. Therefore, this article reviewed different frequency regulation strategies for PV systems accessible in the literature, primarily focusing on those that do not require storage devices. For this, findings from a critical examination of 51 peer-reviewed papers are synthesised. To provide a clear and structured understanding, detailed summary tables with parameters like control technique and type, operating region, consideration of shading scenarios, method evaluation (*software tools and hardware equipment used)*, key contributions/summary, and limitations are presented in each technique section. In addition to filling a major gap noted in previous reviews, this paper also offers a unique section of 26 different optimisation algorithms used in this research domain. It details the dedicated objective functions of these algorithms, giving researchers a clear look at the computational tools and strategies used to improve the performance of PV-based frequency response. It is worth noting that the characterisation of highlighted limitations is predominantly shaped by the author's interpretation and critical assessment of the reviewed literature.

The review highlights the following key findings.

- Methods utilising DC-link capacitors and ELDC for inertia emulation offer quick responses and high efficiency, demonstrating their potential for dynamic stability.
- De-loading/FPPT have emerged as an economical solution for large-scale power plants, providing a dispatchable power reserve without additional hardware.
- Soft computing-based approaches, while computationally intensive, show promise in providing quick and accurate MPP tracking and dynamic operating point modification.
- Conventional power curtailment and PRRC methods are also viable but face limitations in their adaptability to dynamic conditions like fast-changing irradiance and shading scenarios.

A significant gap remains in the robustness of most frequency control methods under partial shading scenarios. The reviewed literature suggests a clear trade-off between the benefits of these control methods and their associated challenges, such as cost, complexity, and robustness under diverse operational conditions. Ultimately, the analysis reveals that while no single solution is universally optimal, the inherent trade-offs of individual strategies underscore the need for holistic and integrated approaches tailored to system-specific requirements and grid architecture. Therefore, future research should focus more on developing hybrid control techniques such as unsupervised ML for predictive forecasting based de-loading, predictive modelling and pattern recognition for partial shading, intelligent droop control with dynamic control and action while considering the associated computational cost. This can synergistically combine the strengths of individual methods to overcome their inherent limitations. Ultimately, this leads to more robust, flexible, and efficient solutions for diverse operational conditions.

Author's contributions

Ateeb Hassan: Preparing the first draft, conceptualisation, Editing **Jubaer Ahmed:** Supervision, Reviewing, Validation, and Editing, **Savvas Papadopoulos:** Supervision, Reviewing, and Validation., **Fadi Kahwash:** Reviewing and Editing., **Keng Goh:** Supervision, Reviewing, and Validation.

Declaration of competing interest

The authors declare that they have no known competing financial interests or personal relationships that could have appeared to influence the work reported in this paper.

Data availability

Data will be made available on request.

References

[1] Rajan R, Fernandez FM, Yang Y. Primary frequency control techniques for large-scale PV-integrated power systems: a review. Renew Sustain Energy Rev 2021;144.
[2] REN21. In: Mastny L, editor. Renewables 2024 global status report collection, global overview. Paris: REN21 Secretariat; 2024.
[3] Wu X, Kerekes T. Flexible active power control for PV-ESS systems: a review. Energies 2021;14(21).
[4] Khan TA, et al. From design to deployment: a comprehensive review of theoretical and experimental studies of multi-energy systems for residential applications. Electronics 2025;14(11):2221.
[5] Alam M, et al. Solar and wind energy integrated system frequency control: a critical review on recent developments. Energies 2023;16(2).
[6] Hadjipaschalis I, Poullikkas A, Efthimiou V. Overview of current and future energy storage technologies for electric power applications. Renew Sustain Energy Rev 2009;13(6):1513–22.
[7] Nazemi M, Liang X. Frequency control techniques for solar PV systems: a review. In: 2023 IEEE Canadian conference on electrical and computer engineering (CCECE); 2023. p. 43–8.
[8] Hartmann B, Vokony I, Táczi I. Effects of decreasing synchronous inertia on power system dynamics—Overview of recent experiences and marketisation of services. International Transactions on Electrical Energy Systems 2019;29(12): e12128.
[9] Wu D, et al. Coordinated control based on bus-signaling and virtual inertia for islanded DC microgrids. IEEE Trans Smart Grid 2015;6(6):2627–38.
[10] Messasma C, Chouaba SE, Sari B. The primary frequency control techniques for grid connected PV systems: a review. In: Artificial intelligence and heuristics for smart energy efficiency in smart cities; 2022. p. 220–9.
[11] Dreidy M, Mokhlis H, Mekhilef S. Inertia response and frequency control techniques for renewable energy sources: a review. Renew Sustain Energy Rev 2017;69:144–55.
[12] Akram U, et al. A review on rapid responsive energy storage technologies for frequency regulation in modern power systems. Renew Sustain Energy Rev 2020; 120:109626.
[13] You S. Use energy storage for primary frequency control in power grids. arXiv preprint arXiv:2101 05165 2021.
[14] Liu X, et al. Coordinated control of distributed energy storage system with tap changer transformers for voltage rise mitigation under high photovoltaic penetration. IEEE Trans Smart Grid 2012;3(2):897–906.
[15] Chua K, et al. Energy storage system for mitigating voltage unbalance on low-voltage networks with photovoltaic systems. IEEE Trans Power Deliv 2012;27(4): 1783–90.
[16] Tan Z, et al. Primary frequency control with BESS considering adaptive SoC recovery. Int J Electr Power Energy Syst 2020;117:105588.
[17] Zimann FJ, et al. Energy storage system control algorithm for voltage regulation with active and reactive power injection in low-voltage distribution network. Elec Power Syst Res 2019;174:105825.
[18] Kewat S, Singh B, Hussain I. Power management in PV-battery-hydro based standalone microgrid IET Renew Power Gener 2017;12:391–8.
[19] Datta U, Kalam A, Shi J. Battery energy storage system for aggregated inertia-droop control and a novel frequency dependent state-of-charge recovery. Energies 2020;13(8):2003.
[20] Lee D-J, Wang L. Small-signal stability analysis of an autonomous hybrid renewable energy power generation/energy storage system part I: time-domain simulations. IEEE Trans Energy Convers 2008;23(1):311–20.
[21] Belila A, et al. On energy management control of a PV-Diesel-ESS based microgrid in a stand-alone context. Energies 2018;11(8):2164.
[22] Yi Z, Dong W, Etemadi AH. A unified control and power management scheme for PV-battery-based hybrid microgrids for both grid-connected and islanded modes. IEEE Trans Smart Grid 2017;9(6):5975–85.
[23] Philip J, et al. A simplified configuration and implementation of a standalone microgrid. In: 2015 IEEE power & energy society general meeting. IEEE; 2015.
[24] Philip J, et al. Control and implementation of a standalone solar photovoltaic hybrid system. IEEE Trans Ind Appl 2016;52(4):3472–9.
[25] Kim A-R, et al. SMES application for frequency control during islanded microgrid operation. Phys C Supercond 2013;484:282–6.
[26] Gouda EA, Abd-Alaziz A, El-Saadawi M. Design modeling, and control of multi-stage SMES integrated with PV system. J Energy Storage 2020;29:101399.
[27] Abumeteir HA, Vural AM. Design and optimization of fractional order PID controller to enhance energy storage system contribution for damping low-frequency oscillation in power systems integrated with high penetration of renewable sources. Sustainability 2022;14(9):5095.
[28] Faisal M, et al. Review of energy storage system technologies in microgrid applications: issues and challenges. IEEE Access 2018;6:35143–64.
[29] Showers SO, Raji AK. Benefits and challenges of energy storage technologies in high penetration renewable energy power systems. In: 2019 IEEE PES/IAS PowerAfrica; 2019.
[30] Anika OC, et al. Prospects of low and zero-carbon renewable fuels in 1.5-degree net zero emission actualisation by 2050: a critical review. Carbon Capture Sci Technol 2022;5:100072.
[31] Uzum B, et al. Rooftop solar PV penetration impacts on distribution network and further growth factors—A comprehensive review. Electronics 2021;10(1):55.
[32] Rodat S, Thonig R. Status of concentrated solar power plants installed worldwide: past and present data. Cleanroom Technol 2024;6(1):365–78.
[33] Meng L, et al. Fast frequency response from energy storage systems—a review of grid standards, projects and technical issues. IEEE Trans Smart Grid 2019;11(2): 1566–81.
[34] Garozzo D, Tina GM. Evaluation of the effective active power reserve for fast frequency response of PV with BESS inverters considering reactive power control. Energies 2020;13(13):3437.
[35] Garttan G, et al. Battery energy storage systems: energy market review, challenges, and opportunities in frequency control ancillary services. Energies 2025;18(15):4174.
[36] Verma P, Katal N. Analysing active power reserve strategies for photovoltaic systems under varying shading scenarios: a comparative study. Progress in Energy 2023;5(4).
[37] Maity S, Rather ZH, Doolla S. A comprehensive review of grid support services from solar photovoltaic power plants. Renew Sustain Energy Rev 2025;210: 115133.
[38] Fernández-Guillamón A, Muljadi E, Molina-García A. Frequency control studies: a review of power system, conventional and renewable generation unit modeling. Elec Power Syst Res 2022;211:108191.
[39] Peddakapu K, et al. A state-of-the-art review on modern and future developments of AGC/LFC of conventional and renewable energy-based power systems. Renew Energy Focus 2022;43:146–71.
[40] Fini MH, Golshan MEH. Determining optimal virtual inertia and frequency control parameters to preserve the frequency stability in islanded microgrids with high penetration of renewables. Elec Power Syst Res 2018;154:13–22.
[41] Ulbig A, Borsche TS, Andersson G. Impact of low rotational inertia on power system stability and operation. IFAC Proc Vol 2014;47(3):7290–7.
[42] De la Parra I, et al. PV performance modelling: a review in the light of quality assurance for large PV plants. Renew Sustain Energy Rev 2017;78:780–97.
[43] Chouder A, et al. Modeling and simulation of a grid connected PV system based on the evaluation of main PV module parameters. Simulat Model Pract Theor 2012;20(1):46–58.
[44] Morey M, et al. A comprehensive review of grid-connected solar photovoltaic system: architecture, control, and ancillary services. Renew Energy Focus 2023; 45:307–30.
[45] Bahari MI, et al. Modeling and simulation of hill climbing MPPT algorithm for photovoltaic application. In: 2016 international symposium on power electronics, electrical drives, automation and motion (SPEEDAM). IEEE; 2016.
[46] Selmi T, et al. P&O mppt implementation using matlab/simulink. In: 2014 ninth international conference on ecological vehicles and renewable energies (EVER). IEEE; 2014.
[47] Safari A, Mekhilef S. Incremental conductance MPPT method for PV systems. In: 2011 24th Canadian conference on electrical and computer engineering (CCECE). IEEE; 2011.
[48] Pai F-S, et al. Performance evaluation of parabolic prediction to maximum power point tracking for PV array. IEEE Trans Sustain Energy 2010;2(1):60–8.
[49] Liu K, et al. Research on dynamic modeling and parameter identification of the grid-connected PV power generation system. Energies 2023;16(10):4152.
[50] Yang Y, et al. 6 - flexible active power control of PV systems. In: Yang Y, et al., editors. Advances in grid-connected photovoltaic power conversion systems. Woodhead Publishing; 2019. p. 153–85.
[51] Haghighat M, et al. A review of state-of-the-art flexible power point tracking algorithms in photovoltaic systems for grid support: classification and application. Journal of Modern Power Systems and Clean Energy 2024;12(1): 1–21.
[52] Shazon MNH, Nahid Al M, Jawad A. Frequency control challenges and potential countermeasures in future low-inertia power systems: a review. Energy Rep 2022; 8:6191–219.
[53] Im WS, et al. Distributed virtual inertia based control of multiple photovoltaic systems in autonomous microgrid. IEEE/CAA Journal of Automatica Sinica 2017; 4(3):512–9.
[54] Guo K, Tang Y, Fang J. Exploration of the relationship between inertia enhancement and DC-link capacitance for grid-connected converters. In: 2018 IEEE 4th southern power electronics conference (SPEC). IEEE; 2018.
[55] Pourheydari M, Parniani M, Ravanji MH. Small-signal analysis and enhanced control of large-scale PV-Penetrated power systems from the electromechanical oscillations point of view. IEEE Syst J 2023.
[56] Bakeer M, et al. Resilient virtual synchronous generator approach using DC-link capacitor energy for frequency support of interconnected renewable power systems. J Energy Storage 2023;65:107230.
[57] Fang J, et al. Distributed power system virtual inertia implemented by grid-connected power converters. IEEE Trans Power Electron 2017;33(10):8488–99.
[58] Liu T, et al. Dual-mode fast frequency control of PV systems with inertia emulation from DC-link capacitor considering voltage restoration. CSEE Journal of Power and Energy Systems 2024.
[59] Singh SK, et al. Virtual inertia emulation of inverter interfaced distributed generation (IIDG) for dynamic frequency stability & damping enhancement through BFOA tuned optimal controller. Arabian J Sci Eng 2022:1–18.
[60] Ramos JG, Araújo RE. Virtual inertia and droop control using DC-link in a two-stage PV inverter. In: 2020 IEEE 14th international conference on compatibility, power electronics and power engineering (CPE-POWERENG). IEEE; 2020.
[61] Karpana S, et al. PV-Supercapacitor cascaded topology for primary frequency responses and dynamic inertia emulation. Energies 2021;14(24):8347.
[62] Sarojini RK, Palanisamy K, De Tuglie E. A fuzzy logic-based emulated inertia control to a supercapacitor system to improve inertia in a low inertia grid with renewables. Energies 2022;15(4):1333.

[63] Samanta S, et al. Design and FPGA implementation of a deloading control technique for DC link voltage regulation of a PV system. In: 2020 3rd international conference on energy, power and environment: towards clean energy technologies. IEEE; 2021.
[64] Nakka PC, Mishra MK. Droop characteristics based damping and inertia emulation of DC link in a hybrid microgrid. IET Renew Power Gener 2020;14(6): 1044–52.
[65] Shivashankar S, et al. Mitigating methods of power fluctuation of photovoltaic (PV) sources–A review. Renew Sustain Energy Rev 2016;59:1170–84.
[66] Cormode D, et al. Comparing ramp rates from large and small PV systems, and selection of batteries for ramp rate control. In: 2013 IEEE 39th photovoltaic specialists conference (PVSC). IEEE; 2013.
[67] Riquelme-Dominguez JM, García-López FDP, Martinez S. Power ramp-rate control via power regulation for storageless grid-connected photovoltaic systems. Int J Electr Power Energy Syst 2022;138:107848.
[68] Haghighat M, Niroomand M, Tafti HD. An adaptive power ramp rate control method for photovoltaic systems. IEEE J Photovoltaics 2021;12(2):557–64.
[69] Yinxiao Zhu HW, Guanying Chu. Active power control for grid-connected photovoltaic system: a review. In: 2020 IEEE/IAS industrial and commercial power system Asia (I&CPS Asia); 2020. p. 1506–11.
[70] Chen X, et al. Forecasting-based power ramp-rate control strategies for utility-scale PV systems. IEEE Trans Ind Electron 2018;66(3):1862–71.
[71] Li X, et al. A cost-effective power ramp rate control strategy based on flexible power point tracking for photovoltaic system. Sol Energy 2020;208:1058–67.
[72] Huo Y, Gruosso G. A novel ramp-rate control of grid-tied PV-Battery systems to reduce required battery capacity. Energy 2020;210:118433.
[73] Patarroyo-Montenegro JF, et al. Comparative and cost analysis of a novel predictive power ramp rate control method: a case study in a pv power plant in Puerto Rico. Appl Sci 2021;11(13):5766.
[74] Alam MJE, Muttaqi K, Sutanto D. A novel approach for ramp-rate control of solar PV using energy storage to mitigate output fluctuations caused by cloud passing. IEEE Trans Energy Convers 2014;29(2):507–18.
[75] Lin D, et al. Strategy comparison of power ramp rate control for photovoltaic systems. CPSS Transactions on Power Electronics and Applications 2020;5(4): 329–41.
[76] Sangwongwanich A, Yang Y, Blaabjerg F. High-performance constant power generation in grid-connected PV systems. IEEE Trans Power Electron 2015;31(3): 1822–5.
[77] Sangwongwanich A, et al. Benchmarking of constant power generation strategies for single-phase grid-connected photovoltaic systems. IEEE Trans Ind Appl 2017; 54(1):447–57.
[78] Hou G, Ke Y, Huang C. A flexible constant power generation scheme for photovoltaic system by error-based active disturbance rejection control and perturb & observe. Energy 2021;237:121646.
[79] Gao Z. Scaling and bandwidth-parameterization based controller tuning. In: Acc; 2003.
[80] Ahmed M, et al. Model-based maximum power point tracking algorithm with constant power generation capability and fast DC-link dynamics for two-stage PV systems. IEEE Access 2022;10:48551–68.
[81] Tafti HD, et al. A general constant power generation algorithm for photovoltaic systems. IEEE Trans Power Electron 2017;33(5):4088–101.
[82] Sangwongwanich A, et al. Delta power control strategy for multistring grid-connected PV inverters. IEEE Trans Ind Appl 2017;53(4):3862–70.
[83] Owais R, Iqbal SJ. A master-slave-based power reserve control approach for solar PV participation in frequency control. Arabian J Sci Eng 2023;48(11):15475–94.
[84] Iqbal M, Gulzar MM. Master-slave design for frequency regulation in hybrid power system under complex environment. IET Renew Power Gener 2022;16(14): 3041–57.
[85] Buticchi G, et al. Analysis of the frequency-based control of a master/slave micro-grid. IET Renew Power Gener 2016;10(10):1570–6.
[86] Yang J, et al. A novel quasi-master-slave control frame for PV-storage independent microgrid. Int J Electr Power Energy Syst 2018;97:262–74.
[87] Xin H, et al. A new frequency regulation strategy for photovoltaic systems without energy storage. IEEE Trans Sustain Energy 2013;4(4):985–93.
[88] Kato T, et al. Impact of power output curtailment control of photovoltaic power generation on grid frequency. IFAC-PapersOnLine 2020;53(2):12157–62.
[89] Riquelme-Dominguez JM, Martinez S. A photovoltaic power curtailment method for operation on both sides of the power-voltage curve. Energies 2020;13(15): 3906.
[90] Luthander R, Lingfors D, Widén J. Large-scale integration of photovoltaic power in a distribution grid using power curtailment and energy storage. Sol Energy 2017;155:1319–25.
[91] Pratama AMN, et al. Method to improve the accuracy of PV curtailment to maintain the system stability in North Sulawesi and gorontalo power grid. In: 2023 4th international conference on high voltage engineering and power systems (ICHVEPS). IEEE; 2023.
[92] Johnson J, et al. Photovoltaic frequency–watt curve design for frequency regulation and fast contingency reserves. IEEE J Photovoltaics 2016;6(6):1611–8.
[93] Zarina PP, Mishra S, Sekhar PC. Exploring frequency control capability of a PV system in a hybrid PV-rotating machine-without storage system. Int J Electr Power Energy Syst 2014;60:258–67.
[94] Yan G, et al. Novel adapted de-loading control strategy for PV generation participating in grid frequency regulation. J Eng 2019;2019(16):3383–7.
[95] Lyu X, et al. Advanced frequency support strategy of photovoltaic system considering changing working conditions. IET Gener, Transm Distrib 2018;12(2): 363–70.
[96] Batzelis EI, Kampitsis GE, Papathanassiou SA. Power reserves control for PV systems with real-time MPP estimation via curve fitting. IEEE Trans Sustain Energy 2017;8(3):1269–80.
[97] Peng Q, et al. Event-triggering virtual inertia control of PV systems with power reserve. IEEE Trans Ind Appl 2021;57(4):4059–70.
[98] Messasma C, et al. PV system frequency regulation employing a new power reserve control approach and a hybrid inertial response. Elec Power Syst Res 2023:223.
[99] Zhong C, Zhou Y, Yan G. A novel frequency regulation strategy for a PV system based on the curtailment power-current curve tracking algorithm. IEEE Access 2020;8:77701–15.
[100] Pawar B, et al. Grid-forming control for solar PV systems with power reserves. IEEE Trans Sustain Energy 2021;12(4):1947–59.
[101] Li Z, et al. Adaptive power point tracking control of PV system for primary frequency regulation of AC microgrid with high PV integration. IEEE Trans Power Syst 2021;36(4):3129–41.
[102] Yan X, et al. Power reserve control strategy in the left-side of maximum power point for primary frequency regulation of grid-connected photovoltaic systems. IET Power Electron 2022;15(2):93–108.
[103] Chen K, et al. An improved MPPT controller for photovoltaic system under partial shading condition. IEEE Trans Sustain Energy 2014;5(3):978–85.
[104] Patel H, Agarwal V. Investigations into the performance of photovoltaics-based active filter configurations and their control schemes under uniform and non-uniform radiation conditions. IET Renew Power Gener 2010;4(1):12–22.
[105] Fezzani A, Mahammed IH, Said S. MATLAB-Based modeling of shading effects in photovoltaic arrays. In: 2014 15th international conference on sciences and techniques of automatic control and computer engineering (STA). IEEE; 2014.
[106] Mohapatra A, et al. A review on MPPT techniques of PV system under partial shading condition. Renew Sustain Energy Rev 2017;80:854–67.
[107] Kermadi M, et al. Recent developments of MPPT techniques for PV systems under partial shading conditions: a critical review and performance evaluation. IET Renew Power Gener 2020;14(17):3401–17.
[108] Worku MY, et al. A comprehensive review of recent maximum power point tracking techniques for photovoltaic systems under partial shading. Sustainability 2023;15(14):11132.
[109] Pati AK, Sahoo N. A new approach in maximum power point tracking for a photovoltaic array with power management system using fibonacci search algorithm under partial shading conditions. Energy Systems 2016;7(1):145–72.
[110] Ramyar A, Iman-Eini H, Farhangi S. Global maximum power point tracking method for photovoltaic arrays under partial shading conditions. IEEE Trans Ind Electron 2016;64(4):2855–64.
[111] Verma P, Kaur T, Kaur R. Power control strategy of PV system for active power reserve under partial shading conditions. Int J Electr Power Energy Syst 2021: 130.
[112] Ghasemi MA, Ramyar A, Iman-Eini H. MPPT method for PV systems under partially shaded conditions by approximating I–V curve. IEEE Trans Ind Electron 2017;65(5):3966–75.
[113] Tafti HD, et al. Global flexible power point tracking in photovoltaic systems under partial shading conditions. IEEE Trans Power Electron 2022;37(9):11332–41.
[114] Kolakaluri VK, Aalam MN, Sarkar V. Metaheuristics assisted efficiency maximizing flexible power point tracking of a photovoltaic array under the partial shading. IEEE Trans Energy Convers 2023;38(3):1576–88.
[115] Batzelis EI, Papathanassiou SA, Pal BC. PV system control to provide active power reserves under partial shading conditions. IEEE Trans Power Electron 2018;33 (11):9163–75.
[116] Dilger EB, de Oliveira RV. Power reserve control for utility-scale PV power plants under cloud conditions. Elec Power Syst Res 2024;229:110099.
[117] Narang A, et al. Dynamic reserve power point tracking in grid-connected photovoltaic power plants. IEEE Trans Power Electron 2023;38(5):5939–51.
[118] Phang J, Chan D, Phillips J. Accurate analytical method for the extraction of solar cell model parameters. Electron Lett 1984;20(10):406–8.
[119] Sekhar P, Mishra S. Storage free smart energy management for frequency control in a diesel-PV-fuel cell-based hybrid AC microgrid. IEEE Transact Neural Networks Learn Syst 2015;27(8):1657–71.
[120] Verma P, Kaur T. Power reserve control strategy of PV system for active power reserve under dynamic shading patterns. Array 2022;16:100250.
[121] Messasma C, et al. An approach for power reserve control (PRC) strategy based on a novel ANN model. In: International conference on artificial intelligence in renewable energetic systems. Springer; 2022.
[122] Gomez JM, Shanmugam PK. Flexible power point tracking using a neural network for power reserve control in a grid-connected PV system. Energies 2022;15(21): 8234.
[123] Jawad A, Masood N-A. A systematic approach to estimate the frequency support from large-scale PV plants in a renewable integrated grid. Energy Rep 2022;8: 940–54.
[124] said Adouairi M, et al. Application of fuzzy sliding mode control on a single-stage grid-connected PV system based on the voltage-oriented control strategy. Results Eng 2023;17:100822.
[125] Gong Z, et al. Forced oscillation analysis of voltage-oriented vector control-based PV inverter connected to weak power grids. IEEE Trans Power Deliv 2025.
[126] Gui Y, Wang X, Blaabjerg F. Vector current control derived from direct power control for grid-connected inverters. IEEE Trans Power Electron 2018;34(9): 9224–35.
[127] Debdouche N, et al. Direct power control for three-level multifunctional voltage source inverter of PV systems using a simplified super-twisting algorithm. Energies 2023;16(10):4103.

[128] Zhao Z, et al. Decentralized grid-forming control strategy for PV-based DC microgrids using finite control set model predictive control. IEEE Trans Smart Grid 2024;15(6):5269–83.
[129] satya nagasri Dangeti L, Marimuthu R. Distributed model predictive control strategy for microgrid frequency regulation. Energy Rep 2025;13:1158–70.
[130] Kermadi M, et al. Model-free deadbeat predictive current control for grid-connected inverters using autoregressive model and recursive least squares. IEEE Journal of Emerging and Selected Topics in Power Electronics 2025.
[131] Ali Khan MY, et al. A comprehensive review on grid connected photovoltaic inverters, their modulation techniques, and control strategies. Energies 2020;13 (16):4185.
[132] Zeng Z, et al. Topologies and control strategies of multi-functional grid-connected inverters for power quality enhancement: a comprehensive review. Renew Sustain Energy Rev 2013;24:223–70.
[133] Azizi A, et al. A review on topology and control strategies of high-power inverters in large-scale photovoltaic power plants. Heliyon 2025;11(3):e42334.
[134] Cam E, Gorel G, Mamur H. Use of the genetic algorithm-based fuzzy logic controller for load-frequency control in a two area interconnected power system. Appl Sci 2017;7(3):308.
[135] Anuradhika K, Dash P. Genetic algorithm-based load frequency control of a grid-connected microgrid in presence of electric vehicles. In: Sustainable energy and technological advancements: proceedings of ISSETA 2021. Springer; 2022. p. 435–47.
[136] Dashtdar M, et al. Improving the power quality of island microgrid with voltage and frequency control based on a hybrid genetic algorithm and PSO. IEEE Access 2022;10:105352–65.
[137] Shabani H, Vahidi B, Ebrahimpour M. A robust PID controller based on imperialist competitive algorithm for load-frequency control of power systems. ISA Trans 2013;52(1):88–95.
[138] Pragallapati N, Sen T, Agarwal V. Adaptive velocity PSO for global maximum power control of a PV array under nonuniform irradiation conditions. IEEE J Photovoltaics 2016;7(2):624–39.
[139] Ali ES, Abd-Elazim SM. Bacteria foraging optimization algorithm based load frequency controller for interconnected power system. Int J Electr Power Energy Syst 2011;33(3):633–8.
[140] Al-Majidi SD, et al. Bacterial foraging algorithm for a neural network learning improvement in an automatic generation controller. Energies 2023;16(6):2802.
[141] Alghamdi H, et al. A novel intelligent optimal control methodology for energy balancing of microgrids with renewable energy and storage batteries. J Energy Storage 2024;90:111657.
[142] Zamee MA, et al. Differential evolution algorithm based load frequency control in a two-area conventional and renewable energy based nonlinear power system. In: 2016 4th international conference on the development in the in renewable energy technology (ICDRET). IEEE; 2016.
[143] Gao S, et al. A state-of-the-art differential evolution algorithm for parameter estimation of solar photovoltaic models. Energy Convers Manag 2021;230: 113784.
[144] Abd-Elazim SM, Ali ES. Load frequency controller design of a two-area system composing of PV grid and thermal generator via firefly algorithm. Neural Comput Appl 2018;30:607–16.
[145] Guha D, Roy PK, Banerjee S. Load frequency control of interconnected power system using grey wolf optimization. Swarm Evol Comput 2016;27:97–115.
[146] Sharma G, et al. Impact of ultracapacitor and redox flow battery with JAYA optimization for frequency stabilization in linked photovoltaic-thermal system. International Transactions on Electrical Energy Systems 2021;31(5):e12883.
[147] Peddakapu K, et al. Stabilization of frequency in multi-microgrid system using barnacle mating Optimizer-based cascade controllers. Sustain Energy Technol Assessments 2022;54:102823.
[148] Kumar V, et al. Stochastic wind energy integrated multi source power system control via a novel model predictive controller based on Harris Hawks optimization. Energy Sources, Part A Recovery, Util Environ Eff 2022;44(4): 10694–719.
[149] Abou El-Ela AA, et al. Design of cascaded controller based on coyote optimizer for load frequency control in multi-area power systems with renewable sources. Control Eng Pract 2022;121:105058.
[150] Hasanien HM, El-Fergany AA. Salp swarm algorithm-based optimal load frequency control of hybrid renewable power systems with communication delay and excitation cross-coupling effect. Elec Power Syst Res 2019;176:105938.
[151] Teekaraman Y, Kuppusamy R, Nikolovski S. Solution for voltage and frequency regulation in standalone microgrid using hybrid multiobjective symbiotic organism search algorithm. Energies 2019;12(14):2812.
[152] Lodhi E, et al. A dragonfly optimization algorithm for extracting maximum power of grid-interfaced PV systems. Sustainability 2021;13(19):10778.
[153] Khamies M, et al. Slime mould algorithm for frequency controller design of a two-area thermal-PV power system. In: 2021 IEEE international conference on automation/XXIV congress of the chilean association of automatic control (ICA-ACCA). IEEE; 2021.
[154] Irudayaraj AXR, et al. Renewable sources-based automatic load frequency control of interconnected systems using chaotic atom search optimization. Appl Soft Comput 2022;119:108574.
[155] Owais R, Javed Iqbal S. Power reserve control of solar photovoltaic system for improved frequency response of a stand-alone power system. Energy Sources, Part A Recovery, Util Environ Eff 2021:1–25.
[156] Ramesh M, Yadav AK, Pathak PK. An extensive review on load frequency control of solar-wind based hybrid renewable energy systems. Energy Sources, Part A Recovery, Util Environ Eff 2021:1–25.
[157] Abriz AF, et al. Modified cuckoo optimization algorithm for frequency regulation of microgrids. In: 2023 8th international conference on technology and energy management (ICTEM). IEEE; 2023.
[158] Kumari S, Shankar G. Maiden application of cascade tilt-integral–tilt-derivative controller for performance analysis of load frequency control of interconnected multi-source power system. IET Gener, Transm Distrib 2019;13(23):5326–38.
[159] Yang B, et al. Novel bio-inspired memetic salp swarm algorithm and application to MPPT for PV systems considering partial shading condition. J Clean Prod 2019; 215:1203–22.
[160] Mahmud I, Masood N-A, Jawad A. Optimal deloading of PV power plants for frequency control: a techno-economic assessment. Elec Power Syst Res 2023:221.
[161] Baskarad T, Kuzle I, Holjevac N. Photovoltaic system power reserve determination using parabolic approximation of frequency response. IEEE Trans Smart Grid 2021;12(4):3175–84.
[162] Zarina P, Mishra S. Cost benefit of using deloaded PV instead of battery. In: 2016 IEEE international conference on power electronics, drives and energy systems (PEDES). IEEE; 2016.